Computational Study of Electrostatic Contribution to Membrane Dynamics

Vladimir Kiselev

Doctor of Philosophy
University of Edinburgh
2011

Declaration

I declare that this thesis was composed by myself, that the work contained therein is my own, except where explicitly stated otherwise in the text, and that no part of this thesis has been submitted to any other university in application for a higher degree.

(*Vladimir Kiselev*)

This thesis is dedicated to my mum, my wife, and my children.

Acknowledgements

I would like to thank my supervisor, Dr. Andrew Goryachev, for his guidance, advice and support throughout my PhD time. His inspiration and bright ideas always motivated me to think differently, as all good scientists do. Under his supervision I have obtained not only new computational and analytical skills, but also an invaluable knowledge of how science works. Moreover, I greatly appreciate his help and proactivity in organization of all the formal stages of my PhD, especially during the admission period.

I would also like to thank our unexpendable collaborator, Dr. Davide Marenduzzo, without whom this project could not get to a happy end. A special thanks to Davide for saving my commitment to a life. Namely, for his ability to instantly find a bug in my code, which I have spent weeks on.

Additional thanks to Dr. Marcin Leda for his priceless knowledge of nonlinear dynamics and statistical mechanics, which he was always happy to share with me. Great thanks to Dr. Alexander Morozov for his help with numerical methods and for his ever positive mood.

This PhD would not be completed without my mum, who has always supported me at every stage of my life, my beloved wife, who is my main motivator, and my children, who make my life happy. Additional warm-hearted thanks to all my Edinburgh friends, who are always nearby and ready to help. A final great thanks to the Darwin Trust of Edinburgh for the financial support.

Abstract

Electrostatics plays a crucial role in the membrane biology. Negatively charged lipids (such as PS, PA and PIP_2) are subject to redistribution under the action of electrostatic forces during various signalling events. Membrane recruitment of multiple signalling proteins (such as MARCKS or Src kinase) is often maintained by positively charged polybasic domains (PD). Even though adsorption of these proteins to the cellular membrane has been extensively investigated, very little is known about how electrostatic interactions contribute to their membrane lateral dynamics. This thesis presents an investigation of the contribution of electrostatic interactions to the membrane lateral dynamics by means of novel computational tools. First, I developed a dynamic Monte-Carlo automaton that faithfully simulates lateral diffusion of the adsorbed positively charged PD of a peripheral membrane protein, as well as the dynamics of mono- (PS, PA) and polyvalent (PIP_2) anionic lipids within the bilayer. This model allowed to investigate the major characteristics of protein-membrane diffusion on the uniform membrane. In agreement with earlier results, the simulations revealed the following microscopic phenomena: 1) Electrostatic lipid demixing in the vicinity of the PD; 2) PD interacts with PIP_2 stronger than with monovalent lipids. On the spatially heterogeneous membrane the automaton predicted a directional drift of the PD, which was validated by a simple mean-field analytical model. The predicted phenomenon could potentially play a major role in membrane domain

formation. To test this hypothesis and to investigate the membrane dynamics on larger scales I developed a continuous model, which was based on the results of the automaton simulations. The results of the continuous model and the Monte-Carlo simulations were shown to be in quantitative agreement. The continuous model allows one to simulate the electrostatic membrane dynamics on micrometer scales and can be used to describe various biologically important processes, such as endocytic cup initiation.

Table of Contents

Acknowledgements **iii**

Abstract **iv**

Table of Contents **vi**

List of Figures **ix**

1 Introduction and motivation **1**

1.1 Membrane composition and properties 3

1.1.1 Phospholipid head group structure and charge 3

1.1.2 PIP_2 and other phosphoinositides 5

1.2 Electrostatics of the membrane adsorption 6

1.2.1 Protein polybasic domain 7

1.2.2 Membrane adsorption of PDs and lipid demixing 8

1.3 Protein and lipid membrane dynamics 9

1.4 Computational modeling of protein and lipid membrane dynamics 10

1.5 Thesis objectives and structure 11

2 Discrete modeling of the dynamics on the spatially uniform membrane **13**

2.1 Monte-Carlo automaton description 13

2.1.1 Lipid lattice structure 15
2.1.2 PD structure 16
2.1.3 Calculation of the interaction energies 17
2.1.4 Calculation of ΔE induced by a system change 18
2.1.5 MCA implementation 22
2.1.6 Testing and calibration of the MCA 22
2.1.7 Limitations of the MCA 23
2.2 Results 24
2.2.1 Lipid sequestration and demixing 24
2.2.2 Peptide diffusion on the uniform membrane 29

3 Discrete modeling of the dynamics on the spatially non-uniform membrane 32
3.1 Analytical estimation of the PD drift 33
3.2 Influence of the membrane hydrophobic core on the peptide drift . 35
3.3 Peptide effective charge 37
3.4 Results 39

4 Continuous modeling of the membrane dynamics 43
4.1 Membrane model 44
4.1.1 Membrane plane in the absence of peptides 44
4.1.2 Free energy 45
4.1.3 Entropy density 46
4.1.4 Internal energy density 49
4.1.5 Membrane incompressibility 50
4.1.6 Minimization of the free energy 51
4.1.7 Poisson-Boltzmann equation 52
4.1.8 Lipid dynamics equations 53
4.1.9 Comparison with Poisson-Botzmann-Nernst-Planck model 55
4.1.10 Lipid production and degradation 56
4.2 Peptide species 57
4.2.1 Peptide transition reactions on binary membranes 58

4.2.2 Limitations of the peptide transition model 59
4.2.3 Peptide transition reaction constants 60
4.2.4 PLCs contributions to free energy and fluxes 63
4.2.5 Average total and effective charges of the peptides 63
4.2.6 General form of membrane dynamics equations 65

5 Comparison of the CM with the MCA **67**
5.1 MCA description 67
5.2 General solution of the CM using FlexPDE 68
5.3 Numerical solution of the simplified CM 69
5.3.1 Quasi steady state approximation 69
5.3.2 Analytical solution of peptide transition reactions 70
5.3.3 Discretization of Nernst-Planck equation 71
5.3.4 Discretization of Poisson-Boltzmann equation 74
5.4 Importance of membrane incompressibility 79
5.5 Results 80
5.5.1 Determination of parameters and calibration of CM 80
5.5.2 Lipid gradients on binary membrane 82
5.5.3 Lipid gradients on ternary membrane 86
5.5.4 Distribution profiles of PLCs on binary membrane 88

6 Conclusions and directions for future work **91**
6.1 Conclusions 91
6.2 Directions for future work 93

Appendix A Effective friction in the peptide drift **95**

Appendix B Additional validation of the MCA **99**

Appendix C Concentrations of lipids and peptide complexes **101**

Bibliography **103**

List of Figures

1.1 Cell membrane structure 2
1.2 Phospholipid structures 4
1.3 Diagram of phoshoinositides regulation 5
1.4 Schematic representation of MARCKS interacting with the membrane 7

2.1 Schematic representation of the membrane lattice 15
2.2 Projection of Lys-5 peptide backbone on the lipid lattice. 16
2.3 Dependence of the interaction energy of lipids on distance 18
2.4 The neighborhood used to calculate ΔE of the lipid movement . . 19
2.5 The neighborhoods used to calculate ΔE of the peptide translational and rotational movements 21
2.6 Probability density functions of lipid association for PS and PIP_2 25
2.7 Average numbers of PS and PIP_2 molecules associated with the peptide 26
2.8 Total peptide charge 26
2.9 Average peptide association times of PS and PIP_2 27
2.10 Lipid demixing profiles 28
2.11 Dependence of the peptide diffusion coefficient on the membrane composition 30

3.1 Characteristic peptide charges 38
3.2 Peptide drift in the gradient of a monovalent lipid (1) 40
3.3 Peptide drift in the gradient of a monovalent lipid (2) 41
3.4 Peptide drift in the gradient of a monovalent lipid with a constant PIP_2 concentration 42

4.1 Transitions between PLCs 58
4.2 Comparison of CM and MCA for the probability density functions of peptide-PS association 62
4.3 Average total and effective charges of the peptides in CM and in MCA 64

5.1 Numerical five-point scheme used in MED method 73
5.2 Dimension reduction in the general form of the discretized Poisson-Boltzmann equation 78
5.3 Comparison of general and PBNP systems 79
5.4 PC diffusion coefficient computed in MCA 81
5.5 PS diffusion coefficient computed in MCA 81
5.6 PIP_2 diffusion coefficient computed in MCA 82
5.7 Comparison of CM and MCA for a single lipid gradient 84
5.8 Comparison of the corrected CM with MCA for a single lipid gradient 85
5.9 Comparison of CM with MCA for a ternary membrane with PS gradient 87
5.10 Comparison of CM with MCA for a ternary membrane with PIP_2 gradient 88
5.11 Comparison of CM and MCA for peptide probability distributions 89
5.12 Comparison of the corrected CM and MCA for peptide probability distributions 90

A.1 Drift of a particle together with the associated potential well . . . 97

B.1 Peptide drift in the gradient of a monovalent lipid (1D Monte-Carlo simulation model) 100

CHAPTER 1

Introduction and motivation

Cell membrane represents an interface between the cell and its external environment. The first mention of the idea that cells are surrounded by a thin layer called a plasma membrane goes back to the second half of the 19^{th} century. Over the years the structure and biophysical properties of the cell membrane have been extensively investigated and nowadays they are well defined and described [1].

Together with its complicated structure (Fig. 1.1), the membrane has a wide range of biological functions. As an interface the membrane contains receptors which receive information from the extracellular environment. Various external molecules can be engulfed by the cell through the membrane by means of various processes, such as endocytosis, phagocytosis etc [3]. Cell growth and proliferation lead to the increase of the membrane area. Many signaling pathways are initiated on the membrane by activated membrane receptors and further propagate into the cell. All of these processes require the recruitment of various protein molecules to the cell membrane, as well as the alteration of the membrane composition. On the molecular level these processes are governed by physical laws. The well known example is the physical diffusion. The diffusion occurs everywhere in the cell and is particularly significant for the membrane organization [4]. However, an impact of other physical principles involved in the membrane functionality is

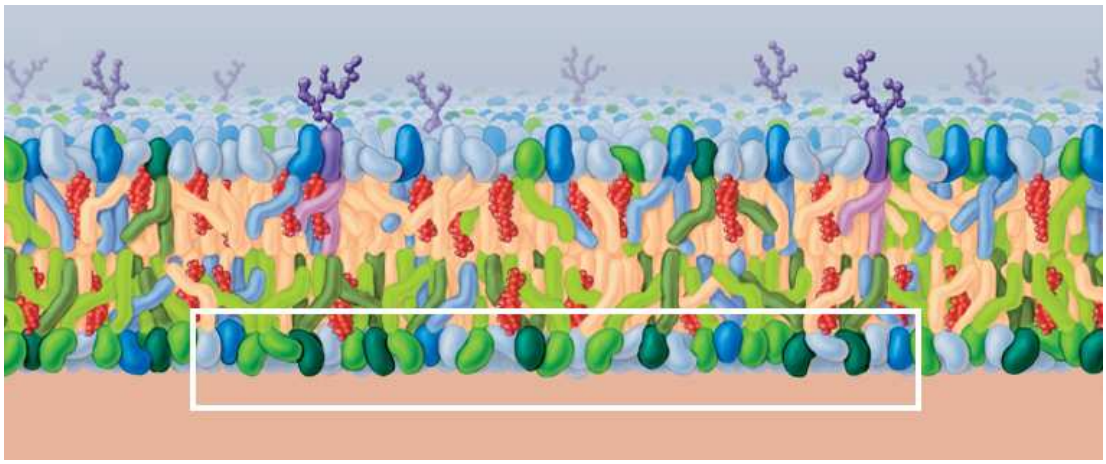

Figure 1.1: Cell membrane structure (adapted from [2]). Top surface (the outer leaflet of the membrane) and the bottom surface (the inner leaflet of the membrane) constitute the membrane bilayer structure. The space between the top and the bottom surfaces is the bilayer interior. White rectangle shows a slice of the inner leaflet with the lipid head groups, which is considered further in the thesis.

yet not well understood.

Electrostatics along with the diffusion is vital for the cell functions. The reason is that, firstly, most of the intracellular proteins, as sequences of amino acids, have parts with charged residues. Secondly, the cell cytoplasm consists of positively and negatively charged ions, that constitute its electrolytic nature [5]. Finally, the cell membrane is also charged and interacts with cytoplasmic proteins and ions by means of electrostatic forces [6].

This thesis represents an investigation of the role of electrostatic interactions in the membrane lateral dynamics. Particularly, I concentrate on the lateral dynamics of membrane lipids and peripheral cytoplasmic proteins recruited and bound to the membrane.

I begin this introductory chapter with the description of the membrane composition and electrostatic properties. Next, I provide an overview of the electrostatic membrane adsorption of peripheral proteins and describe the structure of a specific type of these proteins – proteins with polybasic domains. Then, I introduce the experimental and the theoretical data available on the membrane lateral dynamics. Finally, I define the goals of the thesis and provide its structure.

1.1 Membrane composition and properties

The major components of the cell membrane are various lipid species. Lipids are small amphiphilic molecules consisting of hydrophobic (tails) and hydrophilic (head groups) parts. The human body consists of several kg of membrane lipids with a total surface of about 0.4 km^2/kg and the plasma membrane of one eucariotic cell contains about 10^{10} lipids, organized in a bilayer [7]. The bilayer of the cell membrane is a stable structure, consisting of the bilayer interior, the inner (intracellular, in contact with the cell cytoplasm) and the outer (extracellular, in contact with the extracellular environment) leaflets (Fig. 1.1). The interior of the bilayer is filled with the hydrophobic lipid tails, while the surfaces of the leaflets are populated with the hydrophilic lipid head groups. The outer leaflet of the membrane is generally neutral and does not significantly contribute to the membrane electrostatic properties. In contrast, the inner cytoplasmic leaflet, which consists of about 20–40% of negatively charged lipids [8], constitutes the electrostatic nature of the membrane. The lipids, that create the charge of the inner membrane leaflet, belong to the class of lipids called phosphoglycerides (or phospholipids).

1.1.1 Phospholipid head group structure and charge

Phospholipids is the most abundant class of the membrane lipids. As all other lipids, a phospholipid has a hydrophobic tail connected (through glycerol and a phosphoric acid) to a head group (Fig. 1.2, A). While the tail usually consists of two fatty acids, the head group has a more complicated structure (Fig. 1.2, B).

The main difference between phospholipids is the structure of the alcohol attached to the phosphate. Here I consider four types of membrane phospholipids with different structures of their alcohols: PC – phosphatidylcholine (choline alcohol), PS – phosphatidylserine (serine alcohol), PA – phosphatidic acid (no head group) and PIP_2 – phosphatidylinositol 4,5-bisphosphate (with inositol ring) (Fig. 1.2, B). Since glycerol is neutral and the phosphate is always negatively charged (charge -1 in electron charge units), the net charge of the head group (together with the phosphate) is defined by the structure of the alcohol. For

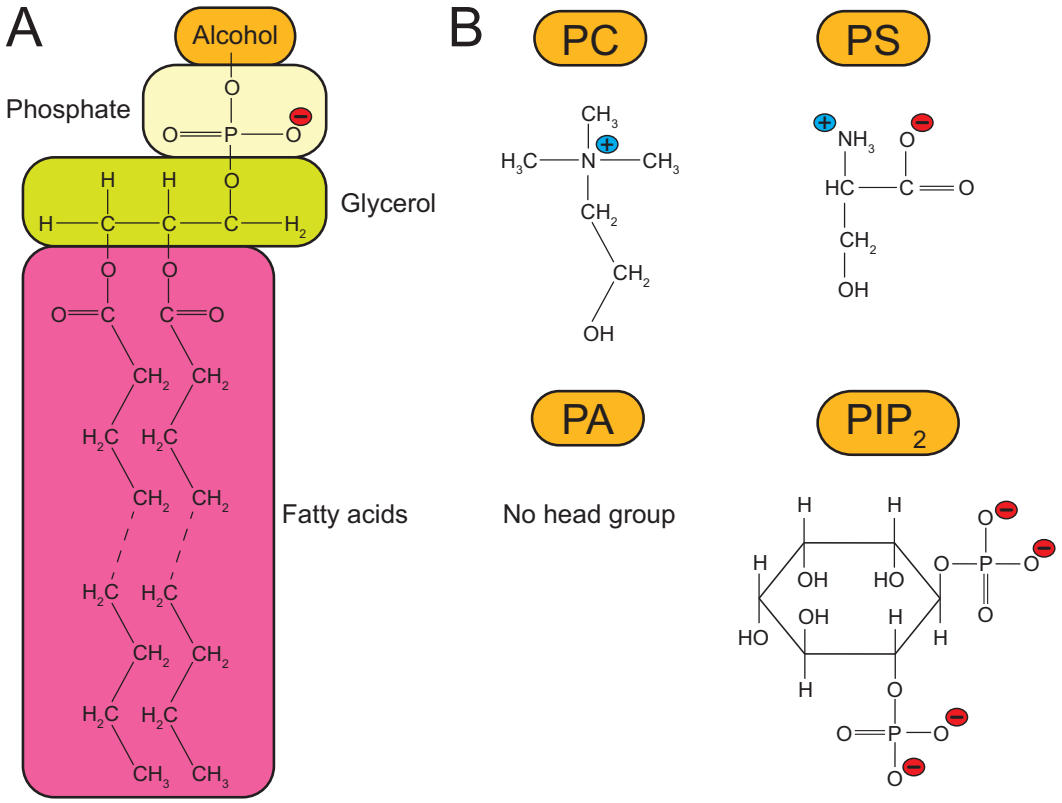

Figure 1.2: Phospholipid structures (adapted from [2]). A, Schematic structure of a phospholipid; B, Structures of the head group alcohols of different phospholipids.

example, the net head group charge of a PC lipid is 0, since the positive charge of its alcohol neutralizes the negative charge of a phosphate group. In contrast, PS lipid has an additional negative charge in its alcohol, thus the net charge of its head group is -1. PA lipid, due to the absence of the alcohol, has only one negative charge in a phosphate group, thus its net charge is -1. PIP_2 has an unusual structure, which makes it a part of the class of lipids called phosphoinositides. The net head group charges of phosphoinositides are generally more negative than charges of other phospholipids. PIP_2 has 4 negative charges on the inositol ring, thus the maximum PIP_2 charge can be -5 (together with the phosphate charge). However, in the relevant biological conditions due to binding of cytoplasmic ions, such as K^+ or H^+, the charge of PIP_2 can be -3, -4 or -5 [9].

1.1.2 PIP_2 and other phosphoinositides

Phosphoinositides constitute a small fraction (5-8%) of the cell membrane lipids [10]. They have a specific inositol head group (the so-called inositol ring – Fig. 1.2, B). The main distinctive feature of the inositol ring is that it has 6 nodes (positions) and can be phosphorylated at them, allowing different structures and consequently different net charges of the ring. Phosphoinositides play a major role in the vital cell processes, such as signaling pathways, exo- and endocytosyses and others. The predecessor of all phosphoinositides is phosphatidylinositol (PI). PI undergoes changes of its structure through phosphorylation and dephosphorylation cycles by specific PI kinases and phosphatases, providing other phosphoinositides (Fig. 1.3).

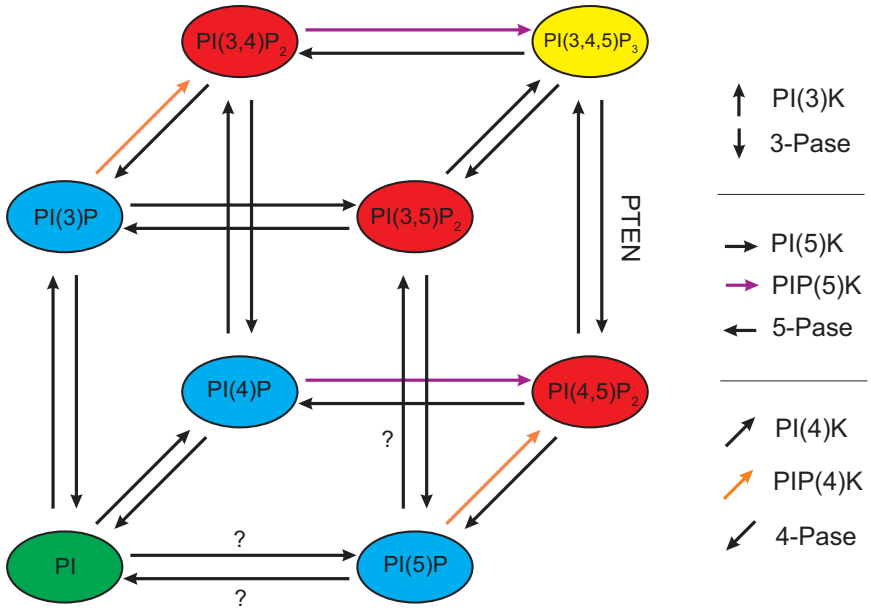

Figure 1.3: Diagram of phoshoinositides regulation. Phosphoinositides are shown in colored ovals. The enzymes involved in the phosphoinositides regulation are shown with arrows of different colors and different directions. Unknown enzymes are shown with "?".

PIP_2 phosphoinositide, which comprises only about 1% of the cytoplasmic leaflet of the plasma membrane, has a large number of functions, such as a source of three major second messengers (DAG, IP_3 and PIP_3), one of the main components of both exo- and endocytosis, an anchor for the peripheral membrane proteins and many others [11–14]. PIP_2 biophysical properties distinguish it from

all other non-inositial membrane components. In addition to its strongly negative charge (-4), described in the previous chapter, PIP_2 headgroup may also protrude much further in the aqueous phase than a typical phospholipid [15]. Due to these distinguishing characteristic PIP_2 is able to interact with cytoplasmic proteins with high affinity, especially with strongly positively charged parts of proteins.

1.2 Electrostatics of the membrane adsorption

Electrostatic properties of the membrane lipids described above play a crucial role in the membrane binding of the peripheral proteins. Peripheral membrane proteins are able to temporally attach to the membrane by insertion of a covalent lipid modifications in it [16]. A covalent lipid modification is a covalent addition of a fatty acid to one of the protein ends. During the membrane binding the lipid modification is hydophobically inserted to the lipid bilayer and due to the hydrophobic effect the total structure stabilizes. However, in many cases the hydrophobic insertion of a lipid modification is not sufficient to keep a protein attached [17]. In these cases electrostatic interactions of the proteins with membrane negatively charged lipids can effectively facilitate the binding [18, 19]. Remarkably, several highly important signaling proteins, such as Ras small GTPases, phosphatase PTEN, and actin regulators WASP and MARCKS as well as nonreceptor tyrosine kinase Src, along with other binding mechanisms, bind to the membrane using a sequence of positively charged residues in their structure, which is called a polybasic domain (PD) [16, 17, 20–23]. It has been shown experimentally that the PD contributes approximately the same amount of energy to the membrane binding (for 2:1 PC/PS membrane) as the hydophobic insertion of the lipid modification [17]. These examples show that the PD is essential for binding of various signaling proteins to the negatively charged inner leaflet of the cell membrane.

1.2.1 Protein polybasic domain

To provide an example of a PD, I concentrate here on the PD of MARCKS protein (151-175), since it has a common structure and has been extensively studied and well described. The structure of the domain is presented in Fig. 1.4, taken from [18]. The PD of MARCKS protein consists of 13 basic residues that interact electrostatically with negatively charged membrane lipids. The main contribution to the electrostatic PD binding is provided by the first 5 basic residues [24] (Fig. 1.4, shown as blue plus signs at the left side of the domain). Additionally, there

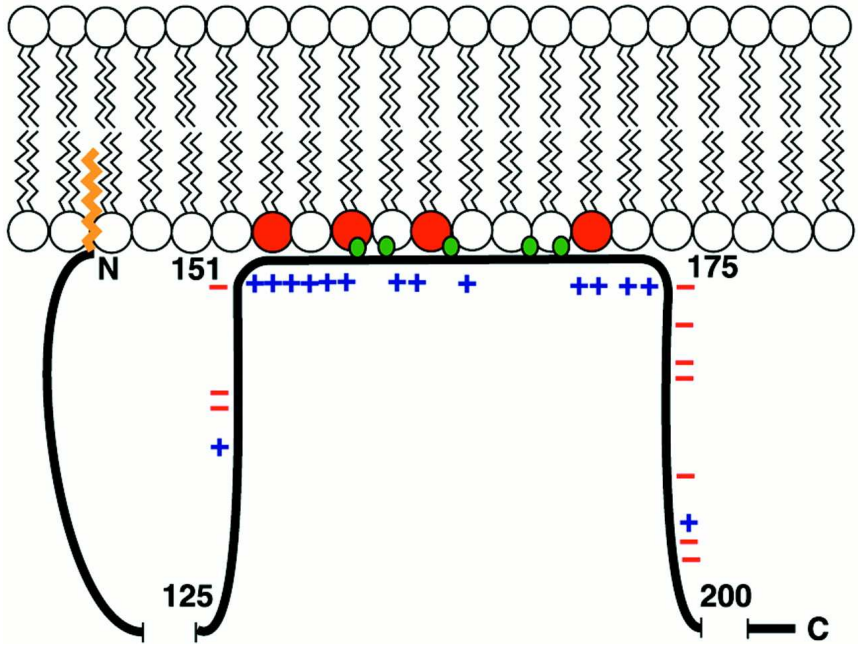

Figure 1.4: Schematic representation of MARCKS interacting with the membrane (from [18]). The PD is a black line between the 151^{th} and the 175^{th} protein residues. The lipid modification inserted in the membrane bilayer is shown in orange. The positively charged residues of the PD are shown as blue plus signs. Negatively charged membrane lipids (PS, PA, PIP_2) are shown as red circles, neutral lipids (PC) are shown as white circles. 5 aromatic residues are shown in green.

are 5 aromatic residues that also contribute to the protein membrane binding (Fig. 1.4, shown in green). These aromatic residues during binding penetrate the polar head group region of the membrane [19]. However, the energy of their interactions with the membrane is insignificant, compared to the contribution from the PD and the lipid modification [17, 22]. Electron paramagnetic resonance [25]

and circular dichroism [18] studies indicated that MARCKS PD is unstructured and elongated when bound to a membrane.

1.2.2 Membrane adsorption of PDs and lipid demixing

Electrostatic adsorption of proteins to the membrane has been a subject of many scientific investigations. A lot of experimental work has been done to measure membrane adsorption isotherms and binding constants of peripheral membrane proteins with PDs, as well as small peptides with characteristic structure, corresponding to the structure of the PD [21, 24, 26, 27]. To describe the mechanism of electrostatic adsorption of the PD to the membrane in detail a large number of computational models have been developed. The structures of the PDs considered in the models vary from simple charged objects (e.g. a sphere or a cylinder) [26,28,29] to more detailed and biologically relevant molecular representations of the PDs [21, 24, 27, 30]. As a result of these studies a new phenomenon of lipid demixing (or sequestration) upon electrostatic protein adsorption has been discovered experimentally and described theoretically [22, 26, 31–35]. Lipid demixing represents a redistribution of lipids in the vicinity of the charged adsorbed molecule (PD). Negatively charged lipids, such as PS, PA or PIP_2 tend to aggregate around the positively charged parts of the adsorbed PD. Thus, the concentration of negatively charged lipids in the vicinity of the PD becomes higher than in the rest of the membrane. Since the area of the membrane with higher density of negatively charged lipids is more attractive for other proteins with PDs, lipid demixing can potentially give rise [24, 29, 34] to formation of recently characterized membrane microdomains [36, 37]. Interestingly, it has been shown that, upon lipid demixing in ternary (PC/PS/PIP_2) membranes, mainly PIP_2 lipids, due to their strong negative charge -4, relocate to the area of adsorption, displacing neutral PC and monovalent PS lipids [22, 31–33, 35].

1.3 Protein and lipid membrane dynamics

Between adsorption to and desorption of any protein from the membrane there is a finite time interval, during which the protein remains bound to the membrane. The average time interval of the protein being bound to the membrane is called the association time and is defined by various factors (e.g. the energy of binding, etc.). The range of associations times varies from sub-seconds to several hours [16]. During the association time the proteins are not static, but generally undergo lateral diffusion on the membrane.

Lateral dynamics of proteins on the biological membranes has been extensively studied in the last decades [38–40]. The development of several biophysical methods, such as fluorescence recovery after photobleaching (FRAP) and fluorescence correlation spectroscopy (FCS) [41] allowed to visualize lipids and proteins on the membrane and explore their diffusive properties. Introduction of artificial membranes, such as supported phospholipid bilayers [42], enabled to perform experiments in a well-controlled *in vitro* environment. The experiments showed that peripheral membrane proteins, such as GPI-anchored proteins and lipid-specific antibodies, are generally 2–8 times slower than lipids [43–45].

It also became clear that electrostatic interactions between proteins and membrane lipids determine lipid lateral mobility. For example, it has been shown that Annexin IV, adsorbed to the surface of a PG (charge -1)/PC bilayer, due to electrostatic interactions, is an important determinant of lipid lateral mobility [46]. As described in section 1.2.2, PIP_2 performs a rapid demixing upon protein membrane adsorption and is strongly sequestered by positively charged residues of the PD. This can be a reason of an experimentally measured slower ($D = 0.8 \pm 0.2$ $\mu m^2/s$) PIP_2 diffusion on the inner leaflet of fibroblasts and epithelial cells compared to its diffusion measured within cellular blebs and artificial phospholipid membranes ($D = 2.5 - 3.3$ $\mu m^2/s$). This finding is also in agreement with other results obtained for both PIP_2 and PIP_3 [47, 48].

The application of the fluorescent protein techniques enabled the *in vivo* analysis of the dynamics of proteins on the inner leaflet of the plasma membrane. These analyses demonstrated that under physiological conditions (20–40% of

monovalent lipids and <1% of PIP_2) diffusion coefficients of proteins attached by a lipid modification and a polybasic domain are similar to those of other peripheral membrane proteins [16]. For example, the inactive (tightly folded) conformation of Src with the PD was shown to diffuse with the mobility $D = 0.57$ $\mu m^2/s$ [49], however, other members of Src family, devoid of polybasic domain, were found to have similar mobilities: $D = 0.1 - 0.6$ $\mu m^2/s$ [50–54]. Analogously, small GTPase KRas with the pronounced PD (+7) was found to diffuse with the mobility $D = 0.2 - 0.35$ $\mu m^2/s$ [50, 53, 55], which is close to that of HRas ($D = 0.35 - 0.5$ $\mu m^2/s$) [55] that has no PD.

Considerably less, however, is known about the influence of different concentrations of negatively charged lipids on the lateral dynamics of proteins with the PDs. Only a few *in vitro* studies revealed the significant changes of the PD diffusion coefficients upon varying the concentrations of anionic lipids. For example, Golebiewska et al. [31] demonstrated that Lys-13, a peptide mimicking the PD of MARCKS protein, diffuses slower on GUVs containing 1% of PIP_2 than on vesicles consisting only of neutral PC and monovalent PS (-1) lipids.

1.4 Computational modeling of protein and lipid membrane dynamics

Computational modeling has been playing a considerable role in characterization of various aspects of protein diffusion on biological membranes [56–59]. Electrostatic interactions between lipids and proteins have also received significant theoretical attention. However, most of it has been focused on the adsorption-desorption dynamics of proteins and the associated demixing of negatively charged lipids (see chapter 1.2.2), while the contribution of electrostatic interactions to the lateral dynamics of adsorbed proteins remained largely unexplored. Only a few studies took this phenomenon into account.

Hinderliter et al. [60] performed Monte-Carlo simulations of multiple proteins on a lattice and, in addition to adsorption and desorption, introduced protein diffusion. However, how electrostatic interaction of proteins with underlying lipids

contributed to the protein lateral dynamics was not considered in detail.

Recently, Khelashvili et al. [61] developed a hybrid (Monte-Carlo simulations coupled to the mean-field approximation) approach in which lateral dynamics of a single poly-lysine peptide and the surrounding lipid was simulated by alternation of random peptide moves and lipid relaxation in accordance with Cahn-Hillard equation. However, due to the absence of explicit thermal fluctuations in the lipid subsystem, lipids did not possess lateral dynamics independent of that of the peptide.

1.5 Thesis objectives and structure

As described above (sections 1.3 and 1.4), the electrostatic contribution to the lateral dynamics of proteins and consequent dynamics of lipids in biological membranes has not been sufficiently studied and the developed modeling tools describe this phenomenon only partially. The goal of this thesis is to uncover new insights into the membrane lateral dynamics by constructing new modeling tools that will be able to describe the electrostatic impact on the membrane dynamics in details. The main objective of the thesis is:

> *To extend the understanding of the electrostatic contribution to the membrane lateral dynamics of proteins and lipids by means of novel computational modeling tools.*

To fulfill this objective, first, I develop a discrete computational model that simulates the behavior of a protein bound to the negatively charged cell membrane. This is a Monte-Carlo simulation model based on the Metropolis algorithm. I describe the details of the model development and implementation in the chapter 2. To test and validate the model I simulate the lipid and protein dynamics on the membrane with the uniform composition. The results of the discrete model obtained on the uniform membrane are provided at the end of chapter 2.

Second, I use the Monte-Carlo model described in chapter 2 to better understand the influence of the distribution of negatively charged lipids on protein lateral dynamics. Particularly, I make the concentrations of lipids in the membrane

non-uniform and run the simulations of the protein diffusion. These simulations are described in the chapter 3.

Thirdly, in chapter 4, based on the results of the Monte-Carlo simulation model and the thermodynamical approach, I construct a novel continuous model of protein and lipid lateral membrane dynamics. I also discuss the limitations of the continuous model and its advantages over the discrete Monte-Carlo simulation model. One of the main advantages of the continuous model is that it allows one to study electrostatic effects on the membrane at larger (several micrometers) scales, as compared to the maximal size (the order of 100 nm) of the membrane domain in the Monte-Carlo simulation model.

In chapter 5 I compare the results obtained in the continuous model with the results of Monte-Carlo simulations for the non-uniform membrane compositions (with lipid gradients).

Finally, I conclude the thesis by explaining how its main objective has been fulfilled and what contributions to the science my work has made. I also provide possible future directions of the research where the developed computational tools can be particularly useful.

CHAPTER 2

Discrete modeling of the dynamics on the spatially uniform membrane

2.1 Monte-Carlo automaton description

The work presented in this chapter has been published in the paper of Kiselev et al. [62] and has been done by me.

To begin a computational investigation of the lateral dynamics of lipids and proteins on the cell membrane, I develop a kinetic Monte-Carlo simulation model (or kinetic Monte-Carlo automaton, MCA hereafter) [63], which faithfully describes the diffusion of lipid species and proteins on the cellular membrane under the action of random thermal noise (Brownian motion) and electrostatic forces.

Generally, any Monte-Carlo simulation procedure is based on a random sampling, which is repeatedly used to decide whether to accept or reject any change in the system configuration. In the MCA under consideration, in order to make this decision, I use Metropolis-Hastings algorithm [64]. Metropolis-Hastings algorithm requires calculation of an expected energy cost (ΔE) caused by the change. Depending on the energy cost the change can be either accepted or rejected. If $\Delta E < 0$ the change brings the system to a state of lower energy, thus it is al-

ways accepted (according to the second law of thermodynamics). If $\Delta E > 0$ the change is accepted with the probability $P = \exp(-\Delta E/k_B T)$, where k_B is Botzmann constant and T is the temperature of the system. To accept the change with the probability P, a random number R ($R \in [0{:}1]$) is generated and compared with P. If $P > R$ then the change is accepted, otherwise it is rejected.

Due to the membrane topology, the MCA is constructed in a two-dimensional space (2D) and consists of two parallel hexagonal lattices, separated by a small distance and embedded into the cytoplasmic solution. The first hexagonal lattice represents the inner leaflet of the cell membrane, while the second one represents the plane of the protein diffusion. In the simulations of the MCA I consider a protein with a PD and a single lipid modification (section 1.2).

Every node of the lipid lattice is occupied by a lipid head group. Since the membrane is not static and lipid head groups are able to move out of the main leaflet plane, I assume that in the MCA the lipid head groups are always surrounded by cytoplasmic ions (alternatively, the cytoplasmic ions can freely penetrate the layer). In this case the lipid head groups in the MCA are always equilibrated with the cytoplasmic ions, due to their high mobility.

To concentrate on electrostatic properties of the protein membrane dynamics in the protein lattice, instead of a whole protein, I consider the diffusion of its PD. Particularly, I simplify the PD by an oligopeptide consisting of only positively charged residues. Similar to the approach described in [24] I choose pentalysine Lys-5 with five basic residues and, consequently, with the charge +5, as such an oligopeptide. In the MCA this peptide always diffuses in the lattice overlying the lipid lattice.

The lipids and the peptide diffuse in their lattices under the action of random thermal noise (Brownian motion) and electrostatic forces. The size of the membrane lattice L is chosen to be less then 100 nm, which allows to simulate the evolution of the membrane in a computationally efficient way. However, since the numerical complexity of the simulations is proportional to L^2, further increase in the lattice dimension reduces the effectiveness of the algorithm. Thus, simulations of the system with larger L have to be performed in the context of a different modeling framework (see chapter 4). The total observation time τ_0 is

chosen to be less than 0.01 s. Experimental data suggests that the characteristic membrane association time of proteins with a PD and a single lipid modification is on the order of seconds [16]. Therefore, since the evolution time in the MCA $\tau_0 \ll 1$ s, I assume that the protein is always bound to the membrane and does not dissociate from it during the simulations.

2.1.1 Lipid lattice structure

To define the unit size (d) of the lipid lattice I use an experimentally measured (at 30° C) value of the average lipid head group area $A_L \sim 0.6$ nm^2 [65]. Using simple geometrical calculations one can derive the following (see Fig. 2.1 for the details):

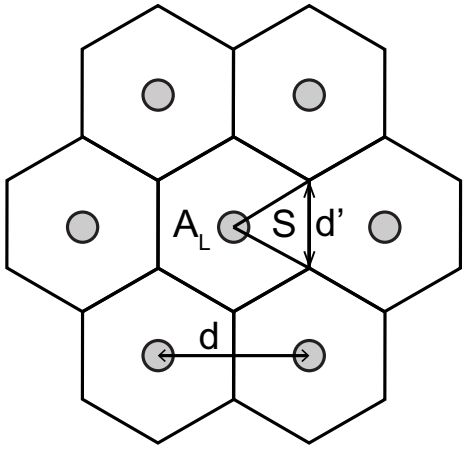

Figure 2.1: Schematic representation of the membrane lattice. Lipids are shown as grey circles; a hexagon around any lipid has an area A_L; d' is the size of the hexagon side; d is the lattice unit size (the distance between two neighboring lipid head groups); S is the area of the equilateral triangle with the side d'.

$$A_L = 6S \tag{2.1}$$

$$S = \frac{\sqrt{3}(d')^2}{4} \tag{2.2}$$

$$d' = \frac{d}{\sqrt{3}} \tag{2.3}$$

Solution of these equations provides an analytical expression for d:

$$d = \sqrt{\frac{2A_L}{\sqrt{3}}} \tag{2.4}$$

For $A_L \sim 0.6$ nm^2 the distance $d \simeq 0.8$ nm. This value of d is used everywhere throughout the simulations. The lipid lattice nodes are populated with 3 types of lipids described in the subsection 1.1.1: neutral PC lipids (with charge 0) monovalent negatively charged PA or PS lipids (with charge -1, referred in the text as PS), and multivalent negatively charged PIP_2 lipids (with charge -4).

2.1.2 PD structure

Previously reported structure of Lys-5 peptide [27], which is chosen as a prototype of a protein with the PD, suggests that the positively charged residues of the peptide can be projected onto the membrane hexagonal lattice with minimal deformations, so that the residues approximately match with some of the lipid nodes (see Fig. 2.2). Utilizing this approximation I use a W-shaped ball-and-stick

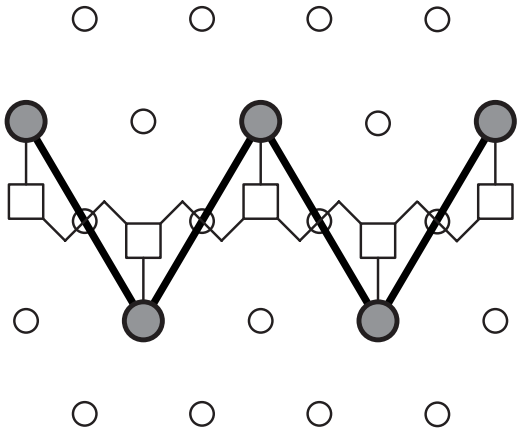

Figure 2.2: Projection of Lys-5 peptide backbone (from [62]) on the lipid lattice (open circles). α-Carbons are denoted by open squares, and positively charged side chains are indicated by solid circles.

structure as a model structure of Lys-5 in the MCA. Due to the matching between the two model lattices, the peptide lattice is chosen to be topologically identical to the lipid one. Thus, during one simulation step, the distance, by which the peptide can be displaced, equals the lipid lattice unit size d. I assume that the peptide and lipid lattices are separated by $D_{H_2O} = 0.28$ nm (the diameter of one

water molecule). This distance is chosen based on the previous studies [66, 67], suggesting that it is optimal for a balance between the Coulombic attraction and desolvation penalties. However, *in vivo*, due to the vertical mobility of the lipid head groups in the membrane plane, this distance can presumably increase, allowing the cytoplasmic mobile ions to freely penetrate and equilibrate in the peptide-membrane space. I use this hypothesis in the MCA, assuming that the peptide-membrane space is always occupied by cytoplasmic mobile ions.

2.1.3 Calculation of the interaction energies

I assume that all lipids and Lys-5 residues are point charges that interact only electrostatically and can populate only lattice discrete nodes. The electrostatic potential of the interaction is chosen to be the screened Coulomb potential (also known as Yukawa potential):

$$V(r) = \frac{q_1 q_2}{4\pi\varepsilon\varepsilon_0}\frac{e^{-r/\lambda}}{r} \tag{2.5}$$

where q_1 and q_2 are the values of the interacting charges, r is the distance between them, ε=80 is the dielectric constant of water, ε_0 is the vacuum permittivity and λ is the Debye length. The Debye length for an ionic solution is a function of the temperature and the ionic strength I:

$$\lambda = \sqrt{\frac{\varepsilon\varepsilon_0 k_B T}{2N_A e^2 I}} \tag{2.6}$$

where N_A is Avogrado's number.

The ionic strength is defined by the following equation:

$$I = \frac{1}{2}\sum_{i=1}^{n} c_i z_i^2 \tag{2.7}$$

Where c_i is the molar concentration of ion i in the cytoplasm, z_i is its charge. The cytoplasmic liquid is usually considered as a 0.1 M 1:1 electrolyte [34, 61]. Thus, I use the value of the Debye length, calculated for this solution, in the majority of the simulations: λ = 1 nm. Since mobile ions are equilibrated with both the

lipids and the peptide the Debye length is assumed to be constant in every point of the MCA system.

According to eq. (2.5) the strongest interactions in the membrane lattice correspond to the minimal possible distance between any two lipids $d = 0.8$ nm. Similarly, the strongest interaction between a peptide residue and a lipid occurs when the lipid is located directly underneath the peptide residue, so that the distance between them is minimal ($D_{H_2O} = 0.28$ nm, see subsection 2.1.2). The values of the maximal interaction energies between any two particles of the MCA can be calculated from the eq. (2.5): $E_{\text{PS-PS}} \simeq 0.4\ k_BT$, $E_{\text{PS-PIP}_2} \simeq 1.6\ k_BT$, $E_{\text{PIP}_2\text{-PIP}_2} \simeq 6.4\ k_BT$, $E_{\text{Lys-PS}} \simeq -1.9\ k_BT$ and $E_{\text{Lys-PIP}_2} \simeq -7.6\ k_BT$.

To illustrate how the interaction energy depends on the distance, I calculate it for a general case of two lipids interacting at different distances (Fig. 2.3).

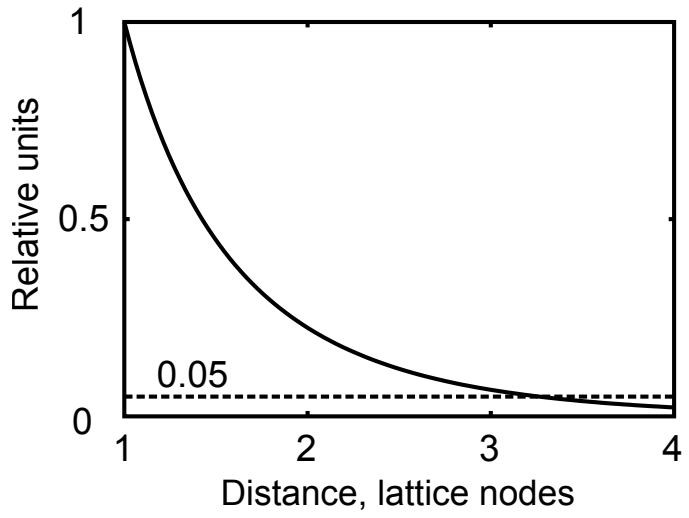

Figure 2.3: Dependence of the interaction energy of lipids on distance. The interaction potential, $V(q_1, q_2, x)$ between any two lipids q_1 and q_2 at the distance x lattice nodes, normalized by its maximal value $V(q_1, q_2, 1)$ at the distance 1 lattice node is shown as a solid black line. Level of the energy corresponding to the 5% of the maximal value is shown as a black dashed line.

2.1.4 Calculation of ΔE induced by a system change

Lipid movements are implemented by means of Kawasaki algorithm [68]. This algorithm represents the diffusion of particles in a compact media, where the particles swap positions during their movements. Each lipid in the model during any

movement swaps its position with a randomly chosen neighboring lipid. The energy cost induced by this swap (ΔE) is required to be computed by the MC algorithm. Since, during the interchange of the two lipids, the rest of the system remains static, the energy cost can be computed by taking into account only interactions of the moving lipids with the rest of the membrane (instead of computing the interactions of all charged particles in the system with each other). Moreover, Fig. 2.3 shows that at the distance of >3 lattice nodes between any two lipids, the energy of interaction of these lipids decreases to less than 5% of the maximal energy. Thus, one can define a 3-node hexagonal neighborhood of the moving lipids, where the energy cost induced by the movement is computed, neglecting the contributions of the lipids lying outside the neighborhood. This is equivalent to cutting off the potential in eq. (2.5) above ∼3 Debye length. The lipid neighborhood is shown schematically in Fig. 2.4. I use this neighborhood in calculations of ΔE induced by the lipid movements.

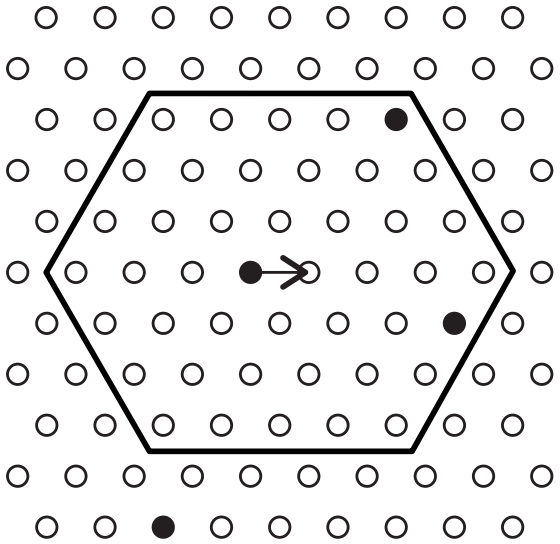

Figure 2.4: The neighborhood (from [62]) used to calculate ΔE of the lipid movement is indicated by the solid line. Charged lipids are shown as solid circles.

In simulations the peptide as a complex rigid structure undergoes two types of movements – translational and rotational. Translational movement is implemented as a displacement of the whole peptide (all five residues) in one out of six directions, chosen at random. Importantly, if the mobility of the peptide is lower than that of the membrane lipids, the lipids will perform a fast demixing, result-

ing in binding of a large number of the negatively charged lipids to the peptide residues. Lys-5 at relevant biological conditions (25% PS, 75% PC) accumulates at its residues about 4 negatively charged PS lipids (see section 2.2.1). If the peptide moved independently from these lipids it would require an energy cost ΔE of about +7.6 k_BT. The probability of such a movement to be accepted is $\exp(-\Delta E/k_BT) \approx 10^{-3}$, resulting in effective immobilization of the peptide. In ternary membranes, containing multivalent PIP_2 the energy cost would be even higher and the peptide immobilization would be stronger. The resulting stalemate in the peptide diffusion was previously described in [61]. However, this phenomenon is known and is called a kinetic trapping. It is usually caused by strong short-range particle interactions. To overcome kinetic trapping, Whitelam and Geissler [69] proposed to introduce collective moves to the system. Thus, instead of the single peptide, the total complex, consisting of the peptide and lipids bound to it, undergoes the lateral diffusion. In this case the energy cost corresponding to the peptide movement does not include the energy of breaking of the peptide-lipid binding. I use this approximation in the MCA. Thus, the peptide movement in the model is always accompanied by a swapping of lipids directly bound to peptide residues with neighboring lipids. The energy cost of the resulting collective movement is then computed (in a similar way, described for the lipids above) within an asymmetrical neighborhood extended in the direction of the proposed movement (Fig. 2.5).

Since the peptide structure is projected onto the hexagonal lattice, I choose a central peptide residue as the best approximation of the center of mass of the peptide. At every simulation step the peptide undergoes rotation around the central node by $\pm 60^\circ$, where the sign is chosen randomly. To avoid kinetic trapping in the case of the peptide rotation, all lipids located in the peptide hexagon envelope (Fig. 2.5) rotate together with the peptide. The energy cost related to the rotation is calculated in the symmetric neighborhood area (Fig. 2.5). Interestingly, the necessity of the peptide rotation becomes clear already at a small fraction of PIP_2 in the membrane, as the peptide accumulates a large negative charge and starts repelling membrane charged lipids. Due to the intrinsic asymmetry of the peptide structure (3 residues on the one side against 2 residues

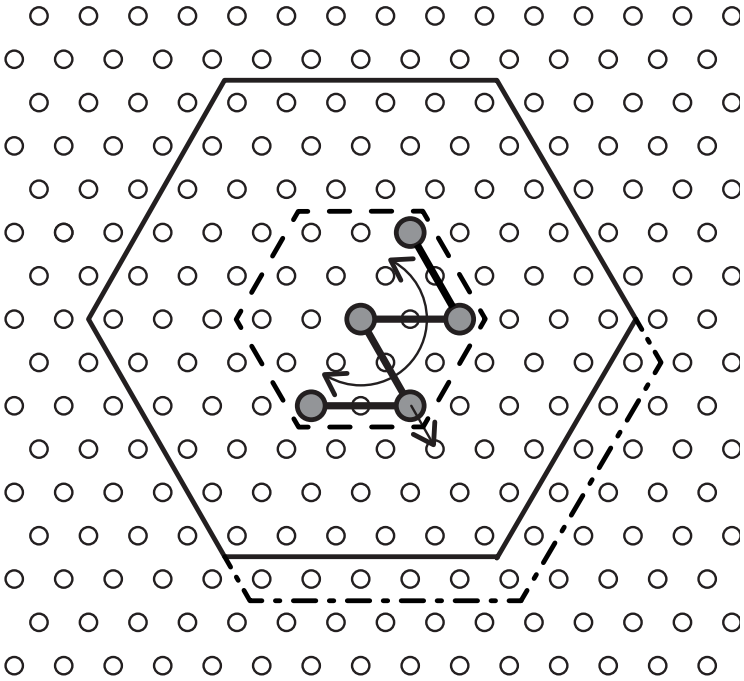

Figure 2.5: The neighborhoods (from [62]) used to calculate ΔE of the peptide translational and rotational movements are shown by dash-dotted and solid lines, respectively. Lipids enclosed within the hexagon shown by the dashed line rotate together with the peptide.

on the other side), its interaction with the membrane lipids is not symmetric. This asymmetry produces an artificial net force acting on the peptide, making its motion biased. Thus, although the rotation mechanism described above does not faithfully represent the corresponding *in vivo* or *in vitro* rotation of a real protein with a PD, it is required for the symmetry of the peptide diffusion.

Note that, since the rotation is discrete, during one rotational step all peptide residues and some of the lipids in the peptide hexagon envelope are displaced by 2 lattice nodes with respect to their initial positions, i.e. their movements are non-local (the displacement is more than 1 node). However, this rotational movement is only important for the interactions of all particles in the peptide hexagon envelope with the lipids that are in the vicinity of the envelope (the peptide nodes and lipids in the hexagon envelope do not change their positions with respect to it). Since the concentration of lipids around the envelope is almost undisturbed (see Fig. 2.10), the rotational move does not significantly change the system configuration. Therefore, I neglect the possible non-Brownian effect that

can be caused by the non-local moves during the discrete peptide rotation.

The energy cost of the rotational movement is computed (in a similar way, described for the translational peptide movement above) within an symmetrical hexagonal neighborhood represented in Fig. 2.5 by a solid line.

2.1.5 MCA implementation

Periodic boundary conditions are imposed on the dynamics of both the lipids and the peptide. One complete time step of the simulations consists of the following:

1. All charged lipids attempt to move by one node in the membrane lattice, including those directly underneath the peptide nodes. This mechanism is implemented using the following procedure. Starting from a randomly chosen corner of the membrane lattice and moving in a typewriter manner, all charged lipids are picked and are forced to move;

2. The peptide tries to move by one node in the peptide lattice;

3. The peptide attempts to rotate around its central node;

All simulations are performed using custom written C code on a multiprocessor Dell Precision T7400 workstation.

2.1.6 Testing and calibration of the MCA

The MCA described above has been extensively tested and validated to ensure that it adequately represents the dynamics of the system at hand. The results are obtained from averaging over several thousand independent realizations. The averaged values of horizontal and vertical displacements $\langle x \rangle$, $\langle y \rangle$ and the mean squared displacement $\langle r^2 \rangle$ are computed for the lipid species. As expected $\langle x \rangle$ and $\langle y \rangle$ are close to and fluctuate around 0 and $\langle r^2 \rangle$ is directly proportional to the time of the simulation ($\langle r^2 \rangle \sim t$). Thus, lipids undergo Brownian diffusion without drift. The rejection rate of lipid dynamics is also checked for the relevant biological conditions (25% PS and 75% PC) and appeared to be negligible

suggesting that lipid moves are mostly accepted. The peptide dynamics has been checked in the same way and has been also proved to be Brownian.

The fact that lipids undergo Brownian diffusion allows one to naturally calibrate the model. Having a fixed value of lattice spatial resolution I computed the diffusion coefficient of lipids in the uncharged membrane from the equation of Brownian law:

$$\langle r^2 \rangle = 4Dt \tag{2.8}$$

The obtained value is D = 0.3 $d^2/\Delta t$, where d is the inter-lipid distance and Δt is the time of one iteration. Remembering that the distance between two neighboring lipids $d = 0.8$ nm $= 8 \cdot 10^{-4}$ μm, the diffusion coefficient can be rewritten in different units: $D = 3.2 \cdot 10^{-7}$ μm$^2/\Delta t$. Assuming that the typical *in vivo* lipid diffusion coefficient is $D_L = 1$ μm^2/s, the "real" time of 1 iteration can be calculated as: $\Delta t = 0.32$ μs. Since the rejection rate of lipid dynamics for relevant biological conditions is negligibly low no further rescaling of the automaton by the acceptance rate is needed (as suggested in [70]).

As described in subsection 2.1.5 the frequencies of peptide and lipid translational moves are equal. This condition automatically defines the maximal achievable diffusion coefficient of the peptide D_0 (when all peptide moves are accepted, i.e. when the system is neutral). As in the lipid case, a suitable experimental value of D_0 can be used to convert the obtained valued of the peptide diffusion coefficient into dimensional units. To make the peptide diffusion coefficient smaller than D_0, the frequency of the peptide moves can be manually reduced to the necessary value, correspondingly slowing down the peptide diffusion.

2.1.7 Limitations of the MCA

It is important to discuss the limitations of the constructed MCA:

1. The model neglects possible hydrodynamic effects beyond the viscous drag. The viscous drag is naturally determined by scaling the model using experimentally measured lipid and protein diffusion coefficients.

2. Although Yukawa potential (2.5) faithfully describes interaction of ions in the electrolyte solution, the model could be improved by using a more detailed Poisson-Boltzmann approach.

3. Ideally, multi-scale or all-atom simulations can be used to better describe the membrane dynamics. However, all of these methods would greatly increase the numerical complexity and, therefore, would require to reduce the size of the system, making it impossible to obtain the effects described in this thesis.

Although these limitations are important, I expect that the simulation results, obtained in the MCA, faithfully describe the membrane dynamics of lipids and proteins.

2.2 Results

This section summarizes the results obtained in the MCA for the case of the uniform lipid distributions in the membrane. All membrane concentrations mentioned in this chapter are fixed, constant and uniform.

2.2.1 Lipid sequestration and demixing

First, I qualitatively measure the electrostatic interactions between the protein PD and the membrane anionic lipids. Since the PD in the MCA is represented by Lys-5 peptide, which structure can be projected to the lipid lattice, there are always 5 nodes in the membrane lattice that are the closest to the Lys-5 basic residues. The interaction of these residues with underlying lipids is the strongest compared to the interactions with other lipids. Thus, the underlying lipids locate in the most preferable positions for interactions. Fig. 2.6, A shows the steady state probability of these positions being occupied by PS in the case of a binary PC/PS membrane. In the physiological range of PS concentrations (15-25%) the peptide basic residues are never fully occupied by monovalent PS lipids. Even at unrealistically high PS concentrations, the total charge of the peptide (the actual

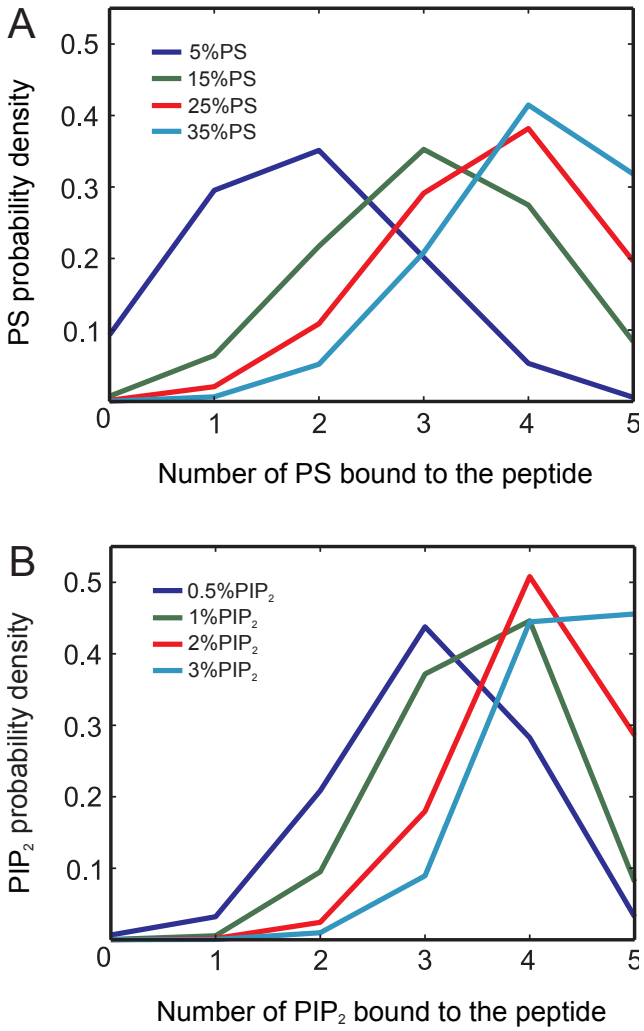

Figure 2.6: Probability density functions of lipid association (from [62]) for PS (A) and PIP_2 (B). For all plots in B, the PS fraction is 25%.

charge of the peptide plus the sum of the charges of all lipids in the underlying positions) remains positive (Fig. 2.8). The situation significantly changes in the case of a ternary PC/PS/PIP_2 membrane (Fig. 2.6, B). Even at a small concentration (0.5%) about three multivalent PIP_2 lipids are associated with the peptide, making the total charge of the peptide strongly negative, -7 (Fig. 2.8).

I also computed the same occupation probabilities for Lys-6 and Lys-7. The data (not presented here) shows that on binary PC/PS membrane the occupations of all three peptides per one peptide residue are almost identical. This suggests that the peptide residues in the constructed MCA interact with anionic membrane lipids independently of each other. Thus, in the case of binary PC/PS membrane,

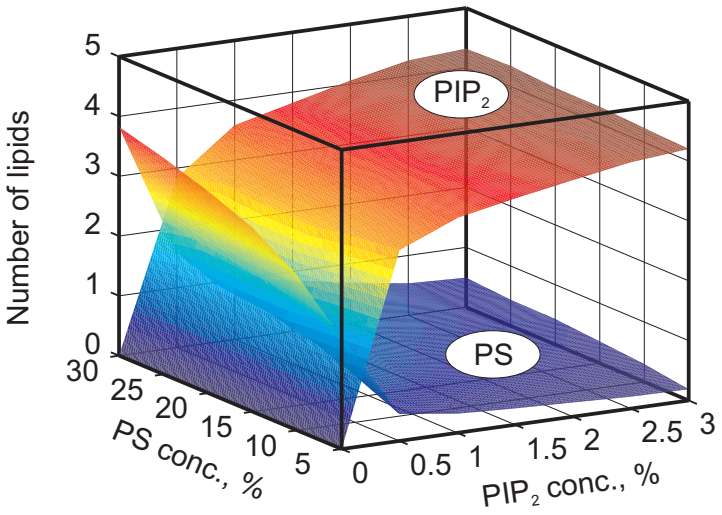

Figure 2.7: Average numbers of PS and PIP_2 molecules (from [62]) associated with the peptide at varying lipid concentrations.

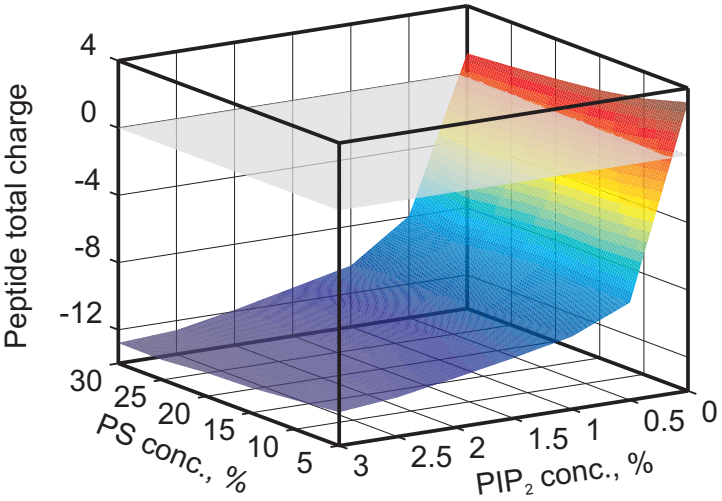

Figure 2.8: Total peptide charge (from [62]) – the charge of the peptide together with associated lipids.

the results above can be also applicable to a peptide with a variable length.

Second, Fig. 2.7 shows that monovalent PS and multivalent PIP_2 lipids effectively compete with each other for the preferable underlying positions underneath the peptide. At concentrations higher than 0.5% PIP_2 lipids practically displace all monovalent PS lipids from the peptide residues.

Next, I measure the average association times of PS an PIP_2 lipids with the peptide residue (Fig. 2.9). Under the assumption that $D_L = 1\ \mu m^2/s$, the association time of PS is about 5-10 simulations steps (1-2 μs), which is about 30-

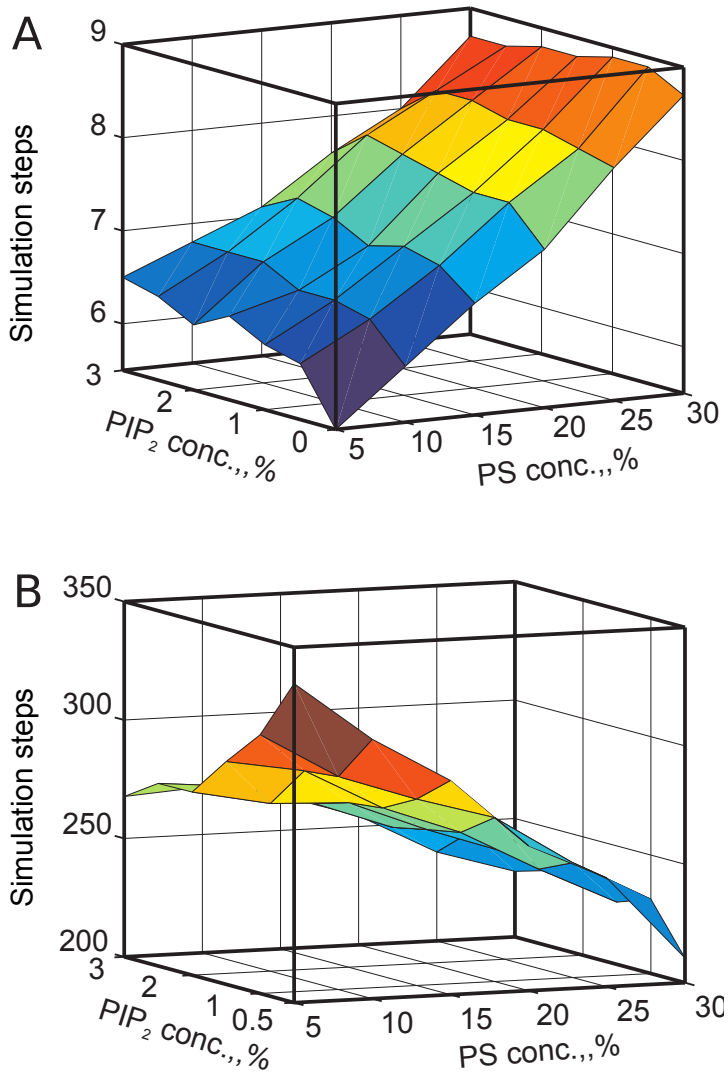

Figure 2.9: Average peptide association times (from [62]) of PS (A) and PIP_2 (B).

50 times shorter than the association time of PIP_2. Therefore, one can conclude that the peptide diffuses mainly together with PIP_2 lipids, but not with PS. These results are in agreement with the experimental data, showing that on the ternary $PS/PIP_2/PC$ membrane, as opposed to the binary PS/PC membrane, the *in vitro* diffusion coefficient of Lys-13 is comparable to the one of the PIP_2 lipids [31].

Finally, I calculate average lipid probability distributions in the vicinity of the peptide. I use a square neighborhood with the center located in the position of the central peptide residue (Fig. 2.10). In the absence of PIP_2, monovalent PS lipids strongly accumulate in between and around peptide residues. However, due to Debye screening, accumulation profiles do not extend further than 1 lipid node

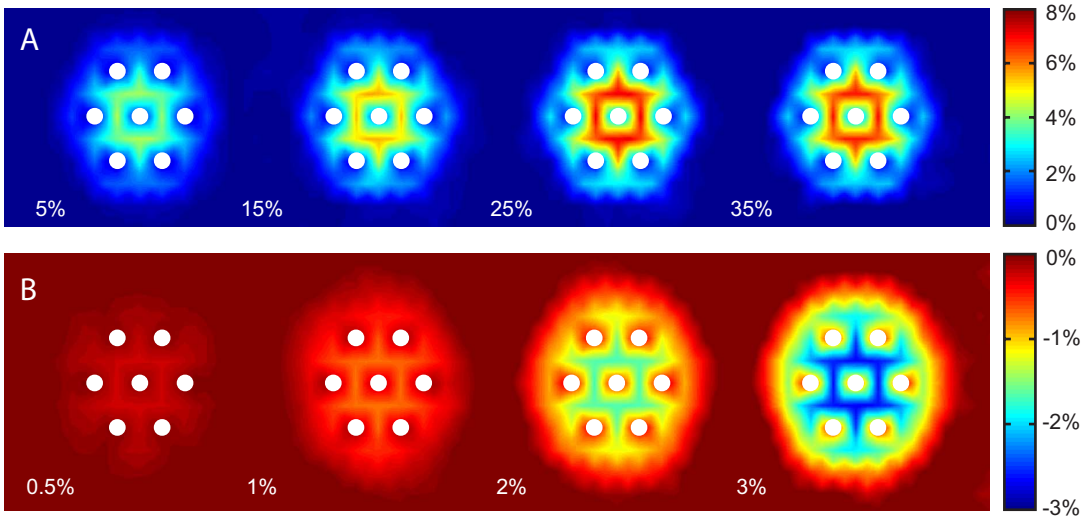

Figure 2.10: Lipid demixing caused by the peptide (from [62]). Pseudocolor represents deviation of the local concentration of PS (A) and PIP_2 (B) from the expected average values indicated in the figure. (A) PIP_2 concentration is 0%. (B) PS concentration is 25%. To produce a smooth concentration field, the true values were projected from the sparse hexagonal lipid lattice onto a fine square grid and intermediate values were computed by spline interpolation. Large values corresponding to the lipid positions located directly underneath the peptide nodes (solid circles) have been removed to reveal subtle details.

away from the peptide. It is also shown in the figure that the sequestration of PS lipids by the peptide saturates with the PS concentration. An increase of the PS concentration higher than 25% does not significantly change its probability distribution in the vicinity of the peptide. In contrast, PIP_2 probability distributions in the ternary PC/PS/PIP_2 membrane have reversed profiles. As expected, PIP_2 lipids quickly accumulate in the preferable positions underneath the peptide residues. Since the repulsion between two PIP_2 lipids by far overcompensate the attraction to the peptide residues (see subsection 2.1.3), the rest of PIP_2 lipids cannot accumulate in the peptide vicinity. In fact, free PIP_2 lipids are almost never found between the peptide nodes. A similar depletion effect (to a lesser extent) is also observed for the PS lipids in the ternary membrane.

The results shown in this chapter indicate that membrane lipids undergo lateral demixing and are sequestered by the peptide basic residues. However, I also measured the relative values of the lipid enrichment on the peptide, i.e. the ratio between the number of lipids found in the membrane area perturbed

by the peptide and the number of lipids that would be found in the same area in the absence of the peptide. Using a symmetric hexagonal neighborhood (37 nodes) of the central peptide residue and the data presented in Fig. 2.10, I obtain the following values of the relative enrichment: at the concentration of 1% in the ternary membrane, PIP_2 are enriched by about ∼10-fold, whereas PS lipids at 35% concentration in the binary membrane are enriched only by about 1.26. Thus, the peptide mainly sequesters PIP_2 lipids, but not PS. These results are in agreement with previously reported experimental data [22, 31, 32].

2.2.2 Peptide diffusion on the uniform membrane

Having described the lipid demixing effect and obtained an agreement with experimental data, I then measured the peptide lateral diffusion coefficients on different (uniform) membrane compositions. In the case of the binary PC/PS membrane, Fig. 2.11, A shows that there is no systematic variation of the peptide diffusion coefficient in a broad range of PS concentrations (10-30%). These results are in agreement with earlier data [31] and are not surprising, since the peptide only weakly interacts with monovalent PS lipids. However, a small reduction of the peptide diffusion coefficient from its maximal value D_0 to a reduced value $D' \approx 0.86 D_0$ is seen between 0% and 10% of PS. A similar weak reduction was also theoretically observed earlier [61]. This effect can be a consequence of the formation of a lipid shell in the vicinity of the peptide due to the rapid lipid demixing (Fig. 2.10, A). The effective friction associated with the lipid shell can potentially reduce the peptide diffusion coefficient.

Fig. 2.11, B shows the dependence of the peptide diffusion coefficient on PIP_2 concentration. Clearly, PIP_2 lipids, even at a small membrane concentration, significantly reduce the peptide lateral dynamics. This behavior can potentially be explained by the following independent arguments.

First, upon the sequestration of PIP_2 lipids the total charge of the peptide-lipid complex becomes strongly negative (see Fig. 2.8). The diffusion of the complex in the membrane can be compared with the diffusion of a strongly negatively charged particle in the two-dimensional suspension of strongly negatively charged

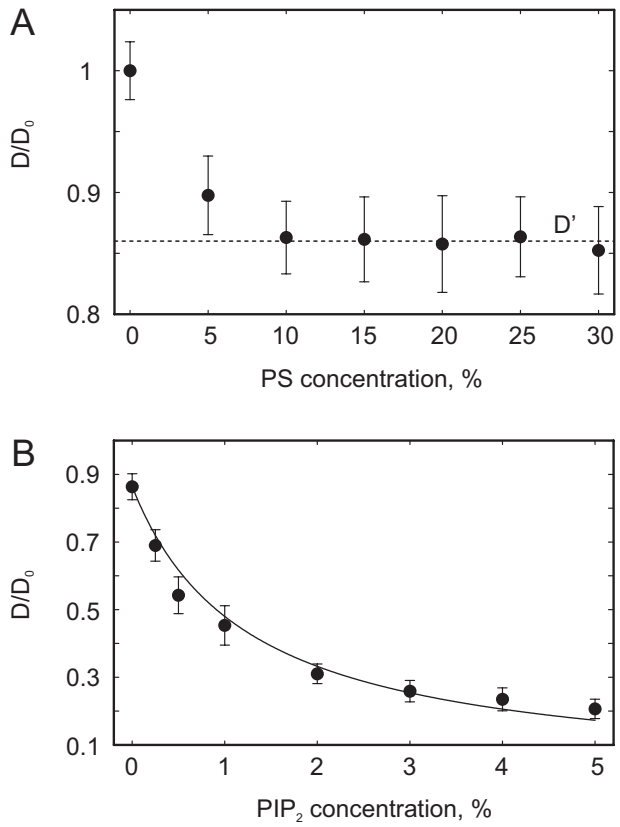

Figure 2.11: Dependence of the peptide diffusion coefficient on the concentration of PS (A) and PIP_2 (B) (from [62]). All simulations in B were performed with 25% of PS; therefore, at 0% of PIP_2, the peptide diffusion coefficient, D', is already $< D_0$.

particles (PIP_2). Due to the Debye screening, Coulombic repulsion between the particles becomes a finite-radius interaction, which can be approximated by the hard-sphere potential. According to Einstein formula for a dilute solution of hard spheres:

$$D^* = \frac{D'}{\eta} = \frac{D'}{1 + \alpha\phi} \tag{2.9}$$

where D^* is the reduced diffusion coefficient, η is the viscosity of the solution, and ϕ is the molar fraction of hard spheres. If one assumes that ϕ is directly proportional to PIP_2 membrane fraction, then it is possible to fit the simulation data of the peptide diffusion coefficient by the analytical function obtained from eq. (2.9) (see Fig. 2.11, B).

Second, Fig. 2.10, B shows that the size of the PIP_2 lipid shell increases together with PIP_2 concentration. The increase of the effective friction associated

with the PIP_2 lipid shell could also reduce the peptide diffusion according to eq. (2.9).

CHAPTER 3

Discrete modeling of the dynamics on the spatially non-uniform membrane

The work presented in this chapter has been published in the paper of Kiselev et al. [62] and has been done by me, except the sections where the work of other authors is explicitly mentioned.

In the previous chapter the peptide lateral dynamics on the uniform membrane was considered. However, the cell membrane is a medium with the ever changing composition. Recent experimental data indicate that various lipid-modifying enzymes can be rapidly recruited and activated on the membrane [71, 72]. Lipid kinases, phosphatases, and some phospholipases alter the lipid charge by adding or removing phosphate groups or using other specific mechanisms. For instance, the monovalent phosphatidic acid (PA) can be produced from the neutral PC lipid by the action of the phospholipase D [73, 74]. PIP_2 can be rapidly produced by phosphatidylinositol 4-phosphate 5-kinase (PIP5K) by phosphorylation of PI(4)P lipid in a large number of cell signaling events [75, 76]. Constant production of the negatively charged lipids on the membrane can generate a gradient of these lipids in the vicinity of the lipid producing enzyme. As a consequence, the associated gradients of the surface charge can generate a temporary electrostatic

potential along the membrane. Since the PDs are located in the closest vicinity of the membrane [27], presumably, they can perceive and respond to the changes in the electrostatic potential. To test this hypothesis, I modified the original MCA by introducing a gradient of the negatively charged monovalent lipids along the membrane width. Particularly, to create a stable gradient, charged lipids are inserted periodically on the left boundary and removed from the lattice once they approach the right boundary. After a large number of iterations (at least 20000) when the gradient becomes stable, the peptide is inserted into the middle of the lattice and its lateral displacement is monitored. Note, that the concentration of the monovalent lipids in the middle of the membrane lattice depends on the value of the lipid gradient, consequently changing the electrostatic properties of the PD (the averaged occupation by monovalent lipids, the peptide total charge etc.). To achieve the constant concentration of monovalent lipids at the lattice center with varying values of the gradient, I introduced two lipid species with the same charge (-1) but distinct boundary conditions. The gradient was generated in the spatial distribution of one species, whereas the other exhibited homogeneous distribution owing to the periodic boundary conditions.

At the time of the peptide insertion into the membrane lattice in the MCA the lipid dynamics is already at the steady state, i.e. the sum of all lipid fluxes at any point of the lattice on average equals 0. Thus, I neglect possible hydrodynamic effects in the peptide diffusion, caused by the lipid fluxes on the membrane.

3.1 Analytical estimation of the PD drift

To analyze the hypothesis of the PD response to the gradient of the electrostatic potential I use a mean-field continuous estimation of the peptide velocity, derived by Davide Marenduzzo. He considers a continuous distribution of lipids, described by a density field $\rho(\vec{\mathbf{r}})$, in the piece of the membrane with the characteristic size $L_d \gg l_p$ (l_p is the characteristic peptide size). The peptide is located at $\vec{\mathbf{r}}^*$ and interacts with negatively charged membrane lipids according to eq. (2.5). The total interaction potential between the peptide and all membrane lipids can

be described as follows:

$$V(\vec{\mathbf{r}}^*) \simeq \int d\vec{\mathbf{r}} \frac{Zq}{4\pi\varepsilon\varepsilon_0} \rho(\vec{\mathbf{r}}^* + \vec{\mathbf{r}}) \frac{e^{-r/\lambda}}{r} \tag{3.1}$$

where the sum over all discrete lipid positions is approximated by the integral over the surface, q is a charge of a single lipid, Z is the peptide charge. The peptide will experience the force created by the gradient of the potential (3.1):

$$\vec{\mathbf{f}}(\vec{\mathbf{r}}^*) = -\frac{\partial V(\vec{\mathbf{r}}^*)}{\partial \vec{\mathbf{r}}^*} \tag{3.2}$$

If $\rho(\vec{\mathbf{r}})$ has a gradient on the membrane, substitution of eq. (3.1) to eq. (3.2) yields:

$$\vec{\mathbf{f}}(\vec{\mathbf{r}}^*) = -\frac{Zq}{4\pi\varepsilon\varepsilon_0} \int d\vec{\mathbf{r}}\, \vec{\nabla}\rho(\vec{\mathbf{r}}^* + \vec{\mathbf{r}}) \frac{e^{-r/\lambda}}{r} \tag{3.3}$$

If the gradient of the lipid density is constant, i.e. if $\vec{\nabla}\rho(\vec{\mathbf{r}}^* + \vec{\mathbf{r}}) \equiv \vec{\nabla}\rho(\vec{\mathbf{r}}^*)$, then it can be taken out of the integral in eq. (3.3), providing the following:

$$\vec{\mathbf{f}}(\vec{\mathbf{r}}^*) = -\frac{Zq}{4\pi\varepsilon\varepsilon_0}\, \vec{\nabla}\rho(\vec{\mathbf{r}}^*) \int d\vec{\mathbf{r}}\, \frac{e^{-r/\lambda}}{r} \tag{3.4}$$

Transforming to the polar coordinates, one can obtain:

$$\vec{\mathbf{f}}(\vec{\mathbf{r}}^*) = -\frac{Zq}{4\pi\varepsilon\varepsilon_0}\, \vec{\nabla}\rho(\vec{\mathbf{r}}^*) \int_0^{2\pi} d\theta \int_0^{\infty} r dr\, \frac{e^{-r/\lambda}}{r} \tag{3.5}$$

Since the last integral in (3.5) equals to λ, the final equation for the force, acting on the peptide, will have the following form:

$$\vec{\mathbf{f}}(\vec{\mathbf{r}}^*) = -\frac{Zq}{2\varepsilon\varepsilon_0}\, \lambda\, \vec{\nabla}\rho(\vec{\mathbf{r}}^*) \tag{3.6}$$

Using Stokes-Einstein's relation, one can express the velocity of the peptide propelled by the force $\vec{\mathbf{f}}$ in a viscous (membrane) medium:

$$\vec{\mathbf{v}} = \frac{D_p}{k_B T} \vec{\mathbf{f}} = -\frac{Zq}{2\varepsilon\varepsilon_0} \frac{\lambda D_p \vec{\nabla}\rho(\vec{\mathbf{r}}^*)}{k_B T} \tag{3.7}$$

where D_p is the peptide diffusion coefficient and k_B is the Boltzmann's constant.

This velocity can be also expressed through the Bjerrum length:

$$l_B = \frac{e^2}{4\pi\varepsilon\varepsilon_0 k_B T} \tag{3.8}$$

which represents the distance at which two ions with elementary charges interact with the energy $k_B T$. Thus, the velocity will have the following form:

$$\vec{\mathbf{v}} = -2\pi \frac{Zq}{e^2} l_B \lambda D_p \vec{\nabla}\rho(\vec{\mathbf{r}}^*) \tag{3.9}$$

Eq. (3.9) shows that in the mean-field approximation, when fluctuations of lipid density can be neglected, the charged peptide experiences a directional drift along the gradient of the lipid concentration with a constant velocity. The velocity of the drift is directly proportional to the peptide charge Z, its diffusion coefficient D_p, Debye length λ, the lipid charge q and the value of the lipid gradient $\vec{\nabla}\rho(\vec{\mathbf{r}}^*)$ at position $\vec{\mathbf{r}}^*$.

3.2 Influence of the membrane hydrophobic core on the peptide drift

The calculations, shown in this section, are done by Davide Marenduzzo.

In section 3.1 the velocity of the peptide on the gradient of anionic lipids was derived without considering of the membrane hydrophobic core. However, due to hydrophobic properties of lipid tails the dielectric constant in the membrane core can be negligible compared to the one in the cytoplasm. This discontinuity of the dielectric constant at the membrane-water interface changes the nature of interaction between charged particles located close to this interface. To investigate how such a refinement impact on the results for the drift velocity of the peptide in a lipid gradient (eq. (3.9)) one can follow the approach developed by Tzlil [30] on the basis of the original work by Netz [77]. Within this framework the electrostatic potential (2.5) is modified to account for the presence of the membrane hydrophobic core (the potential is calculated for the metallic half-space with negligible dielectric constant under the assumption of a finite dielectric constant in

the rest of the space):

$$V^h = \frac{qq'}{4\pi\varepsilon\varepsilon_0} \frac{e^{-\frac{\sqrt{r^2+4zz'}}{\lambda}}}{\sqrt{r^2+4zz'}} \tag{3.10}$$

where q and q' are the charges of the interacting particles, λ is the Debye length, z and z' are the distances of the two charges q and q' from the membrane-water interface.

To estimate the distances z and z', one can use a recently calculated distances between the membrane-water interface and the charged headgroups of phospholipids [78]. In agreement with the previously published data, these distances are shown to be approximately 1 nm. Given the geometry of the MCA, z and z' are approximately equal and are both on the order of one Debye length ($\lambda \approx 1$ nm).

Thus, the two dimensional integrals in eqs. (3.1), (3.3), (3.4) and (3.5):

$$\int_0^{2\pi} d\theta \int_0^{\infty} r dr \frac{e^{-r/\lambda}}{r} \tag{3.11}$$

should be replaced with:

$$\int_0^{2\pi} d\theta \int_0^{\infty} r dr \left[\frac{e^{-r/\lambda}}{r} + \frac{e^{-\frac{\sqrt{r^2+4z^2}}{\lambda}}}{\sqrt{r^2+4z^2}} \right] \tag{3.12}$$

Since the integration of the second term in the integral (3.12) can still be analytically performed, the corrected expression of the peptide drift velocity (3.9) will have the following form:

$$\vec{\mathbf{v}} = -2\pi \frac{Zq}{e^2} l_B \lambda D_p \vec{\nabla} \rho(\vec{\mathbf{r}}^*)(1 + e^{-2z/\lambda}) \tag{3.13}$$

Eq. (3.13) contains the additional term $(1 + e^{-2z/\lambda})$, compared to the original expression of the peptide velocity (3.9). The maximum value of this term is 2, corresponding to the situation when interacting charges are located directly on the membrane-water interface. However, under the assumption $z = z' = 1$ nm, described above, the correction $(1 + e^{-2z/\lambda})$ is rather small (about 14%) and therefore does not significantly change the results obtained by eq. (3.9).

3.3 Peptide effective charge

Due to the lipid demixing effect (see subsection 2.2.1) the nature of the peptide charge Z, introduced in the eq. (3.9) for the peptide drift velocity, can be complicated. Indeed, the intrinsic charge of the peptide is always constant and equals +5. However, upon lipid demixing and consequent sequestration the introduced total peptide charge (see Fig. 2.8) can be significantly smaller and even become strongly negative (in the presence of PIP_2). Since in the MCA the peptide diffuses together with negatively charged lipids that are located directly underneath the peptide residues (according to the model assumption), the reduction of the total peptide charge should be reflected by Z. Moreover, due to the specific mechanism of the lipid moves (Kawasaki step, see subsection 2.1.4), the associated current of lipids, created by the peptide diffusion, in the direction opposite to the peptide drift should also be taken into account.

To include all translocating charges in Z, one should consider one peptide movement in details. I consider a binary PC/PS membrane and describe the peptide movement with respect to one peptide residue with the intrinsic charge +1. As the molar fraction of PS lipid, ρ, grows from 0% to 100%, the total charge of the residue decreases from +1 to 0, as shown by the dashed line in Fig. 3.1, B. If the probability of the peptide residue being associated with PS is $p(\rho)$ then the total residue charge is $1 - p(\rho)$. I denote the initial position of the residue before the movement as "old" and the final position of the residue after the movement as "new". Before the move the "new" position is occupied by PS lipid with the probability ρ and the peptide residue in the "old" position is bound to a PS lipid with the probability $p(\rho)$. One can also assume that these two random events are independent of each other and thus mutual probabilities can be calculated as products of corresponding event probabilities. If the peptide residue is originally bound to a PS lipid, the movement of the residue is associated with the dragging of this lipid resulting in the Kawasaki "swap" with the lipid located in the "new" position. There are four possible scenarios of moving from the "old" to the "new" position (Fig. 3.1, A):

1. The peptide residue is bound to PS and the "new" position is also occupied

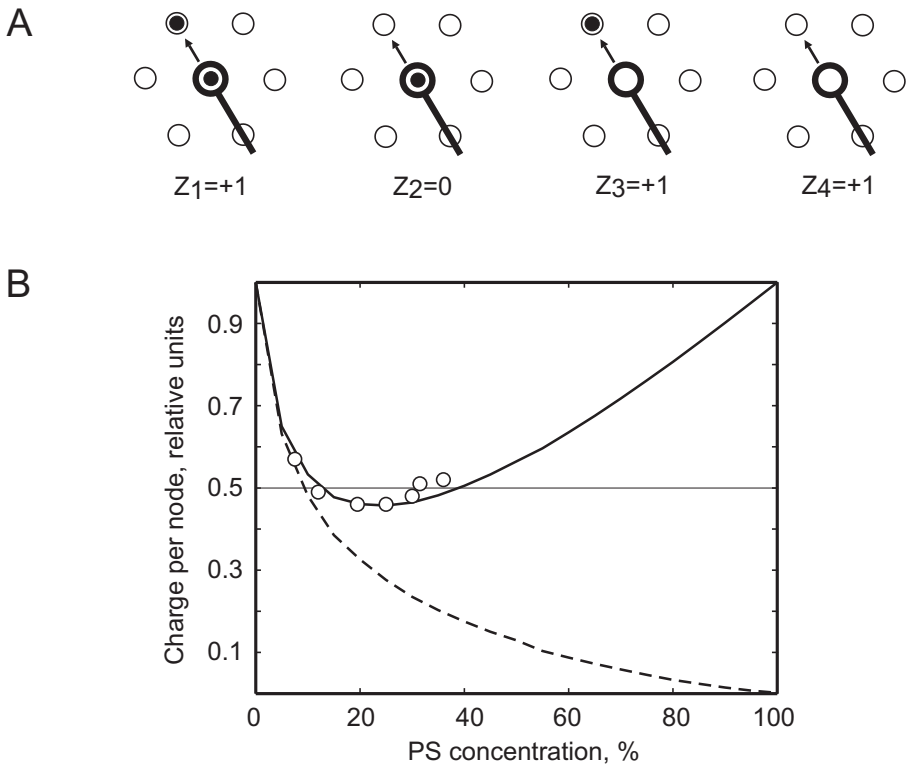

Figure 3.1: Characteristic peptide charges (from [62]). The value of the effective charge Z in eq. (3.9) that translocates during the drift of the peptide is a weak function of the local PS concentration. (A) The four possible elementary translational moves of a peptide node (shown by thick line) projected onto the lipid lattice. Solid circle within the lipid lattice node represents a PS lipid. (B) The value predicted by eq. (3.14) (solid line) is compared to the simulation results (open circles). The total charge of the peptide together with the associated lipids is shown by the dashed line.

by a charged PS lipid. In this case, the effective translocating charge is $Z_1 = +1$ (the charge of the residue) and it occurs with the probability $P_1 = p(\rho) \cdot \rho$;

2. The peptide residue is bound to PS and the "new" position is occupied by a neutral PC lipid. In this case, the effective translocating charge is $Z_2 = 0$ (the charge of the residue plus the charge of the PS lipid) and it occurs with the probability $P_2 = p(\rho) \cdot (1 - \rho)$;

3. The peptide residue is free of a PS lipid and the "new" position is occupied by a charged PS lipid. In this case, the effective translocating charge is $Z_3 = +1$ (the charge of the residue) and it occurs with the probability

$P_3 = (1 - p(\rho)) \cdot \rho$;

4. The peptide residue is free of a PS lipid and the "new" position is occupied by a neutral PC lipid. In this case, the effective translocating charge is $Z_4 = +1$ (the charge of the residue) and it occurs with the probability $P_4 = (1 - p(\rho)) \cdot (1 - \rho)$;

Thus, the average value of the effective translocating charge per one peptide residue is:

$$Z(\rho) = \langle Z_i \rangle = \sum_{i=1}^{4} Z_i P_i = 1 - p(\rho) + p(\rho) \cdot \rho \tag{3.14}$$

Note that $p(\rho)$ can be calculated from the steady state probability density functions of PS lipids, shown in Fig. 2.6, A. The function (3.14) is represented by the solid line in Fig. 3.1, B, in comparison with the simulation data (open circles).

Interestingly, eq. (3.14) suggests that in the broad and physiologically relevant range of the concentration of monovalent PS lipids (10–50%), the effective translocating charge associated with the peptide diffusion does not change significantly and equals to $+0.5 \pm 0.05$ (per peptide residue). Surprisingly, since the effective charge Z does not depend on the concentration of the monovalent lipid, the velocity of the peptide according to the eq. (3.9) remains approximately constant, while the peptide drifts along the lipid gradient.

3.4 Results

Having derived the peptide drift velocity analytically using the mean-field approximation (eq. (3.9)) I compared it with the results of the MCA (Fig. 3.2). In a good agreement with eqs. (3.9) and (3.14), in the MCA the peptide drifts in the direction opposite to the lipid gradient with the velocity approximately proportional to D_p, λ and $\vec{\nabla}\rho(\vec{\mathbf{r}}^*)$.

However, to achieve the best fit between the simulation data and eq. (3.9) an empirical prefactor 0.353 (the velocity obtained in the simulations is smaller), identified with the least mean-square method, is required. Presumably, this

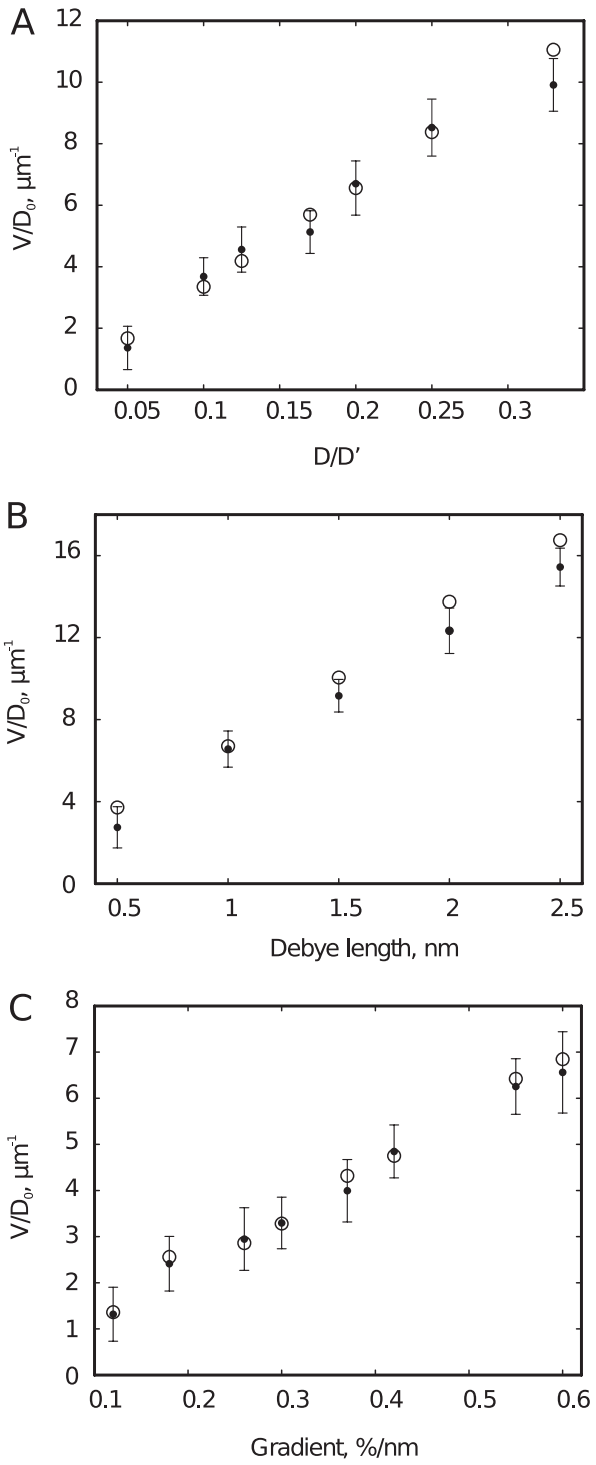

Figure 3.2: Peptide drift in the gradient of a monovalent lipid (from [62]). Dependence of the peptide velocity on the peptide diffusion coefficient (A), Debye length (B) and the magnitude of the lipid gradient (C). Simulation results (solid circles) are compared with the values predicted by eq. (3.9) (open circles). In (A), D_0 is as defined in subsection 2.1.6. When not otherwise shown in the figure, the peptide diffusion coefficient is $0.2D_0$ and the lipid gradient is 0.6%/nm.

velocity reduction is due to the effective friction associated with the lipid shell (forming only in the MCA). The details of the effective friction effect are described in the Appendix A.

To further validate the MCA, I also varied the charge of the peptide residues in the non-physiological range between +0.5 and +2.5. The resulting structure does not represent electrostatic properties of the Lys-5 peptide. However, as shown in Fig. 3.3, the peptide velocities observed in the MCA are in agreement with the prediction of eq. (3.9). In these simulations the effective charge Z is computed for each value of the residue charge from the MCA and then substituted into eq. (3.9).

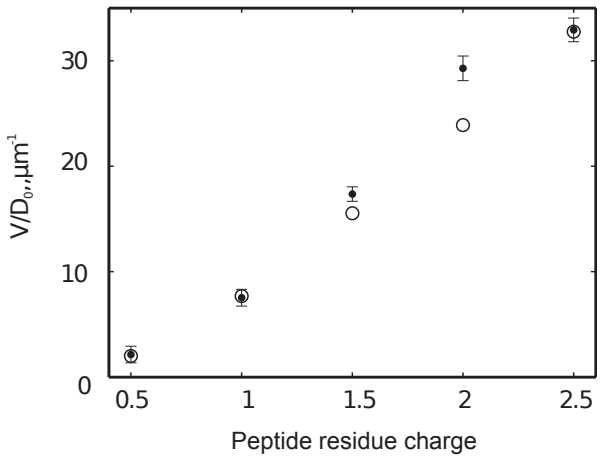

Figure 3.3: Peptide drift in the gradient of a monovalent lipid (from [62]). Dependence of the peptide velocity on the peptide residue charge. The peptide diffusion coefficient and the lipid gradient are $0.2D_0$ and 0.6%/nm, respectively. Simulation results (filled circles) are compared to the values predicted by eq. (3.9) (open circles).

Together with the results presented in Fig. 3.2, this demonstrates that the peptide drift observed in the MCA is fully consistent with the independently derived analytical eqs. (3.9) and (3.14).

Moreover, an additional validation of the MCA by comparison with another simulation technique has been performed (see Appendix B).

As mentioned above the MCA reproduces only about 30% of the velocity predicted by eq. (3.9), however, at the relevant biological conditions the value of the velocity obtained in the MCA is significant. For instance, at $D_p = 0.17D_0$

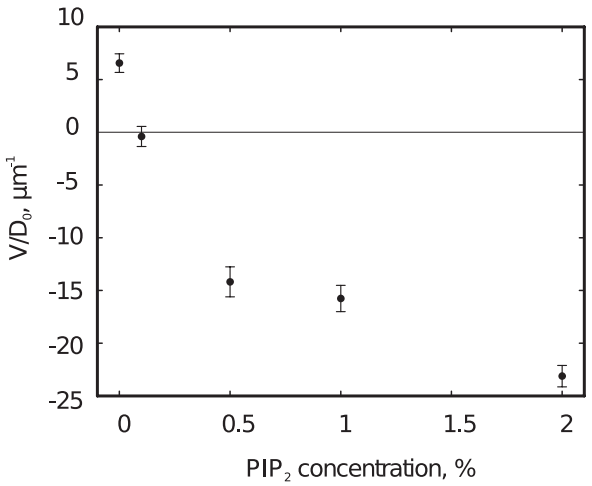

Figure 3.4: Peptide drift in the gradient of a monovalent lipid with a constant PIP_2 concentration (from [62]). Dependence of the peptide velocity on the PIP_2 concentration. The peptide diffusion coefficient is $0.2D_0$ and the PS lipid gradient is 0.6%/nm.

(if $D_0 = 1$ μm^2/s), Debye length $\lambda = 1$ nm and the gradient value 0.3 %/nm the expected velocity value is about 3 μm/s.

Addition of a small concentration of PIP_2 lipids to the membrane with a gradient of PS lipids has an interesting effect on the peptide dynamics. Fig. 3.4 shows that in the absence of PIP_2, as expected, the peptide drifts preferably to the area of a high PS density. However, upon addition of the negligible concentration of PIP_2 ($\sim$0.1%), the peptide becomes effectively electro-neutral and shows no systematic drift in either direction. Upon further addition of PIP_2 the peptide starts drifting in the opposite direction. Thus, PIP_2 lipids significantly change the peptide response to the PS gradient. This effect can be explained by the changes in the total peptide charge at different PIP_2 concentrations. As shown in Fig. 2.7 and Fig. 2.8, in the physiologically relevant PIP_2 range (0–1%), the number of molecules of PIP_2 that are bound to the peptide and, consequently, the total peptide charge change very steeply with the average PIP_2 concentration. Therefore, even a small change in the total membrane PIP_2 content, e.g. due to signal-induced production or degradation, could drastically change the microenvironment and the dynamics of proteins with polybasic domains.

CHAPTER 4

Continuous modeling of the membrane dynamics

The stochastic approach to the biophysical systems described in the previous chapters (Monte-Carlo simulations), due to a significant computational cost, can only be used when the number of particles N, involved in the simulation, is low. Moreover, to faithfully describe the system evolution it is necessary to take into account the interactions of all particles with each other. This detailed description does not allow to significantly increase the size of the system. As shown in the previous chapters, it is only possible to simulate the system behavior at the nano-scale. To simulate an evolution of the system at scales of several micrometers one has to turn to another modeling approximation which is computationally suitable for systems of this size. One particularly effective and commonly used approach is the continuous deterministic framework, which has been extensively used in earlier studies of membrane dynamics [34, 61]. This framework is only applicable to systems with a large number of particles N (comparable to $N_A = 6.02 \cdot 10^{23}$ 1/mol). The concentration of particles in such a system can be approximated by a continuous function. The behavior of this function is governed by initial conditions, system parameters and by a differential equation. Since the solution of any differential equation with fixed parameters is always determined by initial conditions, the framework is deterministic. The continuous deterministic

approach is very fast and computationally efficient, allowing one to work at big (micrometer) scales. The system of differential equations, which describes the behavior of all system components, can be derived from a stochastic description of the same system in the continuous (mean-field) limit, i.e. when N becomes infinitely large. In this case the system noise vanishes, since relative fluctuations typically decrease as $\sqrt{N}$ ($\lim_{N\to\infty} \sqrt{N}/N = 0$).

To extend the model of peptide-membrane dynamics to larger scales I will use such a continuous deterministic approach. Below I describe how the continuous model (CM abbreviation is used throughout the text) of the system is constructed and implemented.

4.1 Membrane model

The peptide-membrane system is defined in the same way as in the MCA (chapter 2), except three major modifications. First, I assume that the lipids and the peptides diffuse in the same plane (membrane plane hereafter). This simplification is sensible due to the fact that in the mean-field approximation the particles can be infinitely close to each other. Second, instead of a single peptide, there is a large number of peptides in the CM, diffusing in the membrane plane. Finally, the membrane plane is not discretized as it was in the MCA, instead the number of lipids and peptides at any point of the plane is defined by their concentrations.

4.1.1 Membrane plane in the absence of peptides

First, I begin the construction of the CM with a description of the membrane plane in the absence of peptides. In this case the membrane plane consists of lipid head groups of 3 lipid species (PS, PIP_2 and PC) with corresponding concentrations c_i ($i \in [1, 3]$) and charges z_i. The cytoplasmic solution is chosen to be the same as was used in the MCA: 0.1 M of 1:1 electrolyte with concentrations of positive and negative ions n_+ and n_-, correspondingly. The concentrations of lipids and mobile ions are smooth functions of distance $\vec{\mathbf{r}}$ in a 2D space and

they are defined in every point of the membrane plane. The behavior of these functions is described by a system of differential equations. The equations are usually dictated by physical properties of the system. In order to derive them I use a universal thermodynamical approach. In this approach a free energy F of a closed system is introduced, which measures a "useful" work obtainable from the system at constant temperature and volume. I assume that the system has a constant volume and is in thermodynamic equilibrium with a heat bath at absolute temperature $T = 298$ K. To obtain the mean-field approximation of the system one has to minimize F [79]. Minimization of F provides important thermodynamical characteristics of the system, such as electro-chemical potentials and distributions of system components. Based on these characteristics one can derive a system of differential equations, which describes the behavior of all components.

4.1.2 Free energy

I start with the definition of a free energy. In thermodynamics a free energy (or Helmholtz free energy) of a closed system at temperature T and volume V is defined as follows:

$$F = U - TS \tag{4.1}$$

where U is the internal energy of the system, T is the absolute temperature (in Kelvin) and S is the entropy of the system. Alternatively, the free energy can be represented by means of a free energy density:

$$F = \int_V f dv = \int_V (u - Ts) dv \tag{4.2}$$

where u and s are an internal energy density and an entropy density, correspondingly. In contrast to the free energy F, the free energy density f is not an integral characteristics of the whole system, but instead it is defined at every point $\vec{\mathbf{r}}$ of the membrane. I will use f for deriving an expression of the free energy F.

4.1.3 Entropy density

I begin a detailed description of the free energy (4.2) with the definition of the entropy (or entropy density). Entropy density is an essential property of any system and it reflects the number of ways in which a system may be arranged. Alternatively, it is a measure of disorder in the system. In order to find an analytical expression of the entropy density I use a statistical mechanics approach. Statistical mechanics describes properties of particle ensembles under different conditions. To analyze the ensemble properties statistical mechanics provides a powerful tool: a partition function. The partition function is introduced to describe thermodynamic properties of a system in equilibrium. The key feature of the partition function is that most of thermodynamic properties of the system, such as the internal energy U, the free energy F or the entropy S can be expressed in terms of the partition function or its derivatives. To derive an expression of the entropy density I use a partition function of the so-called canonical ensemble [80]:

$$Z_N = \int \frac{d^{3N}p \;\; d^{3N}q}{N!h^{3N}} e^{-\beta \hat{H}(p,q)} \tag{4.3}$$

where p and q are momenta and coordinates of particles in the ensemble, N is the total number of particles in the ensemble, $\hat{H}$ is a Hamiltonian of the ensemble, h is a constant of the dimension of momentum×distance (Planck's constant) and $\beta = 1/(k_B T)$, k_B is the Boltzmann's constant.

The partition function shows the volume in (p, q) space, occupied by the ensemble. The pre-exponent term in eq. (4.3) defines the total number of states in (p, q) space, available for the ensemble to occupy. $1/N!$ factor in this term is the so-called "correct Boltzmann counting" factor. It was introduced by Gibb's to resolve Gibb's paradox. The paradox refers to the fact that without this factor in the partition function, the entropy of a closed system of two indistinguishable ideal gases decreases, which is in disagreement with the second law of thermodynamics.

The Hamiltonian $\hat{H}$ is, by definition, a total energy of the ensemble. It is

defined as a sum of kinetic and potential energies of all particles:

$$\hat{H} = \sum_{i=1}^{N} \frac{p_i^2}{2m} + \hat{U} \tag{4.4}$$

To define the analytical expression of the entropy density s I use eq. (4.3) and the definition of the entropy:

$$S = k_B \log(Z_N) \tag{4.5}$$

It is only possible to analytically compute S using eq. (4.5) if one neglects the potential energy (in the membrane plane I consider only electrostatic interactions between system particles) in the Hamiltonian $\hat{H}$. In this case the computed entropy is the translational entropy of an ideal gas of particles. This approximation is necessary due to the complications appearing in the exact calculations of the potential energy contributions to the partition function. This simplification in computing the entropy of a charged solution has been used in many other works and has been extensively validated [34, 35, 61]. Note that other approximations can be used to account for this issue [81].

Using eqs. (4.3) and (4.4) with $\hat{U} = 0$ and remembering the integral of the normal distribution ($\int e^{-\frac{x^2}{a}} dx = \sqrt{\pi a}$), the partition function can be written as:

$$\begin{aligned} Z_N &= \int \frac{d^{3N}p \;\; d^{3N}q}{N! h^{3N}} e^{-\beta \sum_{i=1}^{N} \frac{p_i^2}{2m}} = \\ &= \int e^{-\frac{p_1^2}{2mk_BT}} d^3p_1 \int e^{-\frac{p_2^2}{2mk_BT}} d^3p_2 \;\; ... \int e^{-\frac{p_N^2}{2mk_BT}} d^3p_N \int \frac{d^{3N}q}{N! h^{3N}} = \\ &= \frac{(2\pi m k_B T)^{\frac{3N}{2}}}{N! h^{3N}} \int d^{3N}q = \Big(\frac{2\pi m k_B T}{h^2}\Big)^{\frac{3N}{2}} \frac{V^N}{N!} = \frac{V^N}{V_0^N N!} \end{aligned} \tag{4.6}$$

where V_0 is a constant volume $V_0 = \left(\frac{2\pi m k_B T}{h^2}\right)^{-\frac{3}{2}} = \frac{1}{\lambda_r^3}$, λ_r is the thermal de Broglie wavelength and V is a physical volume occupied by the ensemble. Note that the kinetic energy of particles in the Hamiltonian $\hat{H}$ contributes only as a constant V_0 and does not provide any concentration dependence to the entropy.

Substituting eq. (4.6) in the entropy equation (4.5) one can obtain:

$$S = k_B \log\Big(\frac{V^N}{V_0^N N!}\Big) \tag{4.7}$$

After rearranging the expression under the logarithm in eq. (4.7), the entropy density $s = S/V$ will have the form:

$$s = k_B\Big(\frac{N}{V}\log\Big(\frac{V}{V_0}\Big) - \frac{1}{V}\log N!\Big) \tag{4.8}$$

Application of the Stirling's approximation for large N ($\log N! = N\log N - N + O(log(N))$) to the equation above yields:

$$\begin{aligned} s &= k_B\Big(\frac{N}{V}\log\Big(\frac{V}{V_0}\Big) - \frac{N}{V}\log N + \frac{N}{V}\Big) = \\ &= -k_B\Big(\frac{N}{V}\log\Big(\frac{NV_0}{V}\Big) - \frac{N}{V}\Big) \end{aligned} \tag{4.9}$$

So that (4.9) is equivalent to:

$$s = -k_B(\rho\log(\rho V_0) - \rho) \tag{4.10}$$

where ρ is a concentration of particles of the ensemble (in $1/\mathrm{m}^3$ units).

Eq. (4.10) provides an expression of the translational entropy density of the ensemble, which can be used to define a translation entropy density of each species in the membrane plane. Notice also that entropy is an extensive quantity [82], which means that the total entropy of the system is the sum of the entropies of all species. Thus, for the membrane plane under consideration, consisting of 3 lipid species and n_+ and n_- cytoplasmic ions, the entropy density will have the following form:

$$s = -k_B\Big(\sum_{i=1}^{3}(c_i\log(c_iV_0) - c_i) + n_+\log(n_+V_0) - n_+ + n_-\log(n_-V_0) - n_-\Big) \tag{4.11}$$

4.1.4 Internal energy density

The second term in the right hand side of the free energy F (4.2) is the internal energy density u. By definition, u is an average total energy density of the ensemble, consisting of the average kinetic and the average potential energy densities. Since for the membrane plane the kinetic energy density is already included in the entropy density s (see subsection 4.1.3), in u I consider only the contribution of the potential energy density. However, as described above (subsection 4.1.3), an exact analytical expression of the potential energy density cannot be obtained. To be able to calculate it, the mean-field approximation can be used [80]. In the mean field approximation particles do not interact directly with each other, instead each of them interacts with a mean potential field created by others. The potential is always defined up to a constant, therefore I assume that the value of the potential is 0 in the infinity.

By definition, in the mean field approximation the main part of the internal energy density u of a static electrical system, consisting of identical ions with charges q and the concentration ρ, is defined as a work, required to bring these ions from the infinity to given points, and can be written as: $u = q\rho\phi$, where ϕ is a value of the electrostatic potential at the given point.

If one introduces a non-dimensional electrostatic potential as follows:

$$\psi = \frac{e\phi}{k_B T} \tag{4.12}$$

where e is the electron charge, then the work u can be rewritten as:

$$u = k_B T z \rho \psi \tag{4.13}$$

where z is the valence of ions.

If one applies the mean field approximation to calculate the internal energy density u of the membrane plane, it will have the form:

$$u = k_B T \Big[\Big(\sum_{i=1}^{3} z_i c_i + n_+ - n_- \Big) \psi - \frac{\varepsilon}{8\pi k_B T} |\vec{\nabla}\phi|^2 - \mu_+ n_+ - \mu_- n_- \Big] \tag{4.14}$$

The first term in eq. (4.14) is the work (4.13) required to bring charged lipids and ions from the infinity to a given point of the membrane. The second additional term is the self-energy of the electric field (interaction of an ion with its own field [83]), ε is the dielectric constant of the solution. The last two terms couple the system to the bulk reservoir and represent energy contributions from chemical potentials (μ_+ and μ_-) of positive and negative ions [84].

After substituting the expression for the electrostatic potential ϕ (4.12) to the eq. (4.15) one can obtain the final form of the internal energy density:

$$u = k_B T\Big[\Big(\sum_{i=1}^{3} z_i c_i + n_+ - n_-\Big)\psi - \frac{\varepsilon k_B T}{8\pi e^2}|\vec{\nabla}\psi|^2 - \mu_+ n_+ - \mu_- n_-\Big] \qquad (4.15)$$

4.1.5 Membrane incompressibility

Lipid species perform diffusion in the membrane plane. The total concentration of the membrane at any point equals the sum of concentrations of all lipid species. Since lipids are tightly packed in the membrane, natural total membrane concentrations is approximately constant at any membrane point:

$$\sum_{i=1}^{3} c_i = C_m \qquad (4.16)$$

where C_m is the total membrane concentration.

To include this constraint in the model I introduce a term with a Lagrange multiplier to the free energy. It is a general approach for finding the maxima and the minima of a function with a constraint. The Lagrange multiplier α is a function of coordinates $\vec{\mathbf{r}}$. The term with α has the following form (similar to the approach described in [34]):

$$\int_V -\alpha\Big(\sum_{i=1}^{3} c_i - C_m\Big)dv \qquad (4.17)$$

Thus, combining eqs. (4.2), (4.11), (4.15) and (4.17) one can explicitly define

the free energy of the membrane system:

$$\frac{F}{k_BT} = \int_V \Big[\sum_{i=1}^{3} (c_i \log(c_i V_0) - c_i) + n_+ \log(n_+ V_0) - n_+ + n_- \log(n_- V_0) - n_- + \Big(\sum_{i=1}^{3} z_i c_i + n_+ - n_- \Big) \psi - \frac{\varepsilon k_B T}{8\pi e^2} |\vec{\nabla}\psi|^2 - \mu_+ n_+ - \mu_- n_- - \alpha \Big(\sum_{i=1}^{3} c_i - C_m \Big) \Big] dv \tag{4.18}$$

F can be then used to derive differential equations describing the dynamics of system components in the mean-field approximation.

4.1.6 Minimization of the free energy

The membrane plane consists of five components: three lipid species and two types of mobile ions. Any configuration of these molecules instantly creates the electrostatic potential in the system. However, the responses of these components to the changes in the electrostatic potential are not always instant. Lipid species are generally slow (due to the membrane packing) and their response time to any change in the electrostatic potential is much longer than the response time of mobile ions (they freely diffuse in the cytoplasm). Thus, it is sensible to assume that mobile ions are always equilibrated with the electrostatic potential. To require the minimum of the free energy to be achieved at all times of the dynamics, the free energy should be minimized with respect to the fastest variables – mobile ion concentrations and the electrostatic potential. Such a minimization provides the distributions of mobile ion concentrations and the equation for the electrostatic potential.

Minimization of the free energy with respect to any variable is equivalent to taking a functional derivative of F over this variable and making it equal to 0. The functional derivative is defined as follows. For a given F:

$$F = \int_V f(g, \vec{\nabla} g) dv \tag{4.19}$$

where f and g are functions of coordinates $\vec{\mathbf{r}}$, the functional derivative of F over

g is [85]:

$$\frac{\delta F}{\delta g} = \frac{\partial f}{\partial g} - \vec{\nabla}\Big(\frac{\partial f}{\partial \vec{\nabla} g}\Big) \tag{4.20}$$

Minimization of F (4.18) with respect to ψ thus leads to:

$$\Big(\sum_{i=1}^{3} z_i c_i + n_+ - n_-\Big) + \frac{\varepsilon k_B T}{4\pi e^2}\vec{\nabla}^2\psi = 0 \tag{4.21}$$

This is equivalent to Poisson equation for the electrostatic potential:

$$\vec{\nabla}^2\psi = -\frac{4\pi e^2}{\varepsilon k_B T}\Big(\sum_{i=1}^{3} z_i c_i + n_+ - n_-\Big) \tag{4.22}$$

Minimization of F (4.18) with respect to concentrations of mobile ions n_+ and n_- provides:

$$\begin{aligned} \log(n_+ V_0) + \psi - \mu_+ &= 0 \\ \log(n_- V_0) - \psi - \mu_- &= 0 \end{aligned} \tag{4.23}$$

This is equivalent to:

$$n_\pm = \frac{1}{V_0} e^{\mu_\pm \mp \psi} = n'_\pm e^{\mp\psi} \tag{4.24}$$

where $n'_\pm$ are constants.

I assume that concentrations of both types of mobile ions in the bulk cytoplasm are n_0. If electrostatic potential ψ at the infinity is chosen to be 0, then at the infinity constants $n'_\pm$ are equal to n_0 (see eq. (4.24) with $\psi = 0$). Thus ion concentrations in the vicinity of the membrane are distributed according to the Botzmann distribution:

$$n_\pm = n_0 e^{\mp\psi} \tag{4.25}$$

4.1.7 Poisson-Boltzmann equation

The Poisson equation (4.22), which I derived by the minimization of the free energy functional, can be also derived using Gauss's law [86]. Gauss's law relates

the distribution of electric charge to the resulting electric field. In SI units Gauss's law in its differential form is:

$$\vec{\nabla}.\vec{\mathbf{E}} = \frac{\rho}{\varepsilon\varepsilon_0} \tag{4.26}$$

where $\vec{\nabla}.\vec{\mathbf{E}}$ is the divergence of the electric field $\vec{\mathbf{E}}$, ρ is the charge density, ε is the dielectric constant of the solution and ε_0 is the vacuum permittivity. Taking into account that by definition $\vec{\mathbf{E}} = -\vec{\nabla}\phi$, where ϕ is the electrostatic potential, recalling $\rho = eN_A(\sum_{i=1}^{3} z_i c_i + n_+ - n_-)$, where e is the electron charge, concentrations c_i and $n_\pm$ are in M units and using eq. (4.12), eq. (4.26) will take the form:

$$\vec{\nabla}^2\psi = -\frac{e^2 N_A}{k_B T\varepsilon\varepsilon_0}\Big(\sum_{i=1}^{3} z_i c_i + n_+ - n_-\Big) \tag{4.27}$$

Notice that eq. (4.27) is equivalent to eq. (4.22) if one converts the latter from CGSE to SI units and presents concentrations in M.

Concentrations n_+ and n_- are distributed according to Boltzmann distribution (4.25). Substituting them to eq. (4.27) one can obtain:

$$\vec{\nabla}^2\psi = \frac{2e^2 n_0 N_A}{k_B T\varepsilon\varepsilon_0}\frac{e^{\psi} - e^{-\psi}}{2} - \frac{e^2 N_A}{k_B T\varepsilon\varepsilon_0}\sum_{i=1}^{3} z_i c_i \tag{4.28}$$

Eq. (4.28) is equivalent to the following equation:

$$\vec{\nabla}^2\psi = \frac{1}{\lambda^2}\sinh(\psi) - \frac{e^2 N_A}{k_B T\varepsilon\varepsilon_0}\sum_{i=1}^{3} z_i c_i \tag{4.29}$$

where $\lambda = \sqrt{\frac{k_B T\varepsilon\varepsilon_0}{2e^2 n_0 N_A}}$ is the Debye length of the cytoplasmic solution with ionic strength n_0 (by definition ionic strength $I = \frac{1}{2}\sum n_i z_i^2$ and in the membrane model system $I = \frac{n_0 + n_0}{2}$). Since the cytoplasm is assumed to be a 0.1 M of 1:1 electrolyte solution its Debye length $\lambda = 1$ nm. Note that the same Debye length is used in the MCA. Eq. (4.29) is known as the Poisson-Boltzmann equation.

4.1.8 Lipid dynamics equations

Having obtained the equations describing changes in n_+, n_- (4.25) and in ψ (4.29), in this section I derive the equations for the membrane lipids c_i. Since the

membrane lipids are slower than equilibrated mobile ions, the equations describing changes in lipid concentrations should be dynamic, i.e. should contain a time derivative. To find these equations I first derive the electrochemical potentials of the lipid species. By definition the electrochemical potential has the following form [80]:

$$\mu_i = \mu_i^0 + \frac{\partial F}{\partial N_i} \tag{4.30}$$

where N_i is the number of lipid species of type i, and μ_i^0 is the standard chemical potential of the i^{th} membrane lipid species. Substituting the free energy F (4.18) in eq. (4.30) one can obtain electrochemical potentials of lipids in the extended form:

$$\frac{\mu_i}{k_B T} = \frac{\mu_i^0}{k_B T} + \log(c_i V_0) + z_i \psi - \alpha \tag{4.31}$$

Generally, the electrochemical potential (4.31) is derived for an equilibrium state of the system. I assume that (4.31) is also valid at a transient system state while the system evolves to the equilibrium steady state. The gradient of the electrochemical potential then will have a form:

$$\frac{\vec{\nabla}\mu_i}{k_B T} = \frac{\vec{\nabla} c_i}{c_i} + z_i \vec{\nabla}\psi - \vec{\nabla}\alpha \tag{4.32}$$

I also assume that the flux of any lipid species depends only on the gradient of its chemical potential [87]. Thus, it can be written in the following form:

$$\vec{\mathbf{J_i}} = -D_i c_i \frac{\vec{\nabla}\mu_i}{k_B T} = -D_i(\vec{\nabla} c_i + z_i c_i \vec{\nabla}\psi - c_i \vec{\nabla}\alpha) \tag{4.33}$$

where D_i is a diffusion coefficient of the i^{th} lipid species.

The Lagrange multiplier α should be computed by applying the same constraint (4.16) on the system again. From the continuity equation for all lipid species:

$$\frac{\partial c_i}{\partial t} + \vec{\nabla}.\vec{\mathbf{J_i}} = 0 \tag{4.34}$$

one can find that the constraint (4.16) is equivalent to:

$$\sum_{i=1}^{3} \vec{\mathbf{J}}_{\mathbf{i}} = \text{const} \tag{4.35}$$

Since the sum of the fluxes at infinity should be equal to 0, I define the constant in eq. (4.35) as 0. Substitution of eq. (4.33) into eq. (4.35) yields:

$$\vec{\nabla}\alpha = \frac{\sum_{i=1}^{3} D_i \vec{\nabla} c_i + \vec{\nabla}\psi \sum_{i=1}^{3} D_i z_i c_i}{\sum_{i=1}^{3} D_i c_i} \tag{4.36}$$

Note that in some cases α cannot be explicitly found from (4.36), however, only $\vec{\nabla}\alpha$ is needed in the flux definition (4.33).

Combining eqs. (4.33), (4.36) for a flux and Lagrange multiplier and continuity eq. (4.34) one can obtain an equation describing the dynamics of the i^{th} lipid species in the membrane:

$$\frac{\partial c_i}{\partial t} = \vec{\nabla}\left(D_i \Big[\vec{\nabla} c_i + z_i c_i \vec{\nabla}\psi - c_i \frac{\sum_{j=1}^{3} D_j \vec{\nabla} c_j + \vec{\nabla}\psi \sum_{j=1}^{3} D_j z_j c_j}{\sum_{j=1}^{3} D_j c_j} \Big] \right) \tag{4.37}$$

After a rearrangement eq. (4.37) will have the following form:

$$\frac{\partial c_i}{\partial t} = \vec{\nabla}\left(D_i \Big[\Big(\vec{\nabla} c_i - c_i \frac{\sum_{j=1}^{3} D_j \vec{\nabla} c_j}{\sum_{j=1}^{3} D_j c_j} \Big) + c_i \vec{\nabla}\psi \Big(z_i - \frac{\sum_{j=1}^{3} D_j z_j c_j}{\sum_{j=1}^{3} D_j c_j} \Big) \Big] \right) \tag{4.38}$$

Note that any diffusion coefficient in eq. (4.38) can be a function of the lipid concentration c_i. The system of equations (4.38) completely describes the dynamics of lipids within a cytoplasmic ionic solution. Electrostatic potential can be calculated separately from eq. (4.29).

4.1.9 Comparison with Poisson-Botzmann-Nernst-Planck model

At small concentrations ($c_i \ll C_m$) negatively charged lipids in the membrane do not influence each others dynamics. Similarly, in the case of a binary PC/PS membrane, when only PS diffusion is considered explicitly (equivalent to the lipid

diffusion in the MCA), the dynamics of PS is not constrained. In these two cases it can be assumed that lipids diffuse freely without satisfying the condition of the membrane incompressibility (4.16). Mathematically it means that the Lagrange multiplier α equals 0. Thus, the general equation of lipid dynamics (4.38) (coupled with Poisson-Boltzmann equation (4.29)) transforms to:

$$\begin{aligned} \frac{\partial c_i}{\partial t} &= \vec{\nabla}(D_i \vec{\nabla} c_i + z_i c_i \vec{\nabla}\psi) \\ \vec{\nabla}^2 \psi &= \frac{1}{\lambda^2}\sinh(\psi) - \frac{e^2 N_A}{k_B T \varepsilon \varepsilon_0} \sum_{i=1}^{N} z_i c_i \end{aligned} \tag{4.39}$$

The system of equations (4.39) has the form of the Poisson-Boltzmann-Nernst-Planck (PBNP) system of equations [88]. It usually applies to the diffusion of ions in the electrolyte solution and it does not contain any cross-diffusion terms, i.e. the diffusion of a given lipid species in the system does not depend on the concentrations of others. In this sense the system of equations (4.38) is an extension of PBNP to a multicomponent system with non-negligible "solute" concentrations. Similar effects of the complication of PBNP due to system constraints are described in [89] and in [90]. Simplicity of the system (4.39) makes it possible to solve it numerically using known computational techniques (see section 5.3).

4.1.10 Lipid production and degradation

To create a heterogeneous distribution of negatively charged lipids (lipid gradients), similar to the gradient system used in the MCA, I introduce a production and a degradation of negatively charged lipids to the CM by means of chemical reactions. These reactions are implemented as an interconversion of one lipid species (charged/uncharged) to another (uncharged/charged), making the absolute values of both production and degradation equal:

$$K_i = \frac{\partial c_i}{\partial t} = \pm k_l \tag{4.40}$$

where "+" corresponds to the production, and "-" corresponds to the degradation.

Constant k_l (lipid interconversion intensity, LII, hereafter) can be defined by

comparison of the gradient value in the CM with the results obtained in the MCA. The gradients in the CM are maintained by the presence of sources and sinks of lipids on the membrane (see chapter 5.2).

4.2 Peptide species

After describing the membrane plane in the absence of the peptides, in this chapter I introduce peptide species to the system, add their contributions to the free energy and derive the differential equations of their dynamics on the membrane.

To define the peptide species I use the results of the MCA. They show (Fig. 2.10) that the membrane lipids demix and accumulate in the vicinity of a peptide, significantly changing its intrinsic (+5) charge. To introduce the mechanism of lipid accumulation on the peptide in the continuous limit I use a concept of peptide-lipid complexes (PLC hereafter). A PLC is a complex, consisting of a peptide and several lipids bound to it. Since there are 2 types of negatively charged lipids (PS and PIP_2) in the membrane plane and the number of lipids bound to the peptide is restricted to be less or equal 5, there can be 21 PLCs in the system. I will use the following notation throughout the text: $p_{i,j}$ is a concentration of an (i, j) complex, where i is the number of PIP_2 lipids and j is the number of PS lipids bound to the peptide (see Fig. 4.1). Similar to the MCA the total charge of a PLC is defined as (see subsection 2.2.1): $z_{i,j} = z_{0,0} + \sum_k z_k$, where $z_{0,0}$ is the intrinsic (+5) peptide charge and $\sum_k z_k$ is the total charge of lipids in the PLC.

It was hypothesized that any transition between PLCs in Fig. 4.1 can be described by a kinetic equation (see (4.41)–(4.46)). This assumption can be tested by constructing a system of kinetic equations between PLCs and validating its results against the MCA simulation data. I will call a transition between two complexes as a peptide transition reaction (equivalent to an ionic reaction in chemistry) and it will appear as $R^p_{i,j}$ in the mass-action equations of the complexes.

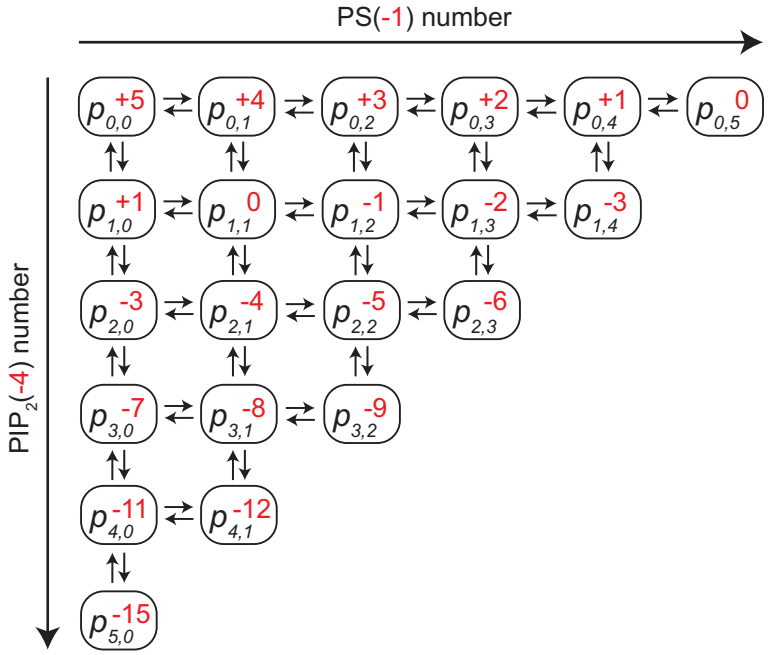

Figure 4.1: Transitions between the peptide complexes $p_{i,j}$ (black arrows) and their total charge (in red), depending on the number of PS and PIP_2 bound to the peptide.

4.2.1 Peptide transition reactions on binary membranes

As a simple case let us consider peptide transition reactions on binary membranes, consisting only of neutral PC and monovalent PS lipids (first row in Fig. 4.1). In this case the peptides can only sequester PS lipids and their charges vary from +5 to 0. One can distinguish between 6 different PLCs: $p_{0,0}$, $p_{0,1}$, $p_{0,2}$, $p_{0,3}$, $p_{0,4}$, $p_{0,5}$. Since I describe a transition between two complexes by a kinetic equation, one can define kinetic constants that determine the rate of the transition. Let $k_{i,j}$ be an association constant of PS with $p_{i,j}$ PLC and $h_{i,j}$ be a dissociation constant of PS from $p_{i,j}$ PLC. Based on the diagram in Fig. 4.1 one can write a system of equations that describes peptide transition reactions on a binary membrane as follows:

$$R^p_{0,0} = \frac{\partial p_{0,0}}{\partial t} = h_{0,1} \cdot p_{0,1} - k_{0,0} \cdot p_{0,0} \cdot c_1 \tag{4.41}$$

$$R^p_{0,1} = \frac{\partial p_{0,1}}{\partial t} = k_{0,0} \cdot p_{0,0} \cdot c_1 + h_{0,2} \cdot p_{0,2} - k_{0,1} \cdot p_{0,1} \cdot c_1 - h_{0,1} \cdot p_{0,1} \tag{4.42}$$

$$R^p_{0,2} = \frac{\partial p_{0,2}}{\partial t} = k_{0,1} \cdot p_{0,1} \cdot c_1 + h_{0,3} \cdot p_{0,3} - k_{0,2} \cdot p_{0,2} \cdot c_1 - h_{0,2} \cdot p_{0,2} \tag{4.43}$$

$$R^p_{0,3} = \frac{\partial p_{0,3}}{\partial t} = k_{0,2} \cdot p_{0,2} \cdot c_1 + h_{0,4} \cdot p_{0,4} - k_{0,3} \cdot p_{0,3} \cdot c_1 - h_{0,3} \cdot p_{0,3} \tag{4.44}$$

$$R^p_{0,4} = \frac{\partial p_{0,4}}{\partial t} = k_{0,3} \cdot p_{0,3} \cdot c_1 + h_{0,5} \cdot p_{0,5} - k_{0,4} \cdot p_{0,4} \cdot c_1 - h_{0,4} \cdot p_{0,4} \tag{4.45}$$

$$R^p_{0,5} = \frac{\partial p_{0,5}}{\partial t} = k_{0,4} \cdot p_{0,4} \cdot c_1 - h_{0,5} \cdot p_{0,5} \tag{4.46}$$

4.2.2 Limitations of the peptide transition model

If the concentration of PLCs is comparable with the concentration of lipids ($c_1 \sim p_{0,j}$) in the membrane then the following statements should be taken into account:

1. Sequestration of lipids on PLCs changes the concentration of free membrane lipids in accordance with equation:

$$R^l_1 = \frac{\partial c_1}{\partial t} = \sum_{j=1}^{5} h_{0,j} \cdot p_{0,j} - \sum_{j=0}^{4} k_{0,j} \cdot p_{0,j} \cdot c_1 \tag{4.47}$$

   Thus, R^l_1 should be added to the lipid diffusion equation (4.38).

2. Since the PLCs consist of both peptide and lipids, their concentrations should be explicitly added to the membrane incompressibility restriction (4.16), to account for the lipids belonging to the PLCs.

However, if one assumes that the concentration of PLCs is much smaller than the concentration of PS:

$$c_1 \gg p_{0,j} \tag{4.48}$$

then peptide transition reactions do not significantly change the PS concentration and, therefore, the concentration of monovalent PS lipids is constant during the time of equilibration of peptide transition reactions:

$$c_1 = \text{const} \tag{4.49}$$

In turn, if eq. (4.49) holds, then R_1^l equals 0 during the time of equilibration and membrane incompressibility restriction (4.16) does not have to be changed.

Since at relevant biological conditions eq. (4.48) is typically satisfied (see Appendix C), hereafter I solve the general system of equations (4.63) under the condition (4.48)

4.2.3 Peptide transition reaction constants

Values of association and dissociation constants $k_{0,j}$ and $h_{0,j}$ (4.41)–(4.46) are defined by obtaining the best fit between the probability density functions of the PS-peptide association in the CM and in the MCA (Fig. 2.6). To obtain the probability density functions in the CM one has to solve the system of ordinary differential eqs. (4.41)–(4.46) numerically (this can also be done by using various software packages, e.g. Matlab) or analytically (subsection 5.3.2) on a uniform membrane.

To minimize the parameter space, available for defining $k_{0,j}$ and $h_{0,j}$, a preliminary estimation of how $k_{0,j}$ and $h_{0,j}$ depend on system variables can be done as follows. Since it has been shown in the MCA that the peptide residues interact with the membrane lipids independently (subsection 2.2.1), one can define the elementary association and dissociation constants of a PS lipid, interacting with the peptide residue – k_{PS} and h_{PS}, so that the total constants $k_{0,j}$ and $h_{0,j}$ are proportional to the elementary ones:

$$k_{0,j} \sim k_{PS}; \qquad h_{0,j} \sim h_{PS}; \tag{4.50}$$

Additionally, the probability of the PS-PLC association, according to the combinatoric rules, is proportional to the number of vacant (not bound to a PS lipids) PLC residues and equals 0, when the PLC is fully occupied by PS. Analogously, the probability of the PS dissociation from the PLC is proportional to the number of occupied (bound to a PS lipids) PLC residues and equals 0, when the PLC is free of PS. Since the number of vacant positions is defined by the charge of the PLC ($z_{0,j}$), the arguments above can be include in the eq. (4.50)

as follows:

$$k_{0,j} \sim \frac{z_{0,j}}{z_{0,0}} k_{PS}; \qquad h_{0,j} \sim \Big(1 - \frac{z_{0,j}}{z_{0,0}}\Big) h_{PS}; \tag{4.51}$$

Finally, in the MCA the dissociation of PS from the peptide leads to a Kawasaki swap between the negatively charged PS and neutral PC, so that the PC occupies the position directly underneath the peptide residue, instead of the PS. In the case of the membrane fully occupied by PS (without PC lipids) the dissociation of the PS lipid from the peptide residues is impossible, since the Kawasaki swap of the lipids does not change the system configuration, making all peptide residues always occupied by PS lipids. To implement this phenomenon in the CM I assume that the dissociation constant $h_{0,j}$ is proportional to the concentration of neutral PC lipids (c_3) in the membrane plane. This assumption automatically vanishes $h_{0,j}$ if the concentration of PC is 0. Thus, the final forms of $k_{0,j}$ and $h_{0,j}$ are the following:

$$k_{0,j} = \frac{z_{0,j}}{z_{0,0}} k_{PS}; \qquad h_{0,0} = \Big(1 - \frac{z_{0,j}}{z_{0,0}}\Big) \frac{c_3}{C_m} h_{PS}; \tag{4.52}$$

The elementary constant h_{PS} can be estimated from the averaged association time τ of PS with the peptide (Fig. 2.9), obtained in the MCA. On the binary membrane τ does not significantly change with the PC concentration and is about 10 iteration steps. Since the "real" time of one iteration step was defined as $\sim$0.1 μs (subsection 2.1.6) the "real" association time of PS with the peptide can be chosen as $\tau = 1$ μs. Assuming that the frequency of the dissociation events is normally distributed (mathematical analogy with a radioactive decay) the average dissociation constant h_{PS} should be inversely proportional to τ:

$$h_{PS} \sim \frac{1}{\tau} \approx 10^6 \ \ \frac{1}{\mathrm{s}} \tag{4.53}$$

I use this value of h_{PS} in the solution of the CM with the following initial conditions (estimated in the Appendix C): $p^0_{0,0} = 100$ μM and the membrane concentration of PS varies from 0.015 M (5% of C_m) to 0.09 M (30% of C_m). Solution of the system (4.41)–(4.46) provides values of PLCs concentrations, that are then normalized by the total peptide concentration $\sum_{j=0}^{5} p_{0,j} = p^0_{0,0}$. The

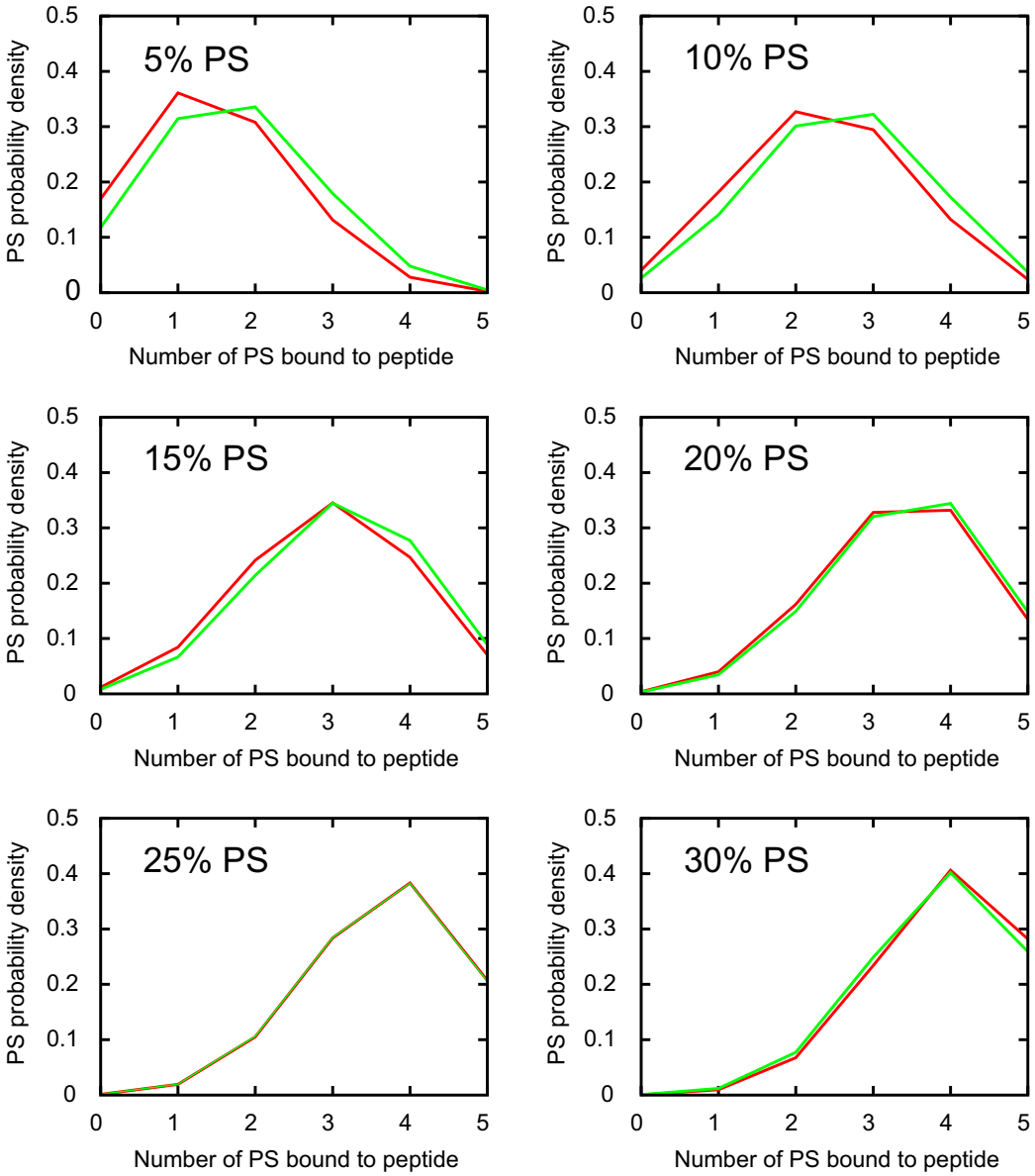

Figure 4.2: Probability densities functions of PS association with the peptides at various concentrations of PS on a homogeneous membrane. Red line - results of the CM, green line - results of the MCA.

best fit (Fig. 4.2) between the peptide occupation probabilities in the CM and in the MC simulations is achieved for $k_{PS} = 2.7{\cdot}10^7\ 1/(M \cdot s)$ (h_{PS} is defined in the eq. (4.53)), using the least mean-square method.

I use the values of $k_{0,j}$ and $h_{0,j}$, defined by eq. (4.52) with estimated values of k_{PS} and h_{PS}, everywhere throughout the calculations in the CM. Note that these constants are derived for a binary membrane only, consisting of neutral PC and monovalent PS lipids. Addition of PIP_2 lipids to the membrane plane with

the peptides requires recalculation of $k_{0,j}$ and $h_{0,j}$.

4.2.4 PLCs contributions to free energy and fluxes

In the CM it is assumed that the PLCs are located in the same plane as membrane lipids. As discussed above (see subchapter 4.2.2), under the assumption (4.48), the membrane incompressibility restriction (4.16) is not imposed on the PLC dynamics. Since PLCs diffuse in the membrane plane their entropic and internal energy contributions to the free energy will have the same forms as for lipids (eqs. (4.11) and (4.15)). Furthermore, the electrochemical potential of the PLCs also has the same form (4.31) except for the Lagrange multiplier:

$$\frac{\mu_{0,j}}{k_B T} = \frac{\mu^0_{0,j}}{k_B T} + \log p_{0,j} + z_{0,j}\psi \tag{4.54}$$

I assume that due to their low concentrations all PLCs diffuse freely and that there are no cross diffusion effects in their dynamics. Then Fick's first law is applicable to the PLCs and the flux of the j^{th} PLC is defined similar to (4.33):

$$\vec{\mathbf{J}}_{0,j} = -D_{0,j}(\vec{\nabla} p_{0,j} + z_{0,j} p_{0,j} \vec{\nabla}\psi) \tag{4.55}$$

4.2.5 Average total and effective charges of the peptides

If all PLCs have the same diffusion coefficients D^p, then eq. (4.55) allows one to calculate the total average electro-flux (considering only the part with the electrostatic potential ψ) of the peptides on the membrane:

$$\vec{\mathbf{J}}_{tot} = \sum_{j=0}^{5} \vec{\mathbf{J}}_{0,j} = -D^p \sum_{j=0}^{5} z_{0,j} p_{0,j} \vec{\nabla}\psi \tag{4.56}$$

The sum $\sum_{j=0}^{5} z_{0,j} p_{0,j}$ in the eq. (4.56), normalized by the total peptide concentration $P_{tot} = \sum_{j=0}^{5} p_{0,j}$, is equivalent to the total peptide charge obtained in the MCA (Fig. 2.8):

$$Z_{tot} = \frac{\sum_{j=0}^{5} z_{0,j} p_{0,j}}{P_{tot}} \tag{4.57}$$

Solution of the system (4.41)–(4.46) (see subsection (4.2.3)) on the membrane

with different PS compositions provides the dependence of Z_{tot} (4.57) on the membrane concentration of PS. Comparison of the total average charge of the peptides in the CM and in the MCA (Fig. 4.3) shows that the peptide transition reaction system (4.41)–(4.46) faithfully describes the reduction of the peptide total charge with the lipid membrane concentration and is in agreement with the MCA results. Note that fig. 4.3 is similar to fig. 3.1.

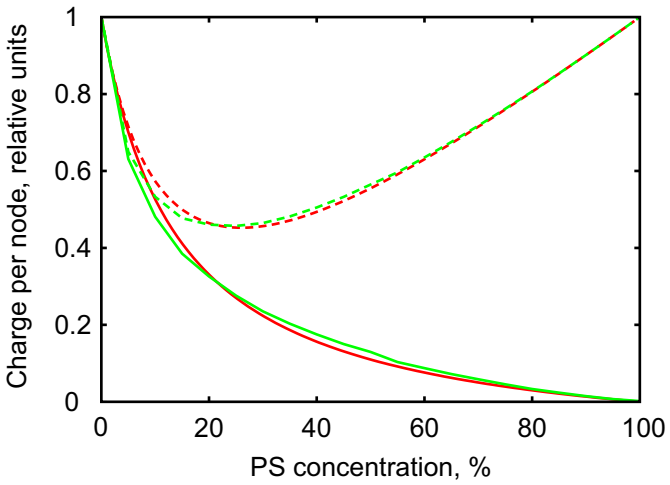

Figure 4.3: Average total and effective charges of the peptides in the CM (red) and in the MCA (green). Solid lines correspond to the total charges, dashed lines correspond to the effective charges.

However, as it was shown in the MCA, the velocity of the peptide on a gradient of monovalent lipids is determined not by the total peptide charge, but by the effective charge associated with the translocating peptide (chapter 3.3), which has the following form (per one peptide residue, eq. (3.14)):

$$Z^{\text{eff}} = 1 - p(\rho) + p(\rho) \cdot \rho \tag{4.58}$$

where ρ is a molar fraction of PS and $p(\rho)$ is the probability of the peptide residue being associated with PS.

In a similar way, in the CM the effective charge can be defined for each PLC. Since $1 - p(\rho)$ is equivalent to the charge of the PLC ($z_{0,j}$) and the probability of association of the peptide residue with PS, $p(\rho)$, is equivalent to the number of the free residues in the PLC ($5 - z_{0,j}$), the effective PLC charge has the following

form:

$$z_{0,j}^{\text{eff}} = z_{0,j} + (5 - z_{0,j})\rho \tag{4.59}$$

Thus, the effective average electro-flux of the peptides on the membrane (similar to the eq. (4.56)) has the following form:

$$\vec{\mathbf{J}}_{tot} = -D^p \sum_{j=0}^{5} \Big(z_{0,j} + (5 - z_{0,j}) \frac{c_1}{C_m} \Big) p_{0,j} \vec{\nabla}\psi \tag{4.60}$$

where c_1 is the PS concentration and C_m is the total concentration of the membrane plane. Therefore the average effective charge of the peptides can be written as:

$$Z^{\text{eff}} = \frac{\sum_{j=0}^{5} \big(z_{0,j} + (5 - z_{0,j}) \frac{c_1}{C_m} \big) p_{0,j}}{P_{tot}} \tag{4.61}$$

Again, solution of the system (4.41)–(4.46) on the membrane with different PS compositions provides the dependence of Z^{eff} (4.61) on the membrane concentration of PS. Comparison of the two approaches (Fig. 4.3) shows that the correction (4.59) of the PLC charge in the CM effectively accounts for the growth of Z^{eff} at high PS concentrations, obtained in MCA, and that both approaches are in a good agreement.

I include the correction (4.59) in the CM calculations. Thus, adding this correction in the equation of the PLC flux (4.55) and using the continuity equation (4.34), one can define a diffusion equation describing the dynamics of PLCs on the membrane:

$$\frac{\partial p_{0,j}}{\partial t} = \vec{\nabla} \Big(D_{0,j} \Big[\vec{\nabla} p_{0,j} + \Big(z_{0,j} + (5 - z_{0,j}) \frac{c_1}{C_m} \Big) p_{0,j} \vec{\nabla}\psi \Big] \Big) \tag{4.62}$$

4.2.6 General form of membrane dynamics equations

Combining together eq. (4.38) with interconversion terms K_i (eq. (4.40)) for lipid dynamics, eq. (4.62) with peptide transition reactions $R_{0,j}^p$ (eqs. (4.41)–(4.46)) and assumption (4.48) for small concentration of PLCs, and Poisson-Boltzmann equation (4.29) with an additional term for PLCs (similar to the term describing lipid contribution – see subsection 4.2.4), one can write a general

form of diffusion equations describing the spatio-temporal dynamics of lipids and PLCs on the binary membranes:

$$\begin{aligned}
\frac{\partial c_i}{\partial t} &= \vec{\nabla}\left(D_i\Big[\Big(\vec{\nabla}c_i - c_i\frac{\sum_{j=1}^{3} D_j\vec{\nabla}c_j}{\sum_{j=1}^{3} D_j c_j}\Big) + c_i\vec{\nabla}\psi\Big(z_i - \frac{\sum_{j=1}^{3} D_j z_j c_j}{\sum_{j=1}^{3} D_j c_j}\Big)\Big]\right) + K_i \\
\frac{\partial p_{0,j}}{\partial t} &= \vec{\nabla}\Big(D_{0,j}\Big[\vec{\nabla}p_{0,j} + \Big(z_{0,j} + (5 - z_{0,j})\frac{c_1}{C_m}\Big)p_{0,j}\vec{\nabla}\psi\Big]\Big) + R^p_{0,j} \\
\vec{\nabla}^2\psi &= \frac{1}{\lambda^2}\sinh(\psi) - \frac{e^2 N_A}{k_B T\varepsilon\varepsilon_0}\sum_{i=1}^{3} z_i c_i - \frac{e^2 N_A}{k_B T\varepsilon\varepsilon_0}\sum_{j=0}^{5} z_{0,j}p_{0,j}
\end{aligned} \tag{4.63}$$

CHAPTER 5

Comparison of the CM with the MCA

To test and validate the system of differential equations (4.63) I compare its solutions at different initial and boundary conditions with the results of MCA simulations. In this chapter I first describe the implementations of the CM and the MCA, that are used for the comparison. Second, I discuss the approximations, where the system (4.63) can be solved numerically, and provide some efficient numerical methods that can be used. Finally, I present the comparison of the CM and the MCA approaches in a number of biophysical situations.

5.1 MCA description

To be able to compare the CM and the MCA models, I modified the MCA by explicit consideration of the diffusion of all lipid species in the membrane (in the CM all lipid species undergo lateral diffusion). However, otherwise the MCA has the same characteristics, described in the chapter 2.

To compute the probability distribution of the peptide on the membrane, the peptide is initially put in the middle of the lattice and then is allowed to undergo $5 \cdot 10^6$ diffusion steps. The position of the peptide at every step is collected. Using averaging over the lattice size and over the number of iterations

the peptide probability distribution is calculated. Additional averaging of the probability distribution over 10 peptide trajectories is also performed. To be able to calculate an energy change corresponding to one peptide movement, the peptide hexagon (dashed line in Fig. 2.5) is not allowed to approach the lattice boundaries closer than 3 lipid distances.

5.2 General solution of the CM using FlexPDE

To solve the general system of membrane dynamics equations (4.63) I take advantage of a commercial software FlexPDE, which is often used for obtaining numerical solutions to partial differential equations. It is based on the Finite Element Method [91].

In the general case the system (4.63) should be solved in a 2D membrane domain. However, since the lipid and peptide distributions in the MCA can be averaged along one dimension, the MCA can be considered as a 1D system. Therefore, for simplicity, in the CM I solve the system (4.63) in 1D. However, in the other situations (when the lipid and the peptide profiles in the MCA are more complicated) solution of the system (4.63) has to be obtained in 2D.

To adjust an accuracy of the solution I define the following parameters required by FlexPDE:

1. Tolerance: ERRLIM = 0.001 (default value);

2. Number of mesh points: NGRID = 100 (initial value) – FlexPDE adjusts it automatically during the calculation;

Boundary conditions are defined explicitly in FlexPDE. In the CM I use two types of boundary conditions: zero flux boundary condition (corresponding to the zero flux of a particular species through the boundary) or fixed value boundary conditions (corresponding to a specific value of concentration at the boundary).

The CM equivalent of the lipid production rate in the MCA are the interconversion terms (LIIs) introduced in subsection 4.1.10. In FlexPDE the interconversion is created by means of a smooth step function (SWAGE) at one of the membrane boundaries.

5.3 Numerical solution of the simplified CM

In the case of small concentrations of negatively charged lipids ($c_i \ll C_m$) or in the case of binary membrane (with neutral and charged species) when the diffusion of only charged lipids is explicitly considered, the general system of membrane equations (4.63) can be reduced to the system of Poisson-Boltzmann-Nernst-Planck equations (see subsection 4.1.9):

$$\begin{aligned}
\frac{\partial c_i}{\partial t} &= \vec{\nabla}\Big(D_i\Big[\vec{\nabla}c_i + z_i c_i \vec{\nabla}\psi\Big]\Big) + K_i \\
\frac{\partial p_{0,j}}{\partial t} &= \vec{\nabla}\Big(D_{0,j}\Big[\vec{\nabla}p_{0,j} + \Big(z_{0,j} + (5 - z_{0,j})\frac{c_1}{C_m}\Big)p_{0,j}\vec{\nabla}\psi\Big]\Big) + R^p_{0,j} \\
\vec{\nabla}^2\psi &= \frac{1}{\lambda^2}\sinh(\psi) - \frac{e^2 N_A}{k_B T \varepsilon\varepsilon_0}\sum_{i=1}^{3} z_i c_i - \frac{e^2 N_A}{k_B T \varepsilon\varepsilon_0}\sum_{j=0}^{5} z_{0,j} p_{0,j}
\end{aligned} \tag{5.1}$$

This system can be solved numerically using known computational techniques. Below I describe some efficient methods that can be used to solve it. I will describe numerical methods of solution of (5.1) in a more general 2D case, but if necessary they can be easily simplified to a 1D case.

In the numerical solution of (4.63) assumptions (4.48) and (4.49) are also used to exclude the impact of the PLCs to the PS membrane concentration.

5.3.1 Quasi steady state approximation

To choose a numerical method of solution of eqs. (5.1) it is necessary to estimate characteristic diffusion and reaction times of the system. If characteristic reaction times are much shorter than diffusion times, it is possible to separate the solution of reaction terms K_i and $R^p_{0,j}$ from the solution of diffusion terms and use an explicit method of solution. Otherwise, an implicit method should be used. As K_1 and K_2 are the constant LIIs, they do not depend on the concentration of any component in the system and can be separated from the diffusion part of the first equation in (5.1).

The characteristic diffusion time in 2D can be estimated as follows:

$$\tau_D = \frac{L^2}{4D} \tag{5.2}$$

where L is the characteristic size of the membrane domain and D is the diffusion coefficient of the membrane species. Using the following values: $L \sim 100$ nm and D=1 μm^2/s, I estimate the characteristic diffusion time as

$$\tau_D \approx 10^{-3} \text{ s} \tag{5.3}$$

Characteristic times of peptide transition reactions $R^p_{0,j}$ can be estimated using the values of the transition reaction constants (4.52):

$$\tau_R \sim \frac{1}{k_{PS} c_1} \approx \frac{1}{h_{PS}} = 10^{-6} \text{ s} \tag{5.4}$$

Comparing two characteristic times one can conclude:

$$\tau_D \gg \tau_R \tag{5.5}$$

Condition (5.5) means that the peptide diffusion and the peptide transition reactions occur on different time scales. Based on this fact, one can assume that the peptide transition reactions are always equilibrated (a quasi steady state approximation), regardless of the state of the PLCs, and their solution can be separated from the solution of the diffusion part of the peptide equation in (5.1). Thus, an explicit numerical method can be used to obtain the solution.

5.3.2 Analytical solution of peptide transition reactions

In the quasi steady state approximation (with assumptions (4.48) and (4.49)) described above the system of peptide transition reactions (4.41)–(4.46) can be solved (for its steady state) at every diffusion step. Mathematically, at the steady-state time derivatives of all components become 0. The steady state solution of the peptide transition equations (4.41)–(4.46) has the following form:

$$R^p_{0,j} = 0, \quad j \in [0; 5] \tag{5.6}$$

System (5.6) can be solved analytically:

$$p_{0,1} = \frac{k_{0,0}}{h_{0,1}} \cdot p_{0,0} \cdot c_1 = A_{0,1} \cdot p_{0,0} \cdot c_1 \tag{5.7}$$

$$p_{0,2} = \frac{k_{0,0}k_{0,1}}{h_{0,1}h_{0,2}} \cdot p_{0,0} \cdot c_1^2 = A_{0,2} \cdot p_{0,0} \cdot c_1^2 \tag{5.8}$$

$$p_{0,3} = \frac{k_{0,0}k_{0,1}k_{0,2}}{h_{0,1}h_{0,2}h_{0,3}} \cdot p_{0,0} \cdot c_1^3 = A_{0,3} \cdot p_{0,0} \cdot c_1^3 \tag{5.9}$$

$$p_{0,4} = \frac{k_{0,0}k_{0,1}k_{0,2}k_{0,3}}{h_{0,1}h_{0,2}h_{0,3}h_{0,4}} \cdot p_{0,0} \cdot c_1^4 = A_{0,4} \cdot p_{0,0} \cdot c_1^4 \tag{5.10}$$

$$p_{0,5} = \frac{k_{0,0}k_{0,1}k_{0,2}k_{0,3}k_{0,4}}{h_{0,1}h_{0,2}h_{0,3}h_{0,4}h_{0,5}} \cdot p_{0,0} \cdot c_1^5 = A_{0,5} \cdot p_{0,0} \cdot c_1^5 \tag{5.11}$$

In the system (5.7)–(5.11) concentrations of all PLCs are defined by means of the concentration of the free peptide, $p_{0,0}$, and the concentration of PS lipids, c_1. Thus, one can avoid the solution of all peptide equations in the system (5.1), except $p_{0,0}$, and find concentrations of other PLCs using eqs. (5.7)–(5.11).

5.3.3 Discretization of Nernst-Planck equation

As described in subsection 5.3.1, diffusion and reaction terms in the first two equation of the system (5.1) can be separately solved and explicit numerical method can be used to find the solution of the diffusion part. In this section I describe an efficient method of solution of the diffusion (Nernst-Planck) parts of these equations. First, I rewrite them in the following general form:

$$\frac{\partial c}{\partial t} = \vec{\nabla}[D(\vec{\nabla}c + zc\vec{\nabla}\psi)] \tag{5.12}$$

where c, D and z are correspondingly the concentration, the diffusion coefficient and the charge of any membrane species (lipids or peptides); ψ is the electrostatic potential. This equation represents a class of advection-diffusion equations and can be rewritten in the following form:

$$\begin{aligned} \frac{\partial c}{\partial t} &= \vec{\nabla}(D\vec{\nabla}c) - \vec{\nabla}(c\vec{\mathbf{v}}) \\ \vec{\mathbf{v}} &= -Dz\vec{\nabla}\psi \end{aligned} \tag{5.13}$$

To solve these equations numerically I use a novel explicit, accurate and efficient discretization scheme ("master equation discretization" or MED) proposed by R. Grima and T.J. Newman [92]. They have shown that this scheme is more accurate than commonly used simple Taylor expansion or the "upwind" schemes. They derive a general discretized form of eq. (5.13) in 1D (it can be used for solution of (5.1) in 1D). I use the same procedure to derive a discretized form of equation (5.13) in 2D. To obtain a general form of the equation suitable for MED one has to define two scalar functions f and g as follows:

$$\begin{aligned} D &= fg \\ \vec{\mathbf{v}} &= g\vec{\nabla}f - f\vec{\nabla}g \end{aligned} \tag{5.14}$$

If functions f and g are defined by (5.14), then, by direct differentiation, one can show that eq. (5.13) can be rewritten as:

$$\frac{\partial c}{\partial t} = f\vec{\nabla}^2(gc) - gc\vec{\nabla}^2 f \tag{5.15}$$

To satisfy the eqs. (5.14), the functions f and g can be chosen as follows:

$$f = D\exp(-\frac{z}{2}\psi) \tag{5.16}$$

$$g = \exp(\frac{z}{2}\psi) \tag{5.17}$$

If the membrane is a square mesh with the size of N nodes and spatial resolution h, then all functions in equation (5.15) can be projected on it (on the mesh). Using the five-point discretization scheme shown in Fig. 5.1, one can obtain the discretized form of equation (5.15) on the mesh:

$$\begin{aligned} \frac{c^{t+1}_{m,n} - c^t_{m,n}}{\tau} = & \\ = f^t_{m,n}\Big[\frac{g^t_{m-1,n}c^t_{m-1,n} + g^t_{m+1,n}c^t_{m+1,n}}{h^2} + & \\ + \frac{g^t_{m,n-1}c^t_{m,n-1} + g^t_{m,n+1}c^t_{m,n+1} - 4g^t_{m,n}c^t_{m,n}}{h^2}\Big] - & \\ - g^t_{m,n}c^t_{m,n}\frac{f^t_{m-1,n} + f^t_{m+1,n} + f^t_{m,n-1} + f^t_{m,n+1} - 4f^t_{m,n}}{h^2} & \end{aligned} \tag{5.18}$$

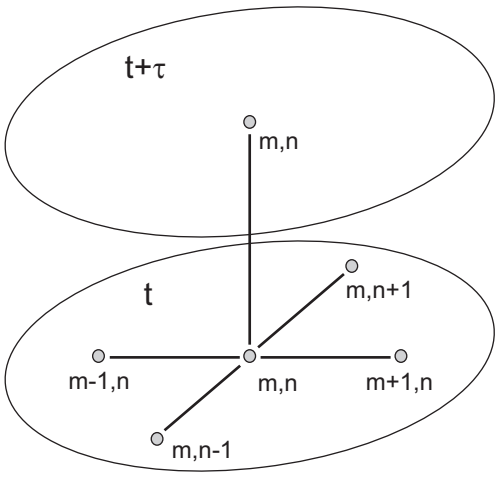

Figure 5.1: Numerical five-point scheme used in MED method. Five known points on the level t are used to calculate a new point on level $t + \tau$.

Equation (5.18) can be simplified to:

$$\begin{aligned} & c_{m,n}^{t+1} - c_{m,n}^{t} = \\ & = \frac{\tau}{h^2}\Big[c_{m-1,n}^{t}(f_{m,n}^{t} g_{m-1,n}^{t}) + c_{m+1,n}^{t}(f_{m,n}^{t} g_{m+1,n}^{t}) + \\ & + c_{m,n-1}^{t}(f_{m,n}^{t} g_{m,n-1}^{t}) + c_{m,n+1}^{t}(f_{m,n}^{t} g_{m,n+1}^{t}) - \\ & - c_{m,n}^{t} g_{m,n}^{t}(f_{m-1,n}^{t} + f_{m+1,n}^{t} + f_{m,n-1}^{t} + f_{m,n+1}^{t})\Big] \end{aligned} \tag{5.19}$$

Substituting functions f and g into equation (5.19), one can obtain the final form of the discretized equation:

$$\begin{aligned} & c_{m,n}^{t+1} - c_{m,n}^{t} = \\ & = \frac{D\tau}{h^2}\Big[c_{m-1,n}^{t} \exp(-\frac{z}{2}(\psi_{m,n}^{t} - \psi_{m-1,n}^{t})) + c_{m+1,n}^{t} \exp(-\frac{z}{2}(\psi_{m,n}^{t} - \psi_{m+1,n}^{t})) + \\ & + c_{m,n-1}^{t} \exp(-\frac{z}{2}(\psi_{m,n}^{t} - \psi_{m,n-1}^{t})) + c_{m,n+1}^{t} \exp(-\frac{z}{2}(\psi_{m,n}^{t} - \psi_{m,n+1}^{t})) - \\ & - c_{m,n}^{t}\Big(\exp(-\frac{z}{2}(\psi_{m-1,n}^{t} - \psi_{m,n}^{t})) + \exp(-\frac{z}{2}(\psi_{m+1,n}^{t} - \psi_{m,n}^{t})) + \\ & + \exp(-\frac{z}{2}(\psi_{m,n-1}^{t} - \psi_{m,n}^{t})) + \exp(-\frac{z}{2}(\psi_{m,n+1}^{t} - \psi_{m,n}^{t}))\Big)\Big] \end{aligned} \tag{5.20}$$

Using an iterative procedure this discretized equation can be used to find a solution of the original eq. (5.13). I have tested this discretization scheme in 2D and it was stable and accurate in the reasonable range of time steps and mesh

units, allowing to efficiently compute the solution of eq. (5.13).

5.3.4 Discretization of Poisson-Boltzmann equation

The last equation in the system (5.1) is the Poisson-Boltzmann equation. To solve this equation computationally I use Newton-Raphson iterative method [93,94], which has been shown to be accurate and efficient in solutions of different types of equations. This method works as follows. Assume that the following equation, which is equivalent to Poisson-Boltzmann equation in (5.1) has to be solved:

$$\Delta\psi = A\sinh\psi - f(c) \tag{5.21}$$

where ψ is the electrostatic potential, A is a constant and $f(c)$ is a function of concentrations of system components. One can define an iterative process of finding a solution of eq. (5.21) as:

$$\psi^{l+1} = \psi^l + \delta\psi \tag{5.22}$$

where ψ^{l+1} is an approximate solution of eq. (5.21) on $(l+1)$ iteration and $\delta\psi$ is an increment of the previous estimate of the solution ψ^l. Substitution of (5.22) to (5.21) provides:

$$\Delta\psi^l + \Delta(\delta\psi) = A\sinh(\psi^l + \delta\psi) - f(c) \tag{5.23}$$

For a small $\delta\psi$, $\sinh(\psi^l)$ can be linearized as follows:

$$\sinh(\psi^l + \delta\psi) = \sinh(\psi^l) + \sinh'(\psi^l)\delta\psi \tag{5.24}$$

Taking into account that $\sinh'(\psi^l) = \cosh(\psi^l)$, one can derive:

$$\Delta\psi^l + \Delta(\delta\psi) = A\sinh(\psi^l) + A\cosh(\psi^l)\delta\psi - f(c) \tag{5.25}$$

Rearranging of eq. (5.25) and utilizing eq. (5.22), one can obtain a general form of Newton-Raphson iterations for solution of the Poisson-Boltzmann

equation:

$$\Delta\psi^{l+1} - A\psi^{l+1}\cosh(\psi^l) = A\sinh(\psi^l) - A\psi^l\cosh(\psi^l) - f(c) \tag{5.26}$$

The original equation (5.21) is now reduced to a solution of a sequence of linear elliptic equations (5.26). Considering the same lattice as used in the solution of Nernst-Planck equation (see subsection 5.3.3) and the same discretization scheme (Fig. 5.1), one can define a discretized form of eq. (5.26) in 2D space:

$$\begin{aligned}\psi^{l+1}_{m+1,n} + \psi^{l+1}_{m-1,n} + \psi^{l+1}_{m,n+1} + \psi^{l+1}_{m,n-1} - (4 + h^2 A\cosh(\psi^l_{m,n}))\psi^{l+1}_{m,n} = \\ = h^2 A\sinh(\psi^l_{m,n}) - h^2 A\psi^l\cosh(\psi^l_{m,n}) - h^2 f(c)\end{aligned} \tag{5.27}$$

Simplification of eq. (5.27) yields:

$$\psi^{l+1}_{m+1,n} + \psi^{l+1}_{m-1,n} + \psi^{l+1}_{m,n+1} + \psi^{l+1}_{m,n-1} + d_{m,n}\psi^{l+1}_{m,n} = e_{m,n} \tag{5.28}$$

where

$$\begin{aligned}d_{m,n} &= -(4 + h^2 A\cosh(\psi^l_{m,n})) \\ e_{m,n} &= h^2 A\sinh(\psi^l_{m,n}) - h^2 A\psi^l\cosh(\psi^l_{m,n}) - h^2 f(c)\end{aligned} \tag{5.29}$$

Coefficients (5.29) are defined by means of known values of $\psi^l_{m,n}$ and $f(c)$. In order to solve eq. (5.28), one should rewrite it in an extended vector form:

$$\begin{pmatrix} b_1 & c_1 & 0 & 0 & \cdots & 0 & 0 & a_1 \\ a_2 & b_2 & c_2 & 0 & \cdots & 0 & 0 & 0 \\ 0 & a_3 & b_3 & c_3 & \cdots & 0 & 0 & 0 \\ \vdots & \vdots & \vdots & \vdots & \ddots & \vdots & \vdots & \vdots \\ 0 & 0 & 0 & 0 & \cdots & a_{N-1} & b_{N-1} & c_{N-1} \\ c_N & 0 & 0 & 0 & \cdots & 0 & a_N & b_N \end{pmatrix} \times \begin{pmatrix} \vec{\psi_1} \\ \vec{\psi_2} \\ \vec{\psi_3} \\ \vdots \\ \vec{\psi_{N-1}} \\ \vec{\psi_N} \end{pmatrix} = \begin{pmatrix} \vec{g_1} \\ \vec{g_2} \\ \vec{g_3} \\ \vdots \\ \vec{g_{N-1}} \\ \vec{g_N} \end{pmatrix} \tag{5.30}$$

where a_i, b_i and c_i are matrices of sizes $N \times N$; $\vec{\psi_i}$ and $\vec{g_i}$ are vectors of sizes N; N is a number of nodes in the discretized lattice. The forms of matrices a_i, b_i, c_i

and vectors $\vec{\psi_i}$, $\vec{g_i}$ depend on the boundary conditions imposed on the membrane system. In the general case of periodic boundary conditions at every boundary of the membrane, the matrices and vectors have the following structures:

$$a_i = c_i = \begin{pmatrix} 1 & 0 & 0 & \cdots & 0 & 0 \\ 0 & 1 & 0 & \cdots & 0 & 0 \\ 0 & 0 & 1 & \cdots & 0 & 0 \\ \vdots & \vdots & \vdots & \ddots & \vdots & \vdots \\ 0 & 0 & 0 & \cdots & 1 & 0 \\ 0 & 0 & 0 & \cdots & 0 & 1 \end{pmatrix} = I \tag{5.31}$$

$$b_i = \begin{pmatrix} d_{i,1} & 1 & 0 & 0 & \cdots & 0 & 0 & 1 \\ 1 & d_{i,2} & 1 & 0 & \cdots & 0 & 0 & 0 \\ 0 & 1 & d_{i,3} & 1 & \cdots & 0 & 0 & 0 \\ \vdots & \vdots & \vdots & \vdots & \ddots & \vdots & \vdots & \vdots \\ 0 & 0 & 0 & 0 & \cdots & 1 & d_{i,N-1} & 1 \\ 1 & 0 & 0 & 0 & \cdots & 0 & 1 & d_{i,N} \end{pmatrix} \tag{5.32}$$

$$\vec{\psi_i} = \begin{pmatrix} \psi_{i,1}^{l+1} \\ \psi_{i,2}^{l+1} \\ \psi_{i,3}^{l+1} \\ \vdots \\ \psi_{i,N-1}^{l+1} \\ \psi_{i,N}^{l+1} \end{pmatrix}; \quad \vec{g_i} = \begin{pmatrix} e_{i,1} \\ e_{i,2} \\ e_{i,3} \\ \vdots \\ e_{i,N-1} \\ e_{i,N} \end{pmatrix} \tag{5.33}$$

If one defines a matrix on the left hand side of eq. (5.30) as M, then solution of eq. (5.30) can be explicitly derived as follows:

$$\begin{pmatrix} \vec{\psi_1} \\ \vec{\psi_2} \\ \vec{\psi_3} \\ \vdots \\ \vec{\psi_{N-1}} \\ \vec{\psi_N} \end{pmatrix} = M^{-1} \begin{pmatrix} \vec{g_1} \\ \vec{g_2} \\ \vec{g_3} \\ \vdots \\ \vec{g_{N-1}} \\ \vec{g_N} \end{pmatrix} \tag{5.34}$$

This means that, to find the electrostatic potential in every point of the membrane at $(l+1)$ iteration, it is necessary to invert the matrix M and multiply it with the vector $\vec{g}$. Notice that both these values (on the right hand side of eq. (5.34)) are known and explicitly defined through the values of $d_{m,n}$ and $e_{m,n}$ (5.29).

Before reaching a steady state regime lipid and PLCs concentration profiles change with time. Consequently the electrostatic potential has to be constantly updated (it is created by the charged lipids and PLCs), i.e. Poisson-Boltzmann equation (or the inversion of the matrix M) has to be solved at every diffusion step. Thus, the complexity of the matrix inversion algorithm, used in the solution of Poisson-Boltzmann equation, is an important parameter, which defines the effectiveness of the total numerical method of solution of (5.1). Since the size of M is $N^2 \times N^2$, the numerical complexity of the general inversion procedure varies from $O(N^{4.5})$ to $O(N^6)$, depending on the algorithm. However, due to a specific structure of M (periodic block-tridiagonal) it is possible to reduce the complexity of the inversion to about $O(N^{3.5})$–$O(N^4)$, by applying algorithms developed for matrices with such structure [95, 96]. This complexity is minimal to obtain an exact analytical solution of eq. (5.30), however it is still computationally inefficient. To further reduce a complexity of matrix inversion the following simplified method can be used. Namely, instead of the general matrix inversion in 2D, the inversion in 1D (vertical columns or horizontal lines of the mesh) can be performed N times. The reduction of the system from 2D to 1D can be done by assuming that two values of the electrostatic potential in eq. (5.28) at $(l+1)^{\text{th}}$ iteration are known and equal to the values of the potential at l^{th} iteration (see Fig. 5.2). Under this assumption eq. (5.28) transforms to the following form:

$$\psi^{l+1}_{m,n+1} + \psi^{l+1}_{m,n-1} + d_{m,n}\psi^{l+1}_{m,n} = e^*_{m,n} \tag{5.35}$$

where

$$\begin{aligned} d_{m,n} &= -(4 + h^2 A \cosh(\psi^l_{m,n})) \\ e^*_{m,n} &= h^2 A \sinh(\psi^l_{m,n}) - h^2 A \psi^l \cosh(\psi^l_{m,n}) - h^2 f(c) - (\psi^l_{m-1,n} + \psi^l_{m,n}) \end{aligned} \tag{5.36}$$

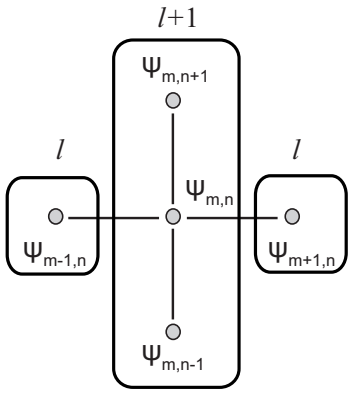

Figure 5.2: Dimension reduction in the general form of the discretized Poisson-Boltzmann equation. Two values of potential $\psi_{m-1,n}$ and $\psi_{m+1,n}$ are assumed to be known and equal the values of potential at the previous iteration. Three unknown values $\psi_{m,n-1}$, $\psi_{m,n}$ and $\psi_{m,n+1}$ then can be found at the next iteration in the reduced 1D dimension.

The advantage of system (5.35)–(5.36) over system (5.28)–(5.29) is that it has a reduced dimensional space – 1D. Matrix M' which has to be inverted in 1D case has a similar structure as matrix M in 2D, except its size is $N \times N$ and instead of matrices a_i, b_i and c_i it has parameters a_i^*, b_i^* and c_i^* with the following values:

$$a_i^* = c_i^* = 1; \quad b_i^* = d_{m,i}(\text{or } d_{i,n}, \text{ depending on the algorithm}) \tag{5.37}$$

In a general form (with periodic boundary conditions) the matrix M' is a periodic tridiagonal matrix. Inversion of this matrix can be done using a very efficient Thomas algorithm [97], the complexity of which is about $O(N)$. However, in this approximation Poisson-Boltzmann equation has to be solved N times in every row or every column of the lattice (to cover the whole lattice). Thus, the total complexity of this approximation method increases to about $O(N^2)$. However, this is still by one order of magnitude more efficient than calculation of an exact analytical solution in 2D space.

I've tested the stability and the accuracy of the simplified method and observed that it was stable in a large range of spatial mesh resolutions and it converged with accuracy of 10^{-8} in about 10 iterations. This method can be used for a solution of Poisson-Boltzmann equation in the system (5.1).

5.4 Importance of membrane incompressibility

To understand how important is the restriction of membrane incompressibility (4.16) in the description of the lipid dynamics I compared the steady state solutions of the general system of equations (4.63) solved in FlexPDE with the simplified PBNP system (5.1) (can be either solved in FlexPDE or using the numerical methods described in the section 5.3 above).

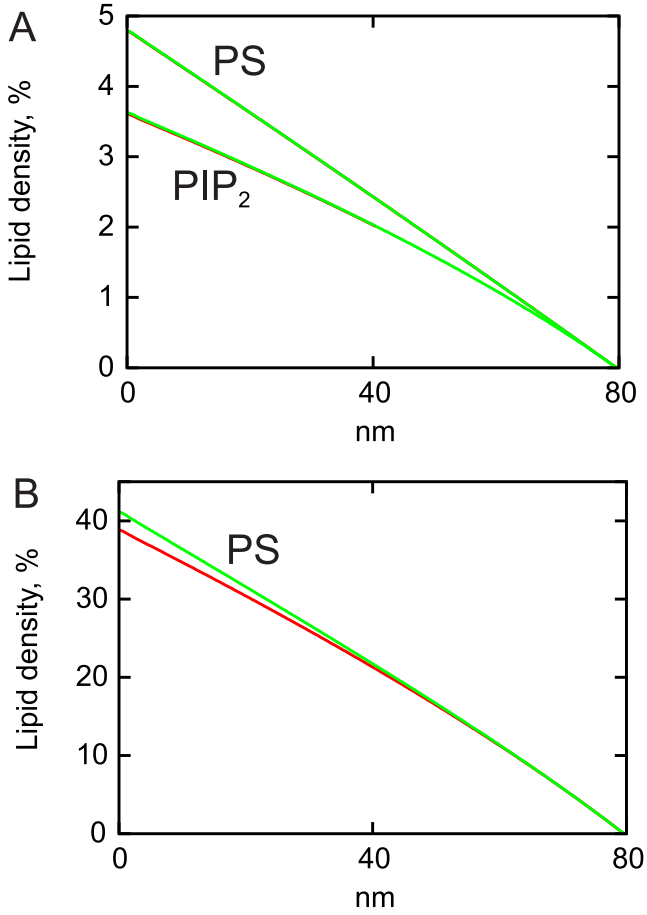

Figure 5.3: Comparison of general (4.63) and PBNP (5.1) systems. Results of the general system are shown in green, results of the PBNP are shown in red. (A) Small gradients of PS and PIP_2; (B) Large gradient of PS.

Fig. 5.3, A shows that as expected for the dilute concentrations of negatively charged lipids ($< 5\%$) discrepancy between two systems (4.63) and (5.1) is negligible and they provide identical results. At higher lipid densities ($\sim 40\%$) the two systems slightly diverge, however, the discrepancy between them is less than 5% (Fig. 5.3, B). Thus, potentially PBNP system can be used to describe the dynamics of lipids in the membrane plane in a large range of concentrations and

the membrane incompressibility restriction (4.16) can be neglected. However, in the systems with densely packed protein-lipid lattices (or with the protein concentrations comparable to the ones of lipids) this restriction in the extended form (including PLCs – see subsection 4.2.2) will become more pronounced and should be explicitly taken into account. Therefore, the general system (4.63) is a more powerful tool (compared to PBNP) which can be further extended to describe systems with different packaging properties.

5.5 Results

Comparison of the peptide occupations and average total and effective charges on the homogeneous membrane in the CM and in the MCA has already been demonstrated in subsections 4.2.3 and 4.2.5. In this section I use the solutions of the CM (obtained in FlexPDE) and the MCA to compare the two approaches for the membrane system with a lipid gradient.

First, I calculate the diffusion coefficients of all membrane lipid species in the MCA to utilized them in the CM. I also calibrate the LIIs of lipids, K_i (subsection 4.1.10), in the CM by comparing the two models in the neutral membrane system (the membrane is binary, but both lipid species are neutral). Second, I compare the two models using a single gradient system (the membrane is binary, one lipid species is neutral, the second lipid species is negatively charged, PS or PIP_2). Finally, I introduce the peptide species to the system and compare the values of the peptide probability distributions on the membrane.

5.5.1 Determination of parameters and calibration of CM

To determine lipid diffusion coefficients (D_i) in the CM, I measure them in the MCA for different membrane compositions. Figs. 5.4, 5.5 and 5.6 show the values of D_i, normalized by the maximal value of the lipid diffusion coefficient D_L in the uncharged membrane (subsection 2.1.6), for PC, PS and PIP_2 lipids, correspondingly. Note different vertical scales in the figures.

Since the obtained values of the lipid diffusion coefficients are discrete, in the

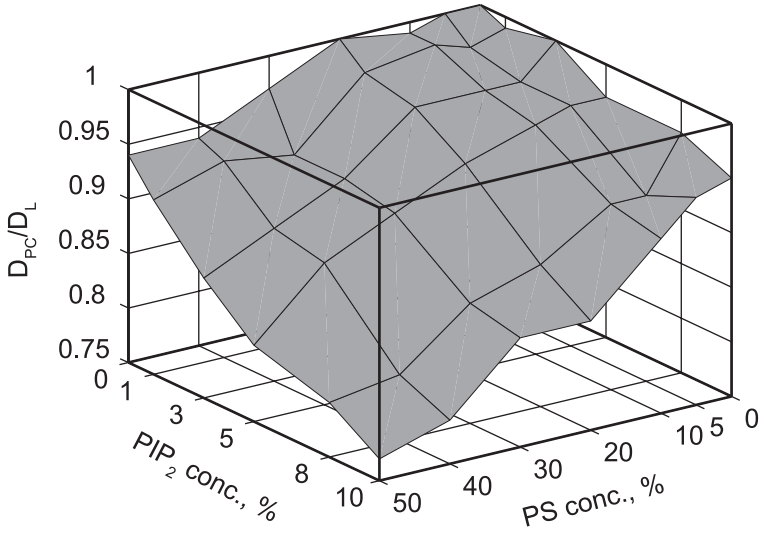

Figure 5.4: Dependence of PC diffusion coefficient, computed in the MCA, on the membrane composition.

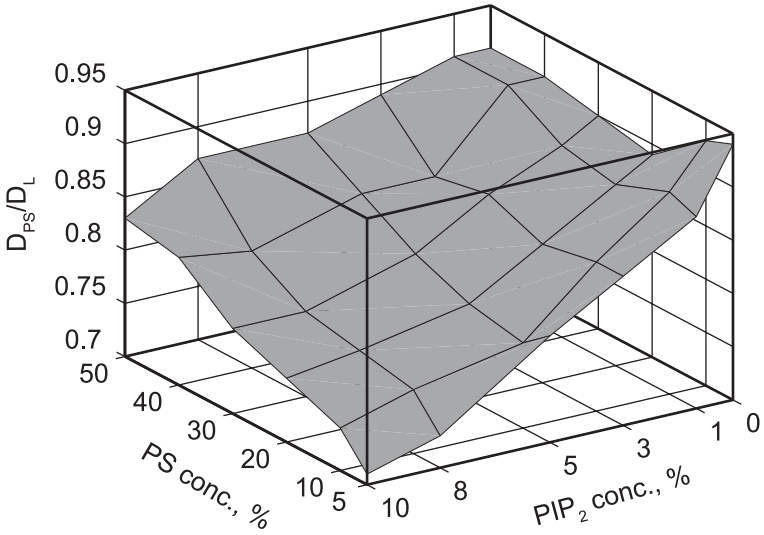

Figure 5.5: Dependence of PS diffusion coefficient, computed in the MCA, on the membrane composition.

CM I approximate them as best fits to the functions shown in Figs. 5.4, 5.5 and 5.6. To find the best fit I use polynomic and exponential functions, since FlexPDE software allows one to define complex functions as input parameters. Exact values of the diffusion coefficients that are used in the CM equations are the following:

$$D_1(\mathrm{PS}) = D_L\Big(\frac{1}{1+3.5\tilde{c_1}} + 3\tilde{c_1}\tilde{c_2}\Big) \tag{5.38}$$

$$D_2(\mathrm{PIP_2}) = D_L\Big(\frac{1}{1+18\tilde{c_1}} + 8\tilde{c_1}\tilde{c_2}\Big)(\exp\left(-3\tilde{c_2}\right) + 0.5\tilde{c_2}) \tag{5.39}$$

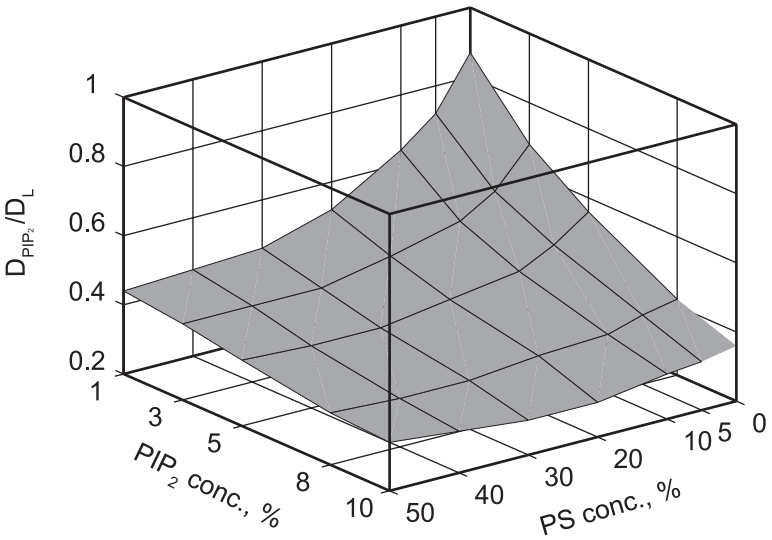

Figure 5.6: Dependence of PIP_2 diffusion coefficient, computed in the MCA, on the membrane composition.

$$D_3(\mathrm{PC}) = D_L\Big(1 - 3.5\tilde{c_1}\tilde{c_2} - 0.3\tilde{c_1} - 0.1\tilde{c_2}\Big) \tag{5.40}$$

where $\tilde{c_i}$, $i = 1, 2, 3$, are the concentrations of PS, PIP_2 and PC, correspondingly, normalized by the total membrane concentration C_m.

To calibrate the LIIs, K_i, in the CM I consider a system of a binary membrane with two identical neutral (PC) lipid species. A gradient of one species is created by the interconversion of lipids at one boundary. By obtaining the best fit of the CM steady state lipid profiles to the MCA simulation results (Fig. 5.7, A), the LII of neutral lipids, K_n, is defined. For the gradient of lipids with 5% peak value the LII is $K_n = 2.34$ M/s (K_1^0 hereafter) and for the gradient of lipids with 50% peak value the LII is $K_n = 10K_1^0 = 23.4$ M/s. The corresponding interconversion rates in the MCA are 0.05 lip/iteration and 0.5 lip/iteration, correspondingly. Thus, in both models, in the case of the neutral membrane system, the peak value of the gradient is directly proportional to the LII. All the values of LIIs, used in the following chapters, lie between K_1^0 and $10K_1^0$.

5.5.2 Lipid gradients on binary membrane

In this section I describe a comparison of the two approaches on the membrane with a single gradient of negatively charged lipids. Fig. 5.7, B, shows the comparison between the CM and the MCA for a system with a single PS gradient for

different values of LIIs. For the small LIIs, K_1^0 and $2.5 \cdot K_1^0$, when the peak value of the gradient is $< 20\%$, the two models provide almost identical results (Fig. 5.7, B and C). However, when the peak value of the gradient is about or more than 20% one can see an explicit deviation of the CM model from the MCA (Fig. 5.7, B). In the MCA automaton the peak value is always lower and the difference between the models grows with the density of negatively charged lipids. Presumably at high PS densities the mean-field approximations breaks down. The theory that can account for this effect is the so-called strong coupling theory [98, 99]. It postulates that highly charged systems are not governed by Poisson-Boltzmann theory (mean-field approximation). Instead, their behavior is better described by the so-called strong coupling limit, where ion-ion correlations are significant. For a system, consisting of a charged surface with a charge density σ and a bulk 1:1 electrolyte solution with ion charges $\pm q$ (similar to the membrane system), its regime can be defined using the Netz-Moreira electrostatic coupling parameter, Σ. This parameter represents a ratio between two characteristic length scales, the Bjerrum length (a typical distance at which two ions q interact with energy $k_B T$, see also eq. (3.8)):

$$l_B = \frac{e^2}{4\pi\varepsilon\varepsilon_0 k_B T} \tag{5.41}$$

where e is the electron charge, ε is the dielectric constant of the medium and ε_0 is the vacuum permittivity, and the Gouy-Chapman length (a typical distance at which a counterion q interacts with a charge surface σ):

$$\mu_{GC} = \frac{e}{2\pi q l_B \sigma} \tag{5.42}$$

So that Σ is defined as follows:

$$\Sigma = \frac{q^2 l_B}{\mu_{GC}} = 2\pi q^3 l_B^2 \frac{\sigma}{e} \tag{5.43}$$

Electrostatic coupling parameter Σ determines to what extent ion-ion interactions are prevalent over ion-surface interactions. When $\Sigma \ll 1$ the system is in the weak coupling regime (mean-field approximation). When $\Sigma \gg 1$ the regime

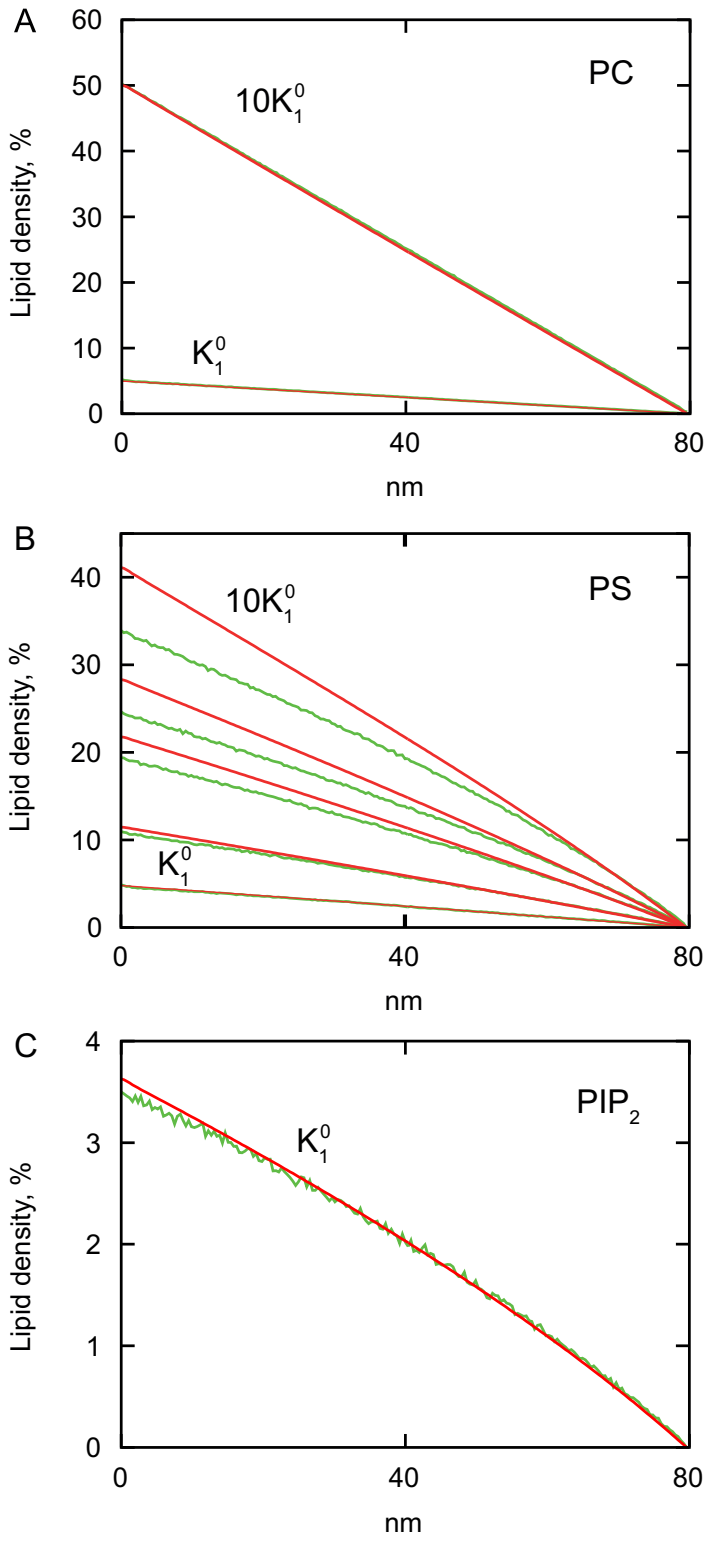

Figure 5.7: Comparison of MCA (green line) and CM (red line) for a single lipid gradient. (A) Gradients of PC in binary PC/PC membrane for two LIIs: K_1^0 and $10K_1^0$; (B) Gradients of PS in binary PS/PC membrane for several LIIs: K_1^0, $2.5K_1^0$, $5K_1^0$, $6.7K_1^0$ and $10K_1^0$; (C) A gradient of PIP_2 in binary PIP_2/PC membrane for the LII K_1^0.

switches to the strong coupling. Although, in (5.43) Σ is derived for a different system (a charged plane interacting with an ion), it can be used as a meaningful dimensionless control parameter in the membrane system. I use it to qualitatively analyze in which regime the membrane system performs.

The coupling parameter for the binary PC/PS membrane system can be estimated by taking $q = -1$ (PS head group charge), $l_B \sim 0.7$ nm (for two ions with -1 charge) and $\sigma/e = 0.34$ 1/nm^2 (for 20%PS, assuming that an average membrane area per lipid head group is 0.6 nm^2, see subsection 2.1.1). Thus, for the membrane system with 20% of PS the coupling parameter is $\Sigma \sim 1$, meaning that already at this modest density of charged monovalent lipids the system is out of the weak coupling limit and the mean-field approximation may not correctly describe lipid interactions.

Interestingly, in the case of binary membrane with one charged lipid species (PS) the CM can be corrected to account for the strong coupling effect without changing the form of equations (4.63). The following correction of PS charge allows the CM to faithfully reproduce the results of the MCA:

$$z_1^* = z_1(1 + \gamma \frac{c_1}{C_m}) \tag{5.44}$$

where γ is a constant.

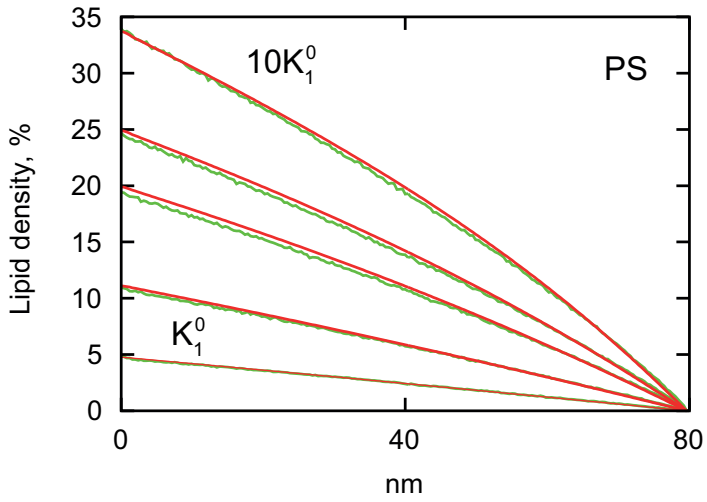

Figure 5.8: Comparison of the corrected CM (5.44), $\gamma = 2$ (red line) with the MCA (green line) for a single lipid gradient. Gradients of monovalent PS lipids on binary PS/PC membrane for several LIIs: K_1^0, $2.5K_1^0$, $5K_1^0$, $6.7K_1^0$ and $10K_1^0$

Fig. 5.8 shows the lipid profiles represented in Fig. 5.7, B after the PS charge correction (5.44) with $\gamma = 2$. For small gradients of PS (with less that 20% peak value) the correction (5.44) does not significantly change the lipid profile. Note that even though the charge correction (5.44) is purely hypothetical and does not have any physical justification, it can efficiently resolve the strong coupling effect in the CM in binary PS/PC membrane systems.

5.5.3 Lipid gradients on ternary membrane

In this section I compare the two approaches in the case when the membrane system is ternary, i.e. consists of three types of lipids: PC, PS and PIP_2. I extend the CM to see how negatively charged lipids with different charges influence each other in the membrane. In this system there is always a gradient of one charged lipid species (PS or PIP_2) and another charged species has zero flux boundary conditions and responds to the gradient by changing its uniform profile.

I begin the comparison with low lipid concentrations and do not use the correction (5.44) for the charge of negatively charged lipids. In Fig. 5.9, A, it is shown how a small gradient of PS lipids (with the LII K_1^0) change the profile of an initially uniform PIP_2. There is a small discrepancy in the PIP_2 profiles between the two models (Fig. 5.9, A). This effect presumably appears due to the large negative charge of PIP_2 lipids, so that the system quickly reaches the strong coupling limit of electrostatic interactions ($\Sigma \sim q^3$).

Secondly, I compare the two models in the case of high PS gradient (with the LII $10K_1^0$) (Fig. 5.9, B). Note that due to the high PS gradient, PIP_2 lipids are completely displaced from the left boundary of the lattice, so that the PS gradient profiles on the left boundary are similar to the ones in the single PS gradient case (see Fig. 5.7, B). At high PIP_2 initial uniform concentration of 5% (see Fig. 5.9, C) the discrepancy between the two models becomes larger, however, it is not surprising, since the value of Σ in this case should be much higher than at the low PIP_2 concentration (Fig. 5.9, A).

Finally, I investigate a reversed situation when a gradient of PIP_2 lipids influences a uniform profile of PS lipids (Fig. 5.10). Since biologically relevant PIP_2

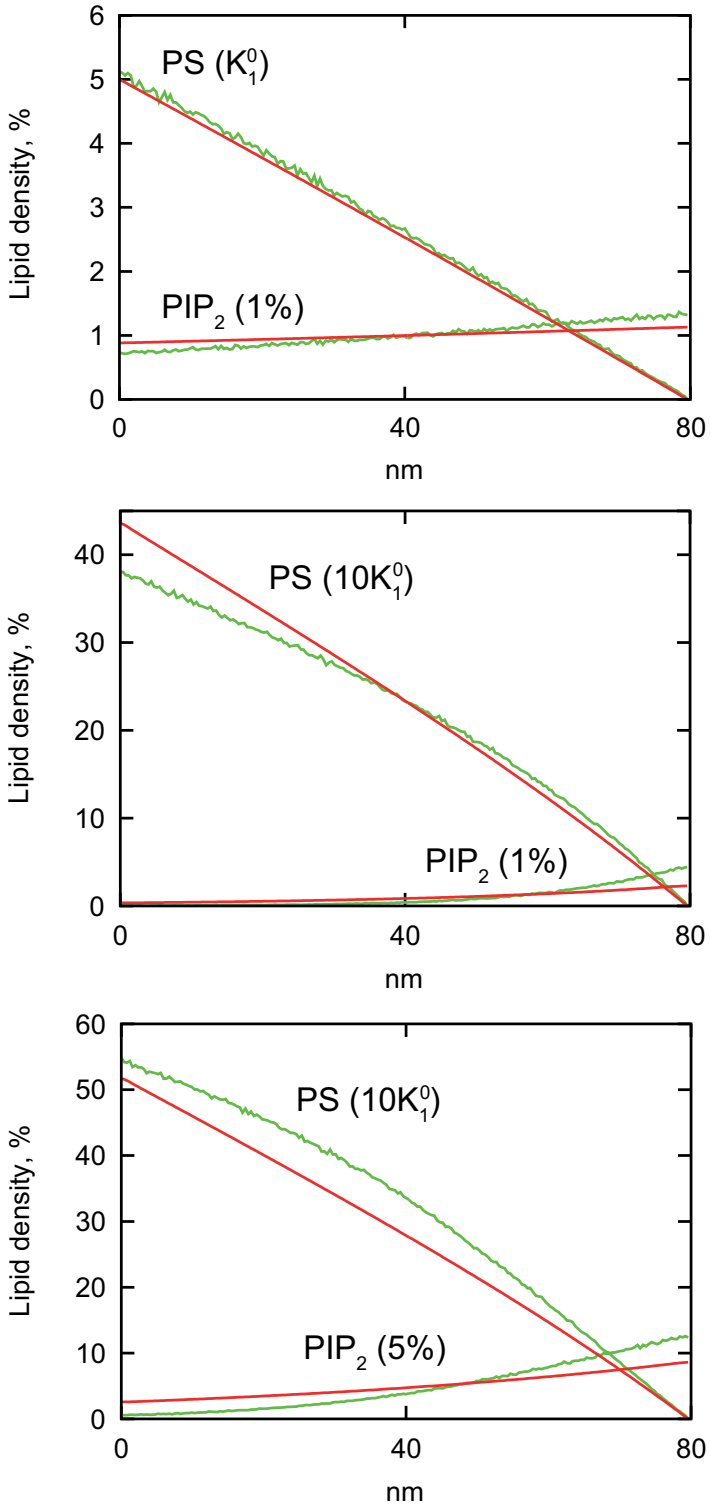

Figure 5.9: Comparison of the CM (red line) with the MCA (green line) for a PS gradient on a ternary membrane. A, LII of PS is K_1^0 and initial uniform PIP_2 concentration is 1%; B, LII of PS is $10K_1^0$ and initial uniform PIP_2 concentration is 1%; C, LII of PS is $10K_1^0$ and initial uniform PIP_2 concentration is 5%.

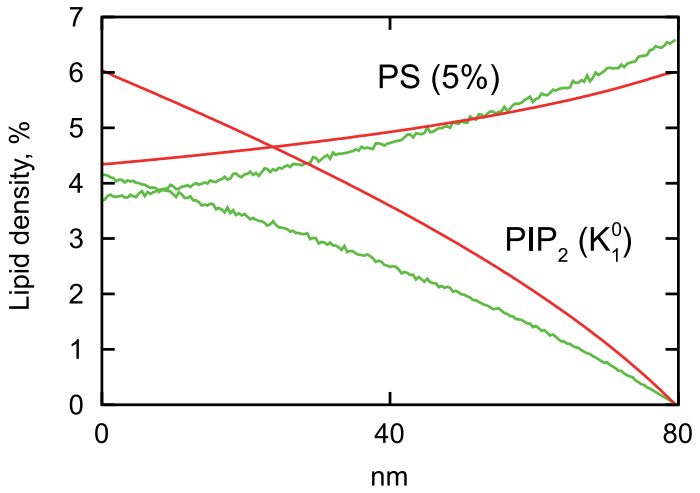

Figure 5.10: Comparison of the CM (red line) with the MCA (green line) for a with PIP_2 gradient on a ternary membrane. LII of PIP_2 is K_1^0 and initial uniform PS concentration is 5%;

concentrations do not exceed at most 10%, I use a small value of PIP_2 LII (K_1^0).

Figs. 5.9 and 5.10 show that, presumably in the mean field approximation used in the CM model, the contribution of multivalent PIP_2 molecules to the electrostatic potential is slightly underestimated. However, quantitatively (trends and functional dependencies) the two models are in a very good agreement.

5.5.4 Distribution profiles of PLCs on binary membrane

Having compared the CM and the MCA approaches in membrane systems with lipid gradients, it is also important to compare them in the presence of the Lys-5 peptide species. For this configuration in the MCA the probability distributions of the peptide on the membrane are calculated as described in section 5.1. Concentrations of PLCs in the CM model are calculated for zero-flux boundary conditions. Lipid boundary conditions are the same as in subsection 5.5.2. Diffusion coefficients of PLCs are chosen to be identical and equal to $D_p^0 = 1\ \mu\text{m}^2/\text{s}$ (the maximal lipid diffusion coefficient D_L, see subsection 2.1.6).

Fig. 5.11 shows the comparison between the PLCs profiles in the CM and in the MCA for two lipid gradients (corresponding to K_1^0 and $10K_1^0$ LIIs). In the MCA, in agreement with the hypothetical peptide drift mechanism, described in chapter 3, in the case of the large PS gradient the peptide significantly ac-

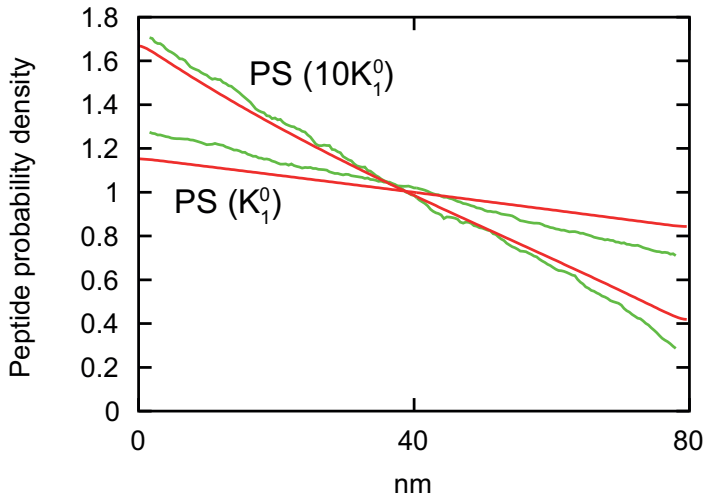

Figure 5.11: Comparison of peptide probability distributions for the MC (green line) and the CM (red line) for two LIIs of PS: K_1^0 and $10K_1^0$.

cumulates on the left membrane boundary with the peak value corresponds to $\sim$1.7 times increase in the peptide concentration. For the small lipid gradient the increase is about 1.3 times. The CM model is in a very good quantitative agreement with the MCA results. The negligible discrepancy between the two models can be corrected by varying of the PLCs diffusion coefficient. For example, if one assumes that complexes with a small number of bound PS lipids are faster than heavy complexes that are fully occupied by PS lipids, so that their diffusion coefficients are corrected as follows:

$$\begin{aligned} D_{0,0} &= 1.3 \cdot D_p^0 \\ D_{0,1} &= 1.2 \cdot D_p^0 \\ D_{0,2} &= 1.1 \cdot D_p^0 \end{aligned} \tag{5.45}$$

the peptide probability distribution profiles in the CM become almost identical to the ones in the MCA (Fig. 5.12).

Based on the comparison of the CM with the MCA, one can conclude that the constructed CM faithfully describes the lateral dynamics of the lipids and the peptides on the cell membrane under the action of electrostatic forces.

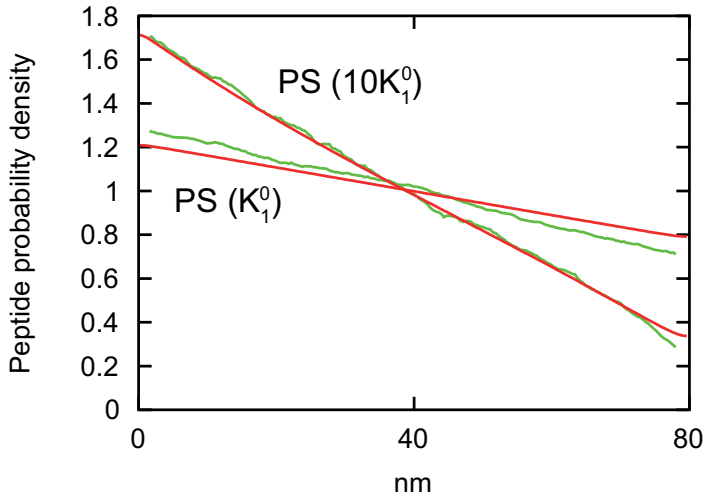

Figure 5.12: Comparison of peptide probability distributions for the MC (green line) and the corrected (5.45) CM (red line) for two LIIs of PS: K_1^0 and $10K_1^0$.

CHAPTER 6

Conclusions and directions for future work

6.1 Conclusions

The main objective of this thesis was:

> *To extend the understanding of the electrostatic contribution to the membrane lateral dynamics of proteins and lipids by means of novel computational modeling tools.*

This objective has been fulfilled by the work described in the previous chapters. In particular:

1. The novel MCA for studying electrostatic effects in the membrane lateral dynamics has been constructed, tested and validated. The results obtained in the MCA on a uniform membrane composition are shown to be in agreement with earlier experimental data. Furthermore, the new electrostatic properties of the peptide, mimicking the PD of a peripheral membrane protein, have been revealed. These include the probability density functions of lipid association with the peptide (Fig. 2.6), the peptide total charge (Fig. 2.8) and the association times of lipids with the peptides (Fig. 2.9). Finally, the reduction of the peptide diffusion coefficient upon the lipid se-

questration has been explained by means of electrostatic properties of the peptide-lipid complex.

2. Using the constructed MCA a novel hypothetical mechanism of the directional peptide drift on the heterogeneous membrane with the lipid gradient has been predicted. Namely, the basic peptide tends to drift to the area of the higher lipid density under the action of the force created by the gradient of the electrostatic potential. This mechanism can have a lot of biological implications (section 6.2 below). Additionally, the results show that the PIP_2 lipids are able to regulate the direction of the peptide drift.

3. The novel CM has been constructed, based on the results of the MCA. The main advantage of the CM over the MCA is that it can be used to study the membrane lateral dynamics on the large (micrometer) scales. The CM has been tested and validated by comparison of its results with the results of the MCA. As a consequence of the peptide directional drift described in the MCA, the CM predicts a local accumulation of the peptide species due to the gradient of the negatively charged membrane lipids (Fig. 5.11).

The constructed computational models significantly contribute to the subject of the membrane modeling. A very small number of studies theoretically describe lateral dynamics of lipids and proteins on the cell membrane under the action of electrostatic forces. Recently, Khelashvili et al. [61] simulated the diffusion of a macroion on the membrane using Monte-Carlo simulation for protein movements and Cahn-Hilliard theory for the lipid dynamics. They have shown that electrostatic sequestration of negatively charged lipids in the vicinity of the moving microion strongly reduces its lateral diffusion. In fact their model predicts that only extremely mobile microions (with the diffusion coefficient 10 times larger than that of lipids) are able to perform lateral movements, whereas slow macroions practically never escape from the lipid shell in the vicinity of the peptide, formed due to electrostatic sequestration. However, as has been shown in subsection 1.3, the measured protein diffusion coefficients are usually comparable to the lipid ones, meaning that model presented by Khelashvili et al. is

not applicable to the description of real biological processes. The second major paper on protein membrane dynamics was presented by Hinderliter et al. [60]. In this study Monte-Carlo simulations of multiple proteins on a lattice are performed and, in addition to adsorption and desorption, protein diffusion is also introduced. Protein domain formation was obtained by varying the energy of interaction between monovalent negatively charged PS lipids and positively charged proteins. However, how the electrostatic interactions of proteins with underlying lipids contribute to the protein lateral dynamics was not considered in detail.

The computational models presented in this thesis are deprived of all the limitations related to the models mentioned above. For example, the MCA provides the detailed description of the electrostatic nature of the membrane dynamics. Moreover, the problem of the restricted diffusion of the protein due to the associated lipid shell is resolved in the MCA by the lipid dragging mechanism. Additionaly, the MCA allows one to further develop it by introduction of other interactions between lipids and proteins. Thus, the improved MCA can be then used in various biological problems, for obtaining of the system detailed characteristics. Since the CM has been shown to be in agreement with the MCA and at the same time it is very computationaly efficient, one could further use it in the description of essential membrane processes.

6.2 Directions for future work

The two constructed MCA and CM models can be further improved and developed to study biologically important phenomena, that include electrostatic interactions on the cell membrane. The possible directions for the future work can be defined as follows:

1. The constructed MCA can be used to identify the role of dense protein clusters in the spatial dynamics of lipids. Multiple proteins with extended polybasic domains, such as MARKCS and GAP-43, or positively charged cytoskeletal polymers like septins are thought to form membrane micro and macro domains that sequester significant amounts of negatively charged

lipids, in particular PIP_2. However, simple reaction-diffusion models demonstrate that within protein clusters, the concentration of free PIP_2 should be lower than in the surrounding protein-free membrane. The constructed MCA can be utilized to thoroughly investigate the dynamics of PIP_2 and monovalent lipids within such clusters at various densities and configurations of the positive charge distribution. The influence of such protein clusters on the diffusion of lipids can be also evaluated.

2. The constructed CM model can be further extended to study various membrane mechanisms. For example, the protein membrane-cytoplasmic shuttling can be included to the system to account for the protein adsorption and desorption, allowing one to simulate the dynamics of the system at large time scales. Relevant protein phosphorylation/dephosphorylation by various enzymes can be also be included to simulate the changes of the intrinsic charge of the PDs. Additionally, the dynamics of the peptide-lipid complexes consisting of both PS and PIP_2 lipids (Fig. 4.1) can be described in details.

3. The modified and extended CM model, which allows to simulate the membrane diffusion at large lateral and temporal scales, can be used to analyze membrane domain formation events, that are potentially governed by the electrostatic interactions. For example, it is known that during clathrin-mediated endocytosis a large number of charged molecules, such as PIP_2 and PA, are produced and they regulate each other on the inner leaflet of the membrane. Thus, electrostatics can play a crucial role in this process and, therefore, the CM can be successfully utilized to study the endocytic cup initiation.

APPENDIX A

Effective friction in the peptide drift

In this appendix I describe the discrepancy of the peptide drift velocity obtained from the MCA and predicted by the eq. (3.9). This work is mainly done by Davide Marenduzzo.

Results of the MCA obtained on the uniform membrane lattice show that negatively charged lipids rapidly demix in the vicinity of the peptide, resulting in their sequestration between and around the peptide residues (Fig. 2.10, A) and in the formation of the lipid shell located underneath and associated with the peptide. Since the profiles shown in Fig. 2.10, A, are steady-state, the shell is permanently attached to the peptide and moves together with it. Thus the drift of the peptide can be potentially hindered by the presence of the lipid shell. I assume that this effect makes the peptide velocity observed in the MCA lower than that predicted by eq. (3.9).

One of the potential explanations of the above hypothesis is that the lipids that constitute the peptide-associated shell, due to their electrostatic potential, form a self-organized potential well, which effectively stabilizes the position of the peptide in its center. Thus, when the peptide attempts to move (to escape from the potential well) it experiences the returning force that prevents its motion and pulls the potential well behind it.

To test the above hypothesis, a simplified one-dimensional model system has been constructed. It consists of a particle (represents the peptide), defined by its position x, diffusing under the action of an external force that simulates the effect of the lipid gradient on the membrane. This particle with diffusion coefficient D_1 is attached to another particle (represents the lipid shell), defined by its position y, with which it interacts via an attractive potential V (e.g., the screened Coulomb potential or a simple Hookean spring, see Fig. A.1, A, for a schematic diagram). The Langevin equations of motion governing the dynamics of this system are:

$$\begin{aligned} \frac{dx}{dt} &= \frac{f}{\gamma_1} - \frac{K}{\gamma_1}(x-y) + \sqrt{2D_1}\eta_1 \\ \frac{dy}{dt} &= \frac{K}{\gamma_2}(x-y) + \sqrt{2D_2}\eta_2 \end{aligned} \tag{A.1}$$

where γ_1 and γ_2 are the friction coefficients of the first and the second particles respectively, D_1 and D_2 are their diffusion coefficients, the interaction between two particles, for simplicity, has been modeled as a Hookean spring with constant K and $\eta_{1,2}$ are two Gaussian (white) noise terms, with variance equal to 1. Two new variables can be introduced as follows: $\zeta = x + y$ (so that the center of mass position is given by $\zeta/2$) and $\xi = x - y$ (the distance between two particles). The characteristic correlation time of the noise terms $\eta_{1,2}$ is of the same order as the unit time step of the MCA (~ 1 μs). However, the peptide drift in the MCA is considered at time scales of about 1000 time steps (~ 1 ms). Thus, at such large time scales the contribution of the noise terms $\eta_{1,2}$ in eqs. (A.1) can be neglected and the steady state value of ξ can be calculated by the subtraction of the second equation from the first one:

$$0 = \frac{d\xi}{dt} = \frac{f}{\gamma_1} - \Big(\frac{K}{\gamma_1} + \frac{K}{\gamma_2}\Big)\xi \tag{A.2}$$

By rearranging of eq. (A.2) one can obtain the steady state value of ξ:

$$\xi = \frac{f/\gamma_1}{K/\gamma_1 + K/\gamma_2} \tag{A.3}$$

An expression, describing the behavior of ζ, can be derived by adding together

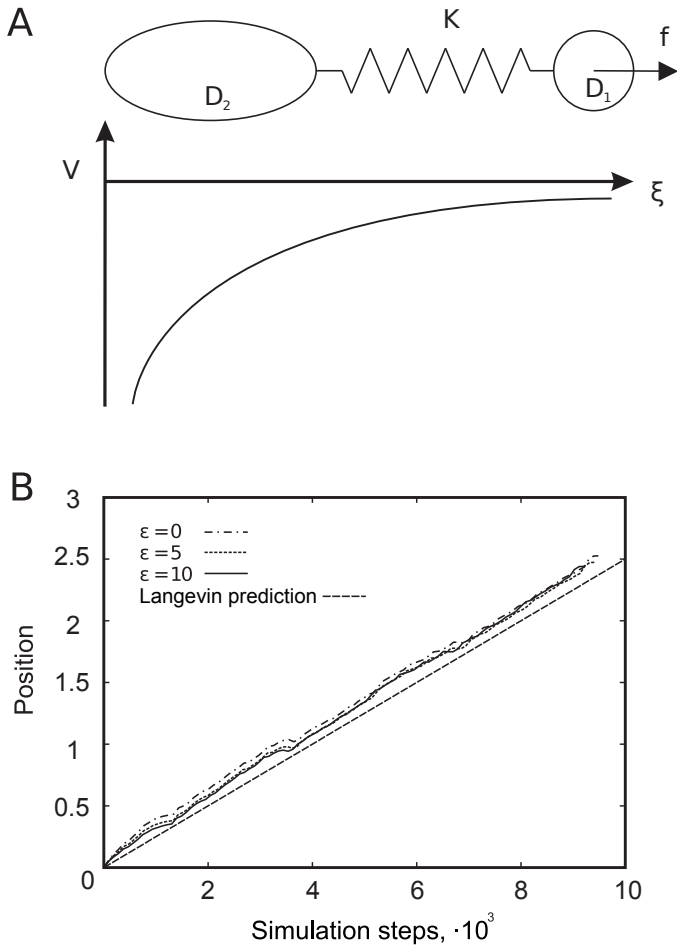

Figure A.1: Drift of a particle together with the associated potential well (from [62]). (A) A sketch of the hypothetical system that consists of a particle (the peptide) that diffuses under the action of a force f while associated with a second particle (lipid shell) via the interaction potential V, symbolically depicted as a spring with constant K. (B) Results of 1D Monte-Carlo simulations for the system shown in A where V is given by eq. (A.9). All quantities are in arbitrary nondimensional units. Time has been rescaled by the Monte-Carlo acceptance rate as suggested in [70].

two equations in the system (A.1):

$$\frac{d\zeta}{dt} = \frac{f}{\gamma_1} + \Big(\frac{K}{\gamma_2} - \frac{K}{\gamma_1}\Big)\xi \tag{A.4}$$

Using eq. (A.3) and taking into account that $\zeta/2$ represents the position of the center of mass of the two particles, the eq. (A.4) can be rewritten in the following form:

$$2v = \frac{f}{\gamma_1} + \Big(\frac{K}{\gamma_2} - \frac{K}{\gamma_1}\Big)\frac{f}{\gamma_1}\frac{\gamma_1\gamma_2}{K(\gamma_1+\gamma_2)} \tag{A.5}$$

where v is the velocity of the center of mass of the two particles. After rearranging of eq. (A.5) the velocity has the following form:

$$v = \frac{f}{\gamma_1 + \gamma_2} \tag{A.6}$$

Remembering Stokes-Einstein's relation:

$$D_{1,2} = \frac{k_B T}{\gamma_{1,2}} \tag{A.7}$$

one can obtain the final form of v:

$$v = \frac{f}{k_B T} \frac{D_1 D_2}{D_1 + D_2} \tag{A.8}$$

Therefore the velocity v does not depend on the spring constant K. Illustrating this fact, Fig. A.1, B, shows kinetic Monte-Carlo simulations of the system of two particles interacting via the sum of a spring and a finite-radius electrostatic potential V' of variable size defined as follows:

$$V' = \begin{cases} \varepsilon r_0 \left[\frac{e^{-r/\lambda}}{r+r_0} - \frac{e^{-r_C/\lambda}}{r+r_0} \right], & r > r_C \\ 0, & r < r_C \end{cases} \tag{A.9}$$

where $r_C = 3\lambda$.

The most relevant prediction of this simplified model for the lateral dynamics of the peptide on the membrane is that a particle interacting with a lipid shell should move slower due to the combined drag term which is equal to $k_B T(D_1 + D_2)/D_1 D_2$. Therefore, any finite diffusivity of the lipid shell associated with the peptide will reduce the peptide effective mobility in the gradient of lipids. I believe that this effect could qualitatively explain the effective coefficient that was found in fitting the simulation results to the theory.

APPENDIX B

Additional validation of the MCA

Additional validation of the MCA was done by Davide Marenduzzo as described below. A coarse-grained 1D kinetic Monte-Carlo algorithm was constructed. It simulates the diffusion of anionic lipids and the peptide on a 1D lattice. Lipids in the model interact with the peptide via the Debye-Hueckel potential which is truncated at three Debye lengths, whereas the mutual interaction of lipids is neglected. One lattice node can be occupied by multiple lipids. To scale the results of the simulations, it is assumed that the number of 10 lipids per node corresponds to the membrane density of 20%. Under this assumption, the length unit corresponds to $\sim$6 nm. To achieve equivalence with the standard Brownian dynamics method (without including hydrodynamics, see [70], and references therein), only single particle moves are used. A steady state lipid gradient is created in the same way as it is done in the MCA (chapter 3). Fig. B.1 shows that the peptide drifts along the lipid gradient with the velocity that is quantitatively similar to that observed in the MCA. Thus, the effect of the peptide drift is not an artifact of a particular configuration of the MCA in 2D, but it is reproducible with and robust to different implementation details.

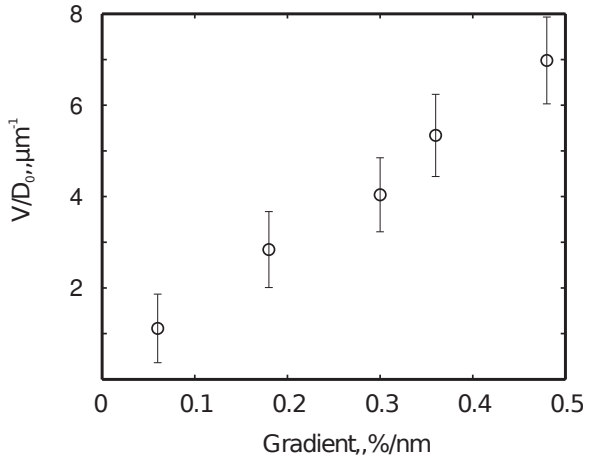

Figure B.1: Peptide drift in the gradient of a monovalent lipid in the coarse-grained 1D Monte-Carlo model (taken from [62]). Velocity of the peptide drift is proportional to the lipid gradient.

APPENDIX C

Concentrations of lipids and peptide complexes

Since the bulk concentration of mobile ions is usually given in M (mol/l), the concentration of lipids is usually given in a percentage of the total membrane concentration C_m and the concentration of peptides is given in molecules/nm^2, it is important to choose one working unit of the concentration and rescale all other units to the chosen one. I choose the working concentration units to be M. To find the concentration of lipids and peptide complexes in M I use the Guggenheim model of a surface [17]. According to this model a piece of the membrane S with two equal vertical extensions $h/2$ should be considered, where h is the height of the resulting parallelepiped. I choose S =1 μm^2. Assume there are N particles (lipids or peptide complexes) evenly distributed on S. Concentration of these particles in M units will be:

$$C = \frac{N}{N_A V} \tag{C.1}$$

where $V = Sh$ is the volume (a parallelepiped) of space where the concentration is measured. The height h can be defined by extending S by 5 nm in the third (vertical) dimension on both sides, so that the h = 10nm. The value of the volume is then: $V = 1\ \mu\text{m}^2 \cdot 10\ \text{nm} = 10^{-2}\ \mu\text{m}^3$. Substitution of this value and

N_A to the eq. (C.1) yields:

$$C = N\frac{10^{-6}}{6.02} \text{ [M]} \tag{C.2}$$

Equation (C.2) allows one to compute a concentration of N uniformly distributed particles on surface S =1 μm^2 in M units. Taking into account that an average area per lipid is about 0.6 nm^2 [65], one can find that there are about $1.7{\cdot}10^6$ lipids in 1 μm^2 piece of the membrane. Substituting this value to eq. (C.2) one can obtain an average total membrane concentration $C_m = 0.3$ M. Based on the experimental data [100, 101], I choose an average concentration of peptide complexes to be about 100 μM.

Bibliography

[1] M. Edidin, "Lipids on the frontier: a century of cell-membrane bilayers," *Nat Rev Mol Cell Biol*, vol. 4, pp. 414–418, May 2003.

[2] T. Pollard, W. Earnshaw, and J. Lippincott-Schwartz, *Cell Biology*. Elsevier Inc., 2008.

[3] G. J. Doherty and H. T. McMahon, "Mechanisms of endocytosis," *Annu Rev Biochem*, vol. 78, pp. 857–902, 2009.

[4] J.-F. Tocanne, L. Dupou-Czanne, A. Lopez, and J.-F. Tournier, "Lipid lateral diffusion and membrane organization," *FEBS Letters*, vol. 257, no. 1, pp. 10 – 16, 1989.

[5] T. Voets, G. Droogmans, G. Raskin, J. Eggermont, and B. Nilius, "Reduced intracellular ionic strength as the initial trigger for activation of endothelial volume-regulated anion channels," *Proceedings of the National Academy of Sciences*, vol. 96, no. 9, pp. 5298–5303, 1999.

[6] S. McLaughlin and D. Murray, "Plasma membrane phosphoinositide organization by protein electrostatics," *Nature*, vol. 438, pp. 605–611, Dec. 2005.

[7] T. Heimburg, *Thermal Biophysics of Membranes*. Wiley-VCH, Weinheim, 2007.

[8] V. Kiessling, C. Wan, and L. K. Tamm, "Domain coupling in asymmetric lipid bilayers," *Biochim Biophys Acta*, vol. 1788, no. 1, pp. 64–71, 2009.

[9] S. McLaughlin, J. Wang, A. Gambhir, and D. Murray, "PIP_2 and proteins: Interactions, organization, and information flow," *Annual Review of Biophysics and Biomolecular Structure*, vol. 31, no. 1, pp. 151–175, 2002.

[10] S. Cockcroft and M. De Matteis, "Inositol lipids as spatial regulators of membrane traffic," *Journal of Membrane Biology*, vol. 180, pp. 187–194, 2001.

[11] T. F. J. Martin, "PI(4,5)P_2 regulation of surface membrane traffic," *Current Opinion in Cell Biology*, vol. 13, no. 4, pp. 493 – 499, 2001.

[12] A. Toker, "The synthesis and cellular roles of phosphatidylinositol 4,5-bisphosphate," *Current Opinion in Cell Biology*, vol. 10, no. 2, pp. 254 – 261, 1998.

[13] S. B. Lee and S. G. Rhee, "Significance of PIP_2 hydrolysis and regulation of phospholipase C isozymes," *Current Opinion in Cell Biology*, vol. 7, no. 2, pp. 183 – 189, 1995.

[14] T. Nebl, S. W. Oh, and E. J. Luna, "Membrane cytoskeleton: PIP_2 pulls the strings," *Current Biology*, vol. 10, no. 9, pp. R351 – R354, 2000.

[15] Z. Li, R. M. Venable, L. A. Rogers, D. Murray, and R. W. Pastor, "Molecular dynamics simulations of PIP_2 and PIP_3 in lipid bilayers: Determination of ring orientation, and the effects of surface roughness on a Poisson-Boltzmann description," *Biophysical Journal*, vol. 97, no. 1, pp. 155 – 163, 2009.

[16] M. Fivaz and T. Meyer, "Specific localization and timing in neuronal signal transduction mediated by protein-lipid interactions," *Neuron*, vol. 40, no. 2, pp. 319–30, 2003.

[17] S. McLaughlin and A. Aderem, "The myristoyl-electrostatic switch: a modulator of reversible protein-membrane interactions.," *Trends Biochem Sci*, vol. 20, pp. 272–276, Jul 1995.

[18] J. Wang, A. Arbuzova, G. Hangys-Mihlyn, and S. McLaughlin, "The effector domain of myristoylated alanine-rich C kinase substrate binds strongly to phosphatidylinositol 4,5-bisphosphate," *Journal of Biological Chemistry*, vol. 276, no. 7, pp. 5012–5019, 2001.

[19] A. Arbuzova, L. Wang, J. Wang, G. Hangys-Mihlyn, D. Murray, B. Honig, and S. McLaughlin, "Membrane binding of peptides containing both basic and aromatic residues. Experimental studies with peptides corresponding to the scaffolding region of caveolin and the effector region of MARCKS," *Biochemistry*, vol. 39, no. 33, pp. 10330–10339, 2000.

[20] J. F. Hancock, H. Paterson, and C. J. Marshall, "A polybasic domain or palmitoylation is required in addition to the CAAX motif to localize p21ras to the plasma membrane," *Cell*, vol. 63, no. 1, pp. 133–9, 1990.

[21] D. Murray, L. Hermida-Matsumoto, C. A. Buser, J. Tsang, C. T. Sigal, N. Ben-Tal, B. Honig, M. D. Resh, and S. McLaughlin, "Electrostatics and the membrane association of Src: theory and experiment," *Biochemistry*, vol. 37, no. 8, pp. 2145–59, 1998.

[22] J. Wang, A. Gambhir, G. Hangyas-Mihalyne, D. Murray, U. Golebiewska, and S. McLaughlin, "Lateral sequestration of phosphatidylinositol 4,5-bisphosphate by the basic effector domain of myristoylated alanine-rich C

kinase substrate is due to nonspecific electrostatic interactions," *J Biol Chem*, vol. 277, no. 37, pp. 34401–12, 2002.

[23] S. Das, J. E. Dixon, and W. Cho, "Membrane-binding and activation mechanism of PTEN," *Proc Natl Acad Sci U S A*, vol. 100, no. 13, pp. 7491–6, 2003.

[24] G. Denisov, S. Wanaski, P. Luan, M. Glaser, and S. McLaughlin, "Binding of basic peptides to membranes produces lateral domains enriched in the acidic lipids phosphatidylserine and phosphatidylinositol 4,5-bisphosphate: an electrostatic model and experimental results," *Biophys J*, vol. 74, no. 2 Pt 1, pp. 731–44, 1998.

[25] Z. Qin and D. S. Cafiso, "Membrane structure of protein kinase C and calmodulin binding domain of myristoylated alanine rich C kinase substrate determined by site-directed spin labeling," *Biochemistry*, vol. 35, no. 9, pp. 2917–2925, 1996.

[26] T. Heimburg, B. Angerstein, and D. Marsh, "Binding of peripheral proteins to mixed lipid membranes: effect of lipid demixing upon binding.," *Biophys J*, vol. 76, pp. 2575–2586, May 1999.

[27] N. Ben-Tal, B. Honig, R. M. Peitzsch, G. Denisov, and S. McLaughlin, "Binding of small basic peptides to membranes containing acidic lipids: theoretical models and experimental results.," *Biophys J*, vol. 71, pp. 561–575, Aug 1996.

[28] S. Tzlil and A. Ben-Shaul, "Flexible charged macromolecules on mixed fluid lipid membranes: theory and Monte Carlo simulations," *Biophys J*, vol. 89, no. 5, pp. 2972–87, 2005.

[29] E. C. Mbamala, A. Ben-Shaul, and S. May, "Domain formation induced by the adsorption of charged proteins on mixed lipid membranes," *Biophys J*, vol. 88, no. 3, pp. 1702–14, 2005.

[30] S. Tzlil, D. Murray, and A. Ben-Shaul, "The "electrostatic-switch" mechanism: Monte Carlo study of MARCKS-membrane interaction," *Biophys J*, vol. 95, no. 4, pp. 1745–57, 2008.

[31] U. Golebiewska, A. Gambhir, G. Hangyas-Mihalyne, I. Zaitseva, J. Radler, and S. McLaughlin, "Membrane-bound basic peptides sequester multivalent (PIP_2), but not monovalent (PS), acidic lipids," *Biophys J*, vol. 91, no. 2, pp. 588–99, 2006.

[32] A. Gambhir, G. Hangyas-Mihalyne, I. Zaitseva, D. S. Cafiso, J. Wang, D. Murray, S. N. Pentyala, S. O. Smith, and S. McLaughlin, "Electrostatic sequestration of PIP_2 on phospholipid membranes by basic/aromatic regions of proteins," *Biophys J*, vol. 86, no. 4, pp. 2188–207, 2004.

[33] J. Wang, A. Gambhir, S. McLaughlin, and D. Murray, "A computational model for the electrostatic sequestration of $PI(4,5)P_2$ by membrane-adsorbed basic peptides," *Biophys J*, vol. 86, no. 4, pp. 1969–86, 2004.

[34] S. May, D. Harries, and A. Ben-Shaul, "Lipid demixing and protein-protein interactions in the adsorption of charged proteins on mixed membranes," *Biophys J*, vol. 79, no. 4, pp. 1747–60, 2000.

[35] E. Haleva, N. Ben-Tal, and H. Diamant, "Increased concentration of polyvalent phospholipids in the adsorption domain of a charged protein.," *Biophys J*, vol. 86, pp. 2165–2178, Apr 2004.

[36] C. A. Day and A. K. Kenworthy, "Tracking microdomain dynamics in cell membranes," *Biochimica et Biophysica Acta (BBA) - Biomembranes*, vol. 1788, no. 1, pp. 245–253, 2009.

[37] A. B. Goryachev and A. V. Pokhilko, "Dynamics of Cdc42 network embodies a Turing-type mechanism of yeast cell polarity," *FEBS Lett*, vol. 582, no. 10, pp. 1437–43, 2008.

[38] S. J. Singer and G. L. Nicolson, "The fluid mosaic model of the structure of cell membranes," *Science*, vol. 175, no. 23, pp. 720–31, 1972.

[39] P. G. Saffman and M. Delbruck, "Brownian motion in biological membranes," *Proc Natl Acad Sci U S A*, vol. 72, no. 8, pp. 3111–3, 1975.

[40] D. Axelrod, "Lateral motion of membrane proteins and biological function," *J Membr Biol*, vol. 75, no. 1, pp. 1–10, 1983.

[41] Y. Chen, B. C. Lagerholm, B. Yang, and K. Jacobson, "Methods to measure the lateral diffusion of membrane lipids and proteins," *Methods*, vol. 39, no. 2, pp. 147–53, 2006.

[42] L. K. Tamm and H. M. McConnell, "Supported phospholipid bilayers," *Biophys J*, vol. 47, no. 1, pp. 105–13, 1985.

[43] F. Zhang, B. Crise, B. Su, Y. Hou, J. K. Rose, A. Bothwell, and K. Jacobson, "Lateral diffusion of membrane-spanning and glycosylphosphatidylinositol-linked proteins: toward establishing rules governing the lateral mobility of membrane proteins," *J Cell Biol*, vol. 115, no. 1, pp. 75–84, 1991.

[44] L. K. Tamm, "Lateral diffusion and fluorescence microscope studies on a monoclonal antibody specifically bound to supported phospholipid bilayers," *Biochemistry*, vol. 27, no. 5, pp. 1450–7, 1988.

[45] M. Stefl, A. Kulakowska, and M. Hof, "Simultaneous characterization of lateral lipid and prothrombin diffusion coefficients by z-scan fluorescence correlation spectroscopy," *Biophys J*, vol. 97, no. 3, pp. L01–3, 2009.

[46] R. Gilmanshin, C. E. Creutz, and L. K. Tamm, "Annexin IV reduces the rate of lateral lipid diffusion and changes the fluid phase structure of the lipid bilayer when it binds to negatively charged membranes in the presence of calcium," *Biochemistry*, vol. 33, no. 27, pp. 8225–32, 1994.

[47] J. M. Haugh, F. Codazzi, M. Teruel, and T. Meyer, "Spatial sensing in fibroblasts mediated by 3' phosphoinositides," *J Cell Biol*, vol. 151, no. 6, pp. 1269–80, 2000.

[48] A. Yaradanakul and D. W. Hilgemann, "Unrestricted diffusion of exogenous and endogenous PIP_2 in baby hamster kidney and Chinese hamster ovary cell plasmalemma," *J Membr Biol*, vol. 220, no. 1-3, pp. 53–67, 2007.

[49] D. E. Shvartsman, J. C. Donaldson, B. Diaz, O. Gutman, G. S. Martin, and Y. I. Henis, "Src kinase activity and SH2 domain regulate the dynamics of Src association with lipid and protein targets," *J Cell Biol*, vol. 178, no. 4, pp. 675–86, 2007.

[50] S. Lu, M. Ouyang, J. Seong, J. Zhang, S. Chien, and Y. Wang, "The spatiotemporal pattern of Src activation at lipid rafts revealed by diffusion-corrected FRET imaging," *PLoS Comput Biol*, vol. 4, no. 7, p. e1000127, 2008.

[51] D. R. Larson, J. A. Gosse, D. A. Holowka, B. A. Baird, and W. W. Webb, "Temporally resolved interactions between antigen-stimulated IgE receptors and Lyn kinase on living cells," *J Cell Biol*, vol. 171, no. 3, pp. 527–36, 2005.

[52] M. Frick, K. Schmidt, and B. J. Nichols, "Modulation of lateral diffusion in the plasma membrane by protein density," *Curr Biol*, vol. 17, no. 5, pp. 462–7, 2007.

[53] P. S. Pyenta, P. Schwille, W. W. Webb, D. Holowka, and B. Baird, "Lateral diffusion of membrane lipid-anchored probes before and after aggregation of cell surface IgE-receptors," *Journal of Physical Chemistry A*, vol. 107, no. 40, pp. 8310–8318, 2003.

[54] L. Zimmermann, W. Paster, J. Weghuber, P. Eckerstorfer, H. Stockinger, and G. J. Schutz, "Direct observation and quantitative analysis of Lck exchange between plasma membrane and cytosol in living T cells," *J Biol Chem*, vol. 285, no. 9, pp. 6063–70, 2010.

[55] H. Niv, O. Gutman, Y. Kloog, and Y. I. Henis, "Activated K-Ras and H-Ras display different interactions with saturable nonraft sites at the surface of live cells," *J Cell Biol*, vol. 157, no. 5, pp. 865–72, 2002.

[56] M. J. Saxton, "Lateral diffusion in an archipelago. Distance dependence of the diffusion coefficient," *Biophys J*, vol. 56, no. 3, pp. 615–22, 1989.

[57] B. J. Sung and A. Yethiraj, "Computer simulations of protein diffusion in compartmentalized cell membranes," *Biophys J*, vol. 97, no. 2, pp. 472–9, 2009.

[58] J. M. Haugh, "Analysis of reaction-diffusion systems with anomalous sub-diffusion," *Biophys J*, vol. 97, no. 2, pp. 435–42, 2009.

[59] T. Gil, J. H. Ipsen, O. G. Mouritsen, M. C. Sabra, M. M. Sperotto, and M. J. Zuckermann, "Theoretical analysis of protein organization in lipid membranes," *Biochimica Et Biophysica Acta-Reviews on Biomembranes*, vol. 1376, no. 3, pp. 245–266, 1998.

[60] A. Hinderliter, P. F. Almeida, C. E. Creutz, and R. L. Biltonen, "Domain formation in a fluid mixed lipid bilayer modulated through binding of the C2 protein motif.," *Biochemistry*, vol. 40, pp. 4181–4191, Apr 2001.

[61] G. Khelashvili, H. Weinstein, and D. Harries, "Protein diffusion on charged membranes: a dynamic mean-field model describes time evolution and lipid reorganization.," *Biophys J*, vol. 94, pp. 2580–2597, Apr 2008.

[62] V. Y. Kiselev, D. Marenduzzo, and A. B. Goryachev, "Lateral dynamics of proteins with polybasic domain on anionic membranes: A dynamic Monte-Carlo study.," *Biophysical Journal*, vol. 100, no. 5, pp. 1261–70, 2011.

[63] R. Rubinstein and D. Kroese, *Simulation and the Monte Carlo method*. Wiley series in probability and mathematical statistics, John Wiley & Sons, 2008.

[64] N. Metropolis, A. W. Rosenbluth, M. N. Rosenbluth, A. H. Teller, and E. Teller, "Equation of state calculations by fast computing machines," *The Journal of Chemical Physics*, vol. 21, no. 6, pp. 1087–1092, 1953.

[65] H. I. Petrache, S. W. Dodd, and M. F. Brown, "Area per lipid and acyl length distributions in fluid phosphatidylcholines determined by H-2 NMR spectroscopy," *Biophysical Journal*, vol. 79, no. 6, pp. 3172–3192, 2000.

[66] D. Murray, N. Ben-Tal, B. Honig, and S. McLaughlin, "Electrostatic interaction of myristoylated proteins with membranes: simple physics, complicated biology," *Structure*, vol. 5, no. 8, pp. 985–9, 1997.

[67] D. Murray, A. Arbuzova, G. Hangyas-Mihalyne, A. Gambhir, N. Ben-Tal, B. Honig, and S. McLaughlin, "Electrostatic properties of membranes containing acidic lipids and adsorbed basic peptides: theory and experiment," *Biophys J*, vol. 77, no. 6, pp. 3176–88, 1999.

[68] K. Kawasaki, *Phase Transition and Critical Phenomena*, vol. 2. Academic, New York, 1972.

[69] S. Whitelam and P. L. Geissler, "Avoiding unphysical kinetic traps in Monte Carlo simulations of strongly attractive particles," *J. Chem. Phys.*, vol. 127, no. 15, p. 154101, 2007.

[70] E. Sanz and D. Marenduzzo, "Dynamic Monte Carlo versus Brownian dynamics: A comparison for self-diffusion and crystallization in colloidal fluids," *The Journal of Chemical Physics*, vol. 132, no. 19, p. 194102, 2010.

[71] F. D. Brown, N. Thompson, K. M. Saqib, J. M. Clark, D. Powner, N. T. Thompson, R. Solari, and M. J. Wakelam, "Phospholipase D1 localises to secretory granules and lysosomes and is plasma-membrane translocated on cellular stimulation," *Current Biology*, vol. 8, no. 14, pp. 835 – 838, 1998.

[72] N.-E.-H. Chatah and C. S. Abrams, "G-protein-coupled receptor activation induces the membrane translocation and activation of Phosphatidylinositol-4-phosphate 5-Kinase I alpha by a Rac- and Rho-dependent pathway," *Journal of Biological Chemistry*, vol. 276, no. 36, pp. 34059–34065, 2001.

[73] R. Cazzolli, A. N. Shemon, M. Q. Fang, and W. E. Hughes, "Phospholipid signalling through phospholipase D and phosphatidic acid," *IUBMB Life*, vol. 58, no. 8, pp. 457–61, 2006.

[74] M. Rizzo and G. Romero, "Pharmacological importance of phospholipase D and phosphatidic acid in the regulation of the mitogen-activated protein kinase cascade.," *Pharmacology & therapeutics*, vol. 94, no. 1-2, pp. 35–50, 2002.

[75] I. van den Bout and N. Divecha, "PIP5K-driven PtdIns(4,5)P_2 synthesis: regulation and cellular functions," *Journal of Cell Science*, vol. 122, no. 21, pp. 3837–3850, 2009.

[76] K. Kwiatkowska, "One lipid, multiple functions: how various pools of PI(4,5)P_2 are created in the plasma membrane.," *Cellular and molecular life sciences : CMLS*, June 2010.

[77] R. R. Netz, "Debye-Hückel theory for interfacial geometries," *Phys. Rev. E*, vol. 60, pp. 3174–3182, Sep 1999.

[78] H. Nymeyer and H.-X. Zhou, "A method to determine dielectric constants in nonhomogeneous systems: Application to biological membranes," *Biophysical Journal*, vol. 94, no. 4, pp. 1185 – 1193, 2008.

[79] P. Chaikin and T. Lubensky, *Principles of condensed matter physics*. Cambridge University Press, 2000.

[80] K. Huang, *Statistical mechanics*. Wiley, 1963.

[81] B. B. Laird and A. D. J. Haymet, "Entropy of electrolytes," *The Journal of Chemical Physics*, vol. 100, no. 5, pp. 3775–3779, 1994.

[82] D. Chandler, *Introduction to modern statistical mechanics*. Oxford University Press, 1987.

[83] V. F. Weisskopf, "On the self-energy and the electromagnetic field of the electron," *Phys. Rev.*, vol. 56, pp. 72–85, Jul 1939.

[84] I. Borukhov, D. Andelman, and H. Orland, "Steric effects in electrolytes: A modified Poisson-Boltzmann equation," *Phys. Rev. Lett.*, vol. 79, pp. 435–438, Jul 1997.

[85] R. Parr and W. Yang, *Density-functional theory of atoms and molecules*. International series of monographs on chemistry, Oxford University Press, 1994.

[86] J. Jackson, *Classical electrodynamics*. Wiley, 1999.

[87] S. Groot and P. Mazur, *Non-equilibrium thermodynamics*. Dover Books on Physics, Dover Publications, 1984.

[88] Q. Zheng and G.-W. Wei, "Poisson-Boltzmann-Nernst-Planck model," *Journal of Chemical Physics*, vol. 134, May 2011.

[89] R. Mills, R. Malhotra, L. A. Woolf, and D. G. Miller, "Distinct diffusion coefficients in binary nonelectrolyte mixtures: Frames of reference," *The Journal of Physical Chemistry*, vol. 98, no. 21, pp. 5565–5575, 1994.

[90] M. S. Kilic, M. Z. Bazant, and A. Ajdari, "Steric effects in the dynamics of electrolytes at large applied voltages. II. Modified Poisson-Nernst-Planck equations," *Phys. Rev. E*, vol. 75, p. 021503, Feb 2007.

[91] O. Zienkiewicz, R. Taylor, R. Taylor, and J. Zhu, *The finite element method: its basis and fundamentals*. Elsevier Butterworth-Heinemann, 2005.

[92] R. Grima and T. J. Newman, "Accurate discretization of advection-diffusion equations," *Phys. Rev. E*, vol. 70, p. 036703, Sep 2004.

[93] S. L. Carnie, D. Y. C. Chan, and J. Stankovich, "Computation of forces between spherical colloidal particles: Nonlinear Poisson-Boltzmann theory," *Journal of Colloid and Interface Science*, vol. 165, no. 1, pp. 116 – 128, 1994.

[94] D. Harries, S. May, W. M. Gelbart, and A. Ben-Shaul, "Structure, stability, and thermodynamics of lamellar DNA-lipid complexes," *Biophysical Journal*, vol. 75, no. 1, pp. 159 – 173, 1998.

[95] M. Napolitano, "A fortran subroutine for the solution of periodic block-tridiagonal systems," *Communications in Applied Numerical Methods*, vol. 1, no. 1, pp. 11–15, 1985.

[96] L. K. Bieniasz, "Extension of the Thomas algorithm to a class of algebraic linear equation systems involving quasi-block-tridiagonal matrices with isolated block-pentadiagonal rows, assuming variable block dimensions," *Computing*, vol. 67, pp. 269–285, 2001.

[97] S. Conte and C. Boor, *Elementary numerical analysis: an algorithmic approach*. International series in pure and applied mathematics, McGraw-Hill, 1980.

[98] M. Kanduc, A. Naji, J. Forsman, and R. Podgornik, "Dressed counterions: Strong electrostatic coupling in the presence of salt," *The Journal of Chemical Physics*, vol. 132, no. 12, p. 124701, 2010.

[99] A. Naji, S. Jungblut, A. G. Moreira, and R. R. Netz, "Electrostatic interactions in strongly coupled soft matter," *Physica A: Statistical Mechanics and its Applications*, vol. 352, no. 1, pp. 131 – 170, 2005.

[100] I. A. Prior, C. Muncke, R. G. Parton, and J. F. Hancock, "Direct visualization of Ras proteins in spatially distinct cell surface microdomains," *The Journal of Cell Biology*, vol. 160, no. 2, pp. 165–170, 2003.

[101] J. F. Hancock and I. A. Prior, "Electron microscopic imaging of Ras signaling domains," *Methods*, vol. 37, no. 2, pp. 165 – 172, 2005.